Aalto University
School of Chemical
Engineering

Katariina Solin

BIOACTIVE NANOCELLULOSE FILMS WITH SPATIAL DEFINITION

Master´s Programme in Chemical, Biochemical and Materials Engineering
Major in Fibre and Polymer Engineering

Master's thesis for the degree of Master of Science in Technology submitted for inspection, Espoo, 30 May, 2018.

Supervisor	Prof. Orlando Rojas
Instructors	Dr. Maryam Borghei
	Dr. Hannes Orelma

Aalto University
School of Chemical
Engineering

Aalto University, P.O. BOX 11000, 00076 AALTO
www.aalto.fi

Abstract of master's thesis

Author Katariina Solin

Title of thesis Bioactive Nanocellulose Films with Spatial Definition

Degree Programme Chemical, Biochemical and Materials Engineering

Major Fibre and Polymer Engineering

Thesis supervisor Prof. Orlando Rojas

Thesis advisor(s) / Thesis examiner(s) Dr. Maryam Borghei and Dr. Hannes Orelma

Date 30.05.2018 **Number of pages** 102+7 **Language** English

Abstract

In this thesis, fluidic channels were prepared on films made from cellulose nanofibers (CNF) and their potential use in biosensor applications was studied. The main goal was to develop hydrophilic-hydrophobic patterns to controllably produce CNF substrates for microfluidic applications. The work included a detailed investigation, to prevent non-specific adsorption of a type of human serum protein, hIgG, on CNF. A suitable antifouling agent for the CNF films was tested. CNF is a cellulosic material that has at least one dimension in the nanometer range and it is mainly produced mechanically from wood fibers. It can be used to make strong, translucent and smooth films. Two different approaches were tested to prepare 2D-channels on the CNF films: photolithography and inkjet printing of hydrophobic materials. The photolithographic method utilized simultaneously thiol-ene and thiol-yne click chemistries. In the inkjet studies, it was observed that polystyrene dissolved in p-xylene worked successfully. The prepared microfluidic CNF materials were characterized with SEM, AFM, contact angle measurements and liquid flow tests. Additionally, the non-specific protein adsorption was studied by using model CNF films with QCM-D, SPR and AFM techniques. Furthermore, the adsorption of fluorescent hIgG was performed on real CNF films and channels with CLSM method. The molecules used for protein blocking included BSA, fibrinogen and PDMAEMA-block-POEGMA copolymers. The results indicated that the best fluid flow was obtained by inkjet printing channels with polystyrene edges on CNF films. In addition, the PDMAEMA-block-POEGMA copolymer was the best antifouling agent for CNF and it reduced the hIgG adsorption up to 95 %. The successful blocking of the channels point out that these systems could be developed further and possibly be used in future biosensing applications.

Keywords CNF films, nanopaper, biosensor substrate, fluidic channel, non-specific protein adsorption

Aalto-yliopisto
Kemian tekniikan korkeakoulu

Aalto-yliopisto, PL 11000, 00076 AALTO
www.aalto.fi

Diplomityön tiivistelmä

Tekijä Katariina Solin

Työn nimi Kuvioidut ja bioaktiiviset nanoselluloosafilmit

Koulutusohjelma Kemian, biokemian ja materiaalien tekniikka

Pääaine Kuitu- ja polymeeriteknologia

Työn valvoja Prof. Orlando Rojas

Työn ohjaaja(t)/Työn tarkastaja(t) TkT. Maryam Borghei ja TkT. Hannes Orelma

Päivämäärä 30.05.2018 **Sivumäärä** 102+7 **Kieli** Englanti

Tiivistelmä

Tässä diplomityössä valmistettiin nestevirtauskanavia nanoselluloosa-filmien pinnoille, ja tutkittiin näiden mahdollista käyttöä biosensoreissa. Työn tavoitteena oli valmistaa kanavia muodostamalla filmeille hydrofobisia ja hydrofiilisiä alueita. Lisäksi tavoitteena oli tutkia hIgG-vasta-aineen epäspesifistä adsorptiota CNF-filmeille sekä löytää sopivia adsorptionestoaineita, jotka soveltuvat tälle materiaalille. Adsorptionestoaineina kokeiltiin BSA:ta, fibrinogeenia ja PDMAEMA-blokki-POEGMA -kopolymeerejä. Selluloosan nanofibrillit (cellulose nanofibrils CNF) ovat nanomateriaali, jota valmistetaan puukuiduista mekaanisella käsittelyllä. Tästä materiaalista voidaan valmistaa mekaanisesti vahvoja, läpinäkyviä ja tasaisia filmejä. Tässä työssä valmistettiin CNF-filmeille kanavia käyttäen CLICK-kemian reaktioita sekä polymeerikuviointi-menetelmää käyttäen mustesuihkutulostusta. Valmistettuja pintakanavia tutkittiin SEM- ja AFM-menetelmillä, kontaktikulmamittauksilla sekä virtaustestein. Proteiinien epäspesifistä adsorptiota tutkittiin CNF-mallipinnoilla QCM-D-, SPR- ja AFM-menetelmien avulla. Lisäksi adsorptiota tutkittiin CNF filmeille valmistetuissa kanavissa fluoresoidun vasta-aineen avulla CLSM-menetelmällä. Tutkimukset osoittivat, että mustesuihkutulostettu polystyreeniliuos muodosti parhaiten toimivan nestevirtauskanavan CNF filmin pinnalle. Lisäksi PDMAEMA-blokki-POEGMA -kopolymeeri osoittautui parhaaksi adsorptionestoaineeksi. Se vähensi hIgG:n adsorptiota 95 %. Yhdistämällä pintakanavien valmistusmenetelmä ei-selektiivisen adsorptionestoaineiden kanssa voidaan valmistaa materiaaleja tulevaisuuden biosensoreihin.

Avainsanat CNF filmit, nanopaperi, biosensorin substraatti, nestevirtauskanava, epäspesifinen proteiiniadsorptio

Preface

First, I would like to thank my supervisor Professor Orlando Rojas for providing me this opportunity to work in his research group and in this inspiring project. I appreciate all the support and positive feedback you have given me. I would also like to thank my instructors Dr. Hannes Orelma and Dr. Maryam Borghei for excellent guidance during this project. Thank you for all the good advice and answers to my questions. In addition, many thanks to Maija Vuoriluoto whom I got help in the laboratory experiments in the beginning of my work. Especially, I would like to thank Maija for broadening my understanding of the QCM-D and SPR methods. I am very grateful to Jiaqi Guo, Risto Koivunen, Guillermo Reyes Torres, Annamari Jukkola, Ritva Kivelä, Marja Kärkkäinen and Rita Hatakka for the practical help in the laboratory. Additionally, I would like to thank VTT Technical Research Centre of Finland for providing me CNF films for this project. Furthermore, special thanks to my friends Nanna Koivula and Katja Utriainen for all the tips and support during this project. Finally, I would like to thank my family and boyfriend for all the patience and encouragement that they have given me during this project and throughout my studies.

Espoo, 30 May, 2018

Katariina Solin

Table of Contents

List of Abbreviations

AFM	Atomic force microscopy
BSA	Bovine serum albumin
CBDs	Cellulose binding domains
CDRs	Complementarity determining regions
CLSM	Confocal laser scanning microscopy
CMC	Carboxymethylated cellulose
CNF	Cellulose nanofibrils
D33-EGMA-110	PDMAEMA-block-POEGMA copolymer
D33-EGMA-137	PDMAEMA-block-POEGMA copolymer
D58-EGMA-118	PDMAEMA-block-POEGMA copolymer
DMSO	Dimethyl sulfoxide
Fab region	Fragment antigen-binding region
Fc region	Fragment crystallizable region
FITC	Fluorescein 5(6)-isothiocyanate
hIgG	Human immunoglobulin G
hIgG-FITC	FITC-stained human IgG
IgG	Immunoglobulin G
μPAD	Microfluidic paper analytical device

MilliQ	Deionized water purified with Millipore Synergy UV unit
PC	Phosphorycholines
PDMAEMA	Poly(2-(dimethylamino)ethyl methacrylate)
PEG	Polyethylene glycol
PEG-SH	Poly(ethylene glycol) methyl ether thiol
PEI	Polyethyleneimine
pI	Isoelectric point
POEGMA	Poly(oligo(ethylene glycol) methyl ether methacrylate
QCM-D	Quartz crystal microbalance with dissipation
SEM	Scanning electron microscopy
SPR	Surface plasmon resonance
SutCo	Roll-to-roll pilot scale manufacturing line for CNF films
WCA	Water contact angle

1. Introduction

Cellulosic nanomaterials exhibit significant potential to develop efficient material platforms in the biomedical field, especially in diagnostics. Diagnostics involve biomolecular recognition, which is changed to a detectable electric or visual signal. Their applications include among other things biosensors. Biosensors produce analytical information by utilizing biological responses. They use sensitive biological elements, bioreceptors, which interact, bind or recognize the analyte of interest. (Schultz and Taylor, 1996) Typical recognition elements include enzymes, nucleic acids, antibodies and cells (Grieshaber et al., 2008). Immunoassays are biosensors that utilize highly specific antibody-antigen interactions. In immunoassays, a physicochemical change occurs when antibody binds the antigen and with the help of tracers, such as fluorescent molecules, enzymes, or radioisotopes, a signal is generated. (O'sullivan, 1979)

Ideal biosensors have high sensitivity, biocompatibility, high specificity, good stability, no background signal and no errors from environmental variables (Aikio et al., 2006). However, especially the presence of the background signal is a common problem in biosensors and usually it is caused by non-specific binding of biomolecules (Aikio et al., 2006; Rusmini et al., 2007). Therefore, in order to get better sensing results, the surface of the biosensor must suppress the non-specific adsorption of biomolecules. Thus, it is important to find ways to reduce the non-specific interactions on substrates when developing new biosensors. In addition, it is important to develop new sensors that are sensitive, specific, user-friendly, robust and affordable.

Traditionally, support materials employed in the medical and diagnostic applications are made from non-renewable resources, such as fossil-based plastics (Lequin, 2005; Wu et al., 2008). Using of these materials provoke among other things environmental concerns. That is why cellulose-based substrates have gained interest in the research of diagnostics applications. The fact that cellulose is a renewable material and the most

abundant biomass material in nature makes it economically interesting material for many applications, including disposable applications. Furthermore, cellulose as well as nanocellulose have properties such as biocompatibility, special morphology and non-toxicity, which make them interesting materials in the development of new functional substrates in diagnostic applications (Salas et al., 2014; Orelma et al., 2012a). Along with sustainability, cellulose could also bring better economy to these applications by replacing some substrates with higher costs. Cellulose is inexpensive material and therefore, it could potentially lower the price of some products (Orelma et al., 2012a).

Paper-based biosensors provide portable, low-cost analytical platforms that could potentially be used in point-of-care (PoC) and in-field assays. In addition, nanomaterial-based lateral flow test strips and paper microfluidic devices have a great potential to improve detection sensitivity and selectivity. (Ge et al., 2014) Some studies have proposed cellulosic substrates to be used in electrochemical paper-based analytical devices (ePADs), microfluidic paper-based analytical devices (μPADs) and electrochemiluminescence (ECL) immunoassays (Lamas-Ardisana et al., 2018; Hu et al., 2014; Ge et al., 2012). In the literature, there are many reports concerning the progress of the development of paper-based microfluidic biosensors (Fenton et al., 2008; Jarujamrus et al., 2012; Li et al., 2008; Li et al., 2010). In addition, the use of nanocellulose materials in biosensors has raised interest in recent years (Vuoriluoto et al., 2016; Orelma et al., 2012a; Edwards et al., 2013).

The objective of this thesis was to produce fluidic channels on nanocellulose films by creating hydrophilic-hydrophobic patterns on the surface of the films. Another goal was to study non-specific adsorption of proteins on nanocellulose films and to find a suitable antifouling agent for this material. In this work, click chemistry and polymer patterning methods were utilized to produce fluidic channels. The non-specific protein adsorption was studied with human IgG antibodies with surface-sensitive techniques, including SPR and QCM-D. The hIgG was chosen as a model protein because of its abundance. IgG is the major antibody isotype in human plasma (Janeway et al., 2001). The protein blocking efficiencies of BSA, fibrinogen and hydrophilic PDMAEMA-

block-POEGMA copolymers with cationic ends were investigated. In addition, the potential use of these channels in future biosensor applications was analyzed.

First in this thesis, a short literature review is presented. In the chapter 2, theoretical background of this work is discussed; cellulose and nanocellulose are introduced and their use in biosensor applications reviewed. In addition, a few surface modification methods of nanocellulose and the theory of protein adsorption are discussed. Then, in the third chapter, experimental part of this thesis is presented and in the chapter 4, results of these experiments and discussion are addressed. Finally, the chapter 5 presents the conclusions of this thesis and the future prospects are discussed.

2. Background

2.1 Cellulose

Cellulose $(C_6H_{10}O_5)_n$ is a linear chain polymer that consists of repeating D-anhydroglucopyranose units linked together with β(1→4)-glycosidic bonds (Figure 1). It is the main structural component in the cell walls of plants (Klemm et al., 1998). Cellulose can also be found in fungi, algae, bacteria and in some invertebrates like tunicates (Wertz et al., 2010). It is one of the most important polysaccharide for humans, along with starch and glycogen. In addition, it is the most abundant polymer in the world and it can be used to make for example paper, cardboard, films, clothes, biofuels and composites. It is also a major source of fiber in our diet.

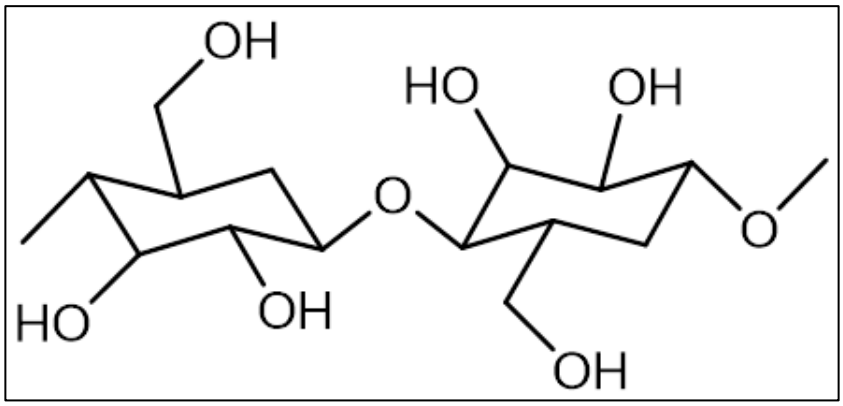

Figure 1. Repeating unit of cellulose: D-anhydroglucopyranose unit linked with β(1→4)-glycosidic bonds.

In plants, cellulose is formed from glucose that is produced by photosynthesis in leafs, in which light energy is transformed into chemical energy. In this process, some of the produced glucose is used as energy, some is stored for later use in the form of starch and the rest is formed into cellulose (Fukuoka and Dhepe, 2006; McKendry, 2002). Cellulose chains pack naturally tightly together via hydrogen bonds and van der Waals forces forming elementary fibrils. The formed cellulose fibrils are rigid, strong and they

have low solubility in water (Moon et al., 2011). As a result, cellulose fibrils have tendency to form organized structures. In plants cellulose fibrils pack further into microfibrils and subsequently into fibers.

2.2 Cellulose nanomaterials

The definition for nanomaterial is that it has at least one dimension in the nanometer range, i.e. between 1 to 100 nm (Khalil et al., 2014). Wood cellulose nanomaterials have many interesting properties such as high strength, low density and high aspect ratio. In addition, they have large surface areas, which make them to be reactive materials with a good binding ability. However, the properties of nanocellulose vary depending on the source material and production method. (Kangas, 2014)

Cellulose nanomaterials can be produced by mechanical, chemical and enzymatic treatments. In addition, some species of bacteria can produce cellulose nanofilaments by using sugars as a carbon source. Cellulose nanomaterials can be classified based on their dimensions, preparation mechanisms and properties. They are generally divided into cellulose nanofibrils (CNF), cellulose nanocrystals (CNC) and bacterial cellulose (BC). Cellulose nanofibrils are mechanically isolated microfibrils. Cellulose nanocrystals are, in turn, highly crystalline rods of cellulose, obtained by acid hydrolysis, and bacterial cellulose is an exopolymer produced by microbes such as *Gluconacetobacter xylinus.* (Kangas, 2014) Bacterial cellulose has the overall structure in the macroscale but the fine structure in the nanoscale. The hierarchical structures from wood fiber to CNF and CNC are illustrated in the Figure 2.

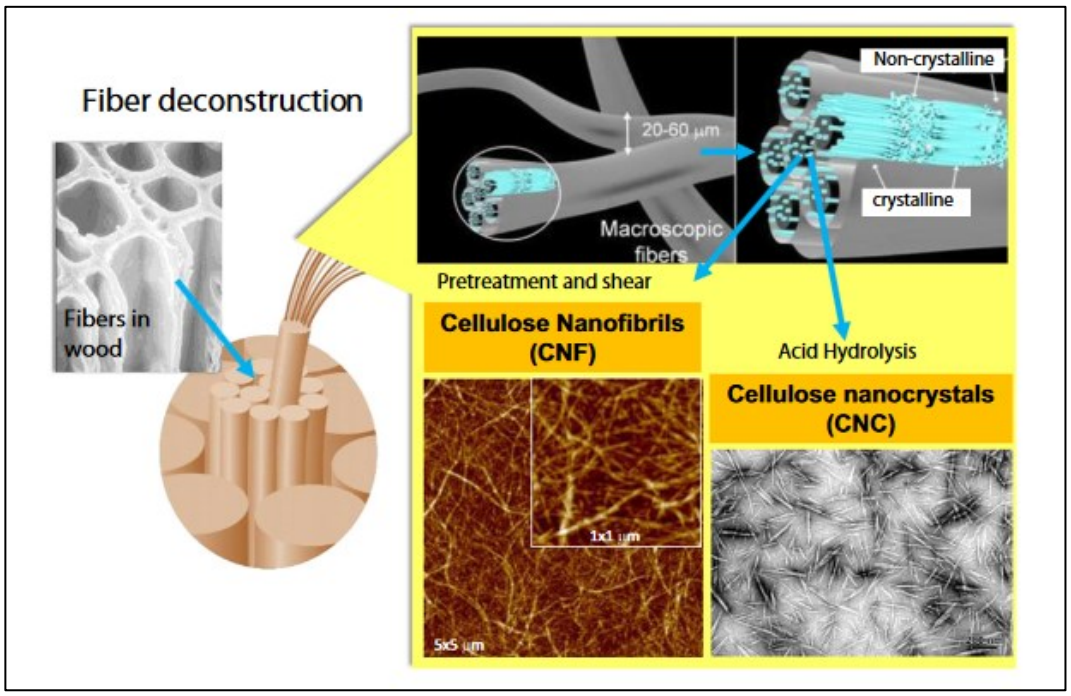

Figure 2. Illustration of nanocellulose production from fiber cell walls by mechanical and chemical treatments (Salas et al., 2014).

2.2.1 Cellulose nanofibrils

Cellulose nanofibrils (CNF) are mechanically isolated microfibrils that contain both crystalline and amorphous domains (Khalil et al., 2014; Brinchi et al., 2013). CNF is mainly produced from wood pulp, but also, raw materials such as cotton, sugar beet, hemp and flax are used. Usually, the fibrils have a width of 20-40 nm and a length of several micrometers. (Kangas, 2014) It is generally produced by mechanical treatment of wood pulp in processes, where mechanical shear causes lateral disintegration of cellulose fibers into nanoscale fibrils. The most common methods used to produce CNF are homogenization, microfluidization and microgrinding. (Missoum et al., 2014) In addition, chemical treatments and combination of mechanical and chemical treatments can be used in the production of CNF (Abitbol et al., 2016). Mechanically produced nanocellulose is a heterogeneous material, consisting of micro- and nanoscale fibers, fiber bundles, non-fibrillated fibers and bigger fiber fractions (Kangas, 2014).

However, by combining suitable pretreatment steps with the mechanical manufacture method, the produced material comprises only individual CNFs. CNF has natural properties such as low thermal expansion, high surface area, very high aspect ratio and excellent mechanical properties (Khalil et al., 2014; Lasseuguette, 2008; Fujisawa et al., 2013). A SEM image of cellulose nanofibrils can be seen in the Figure 3.

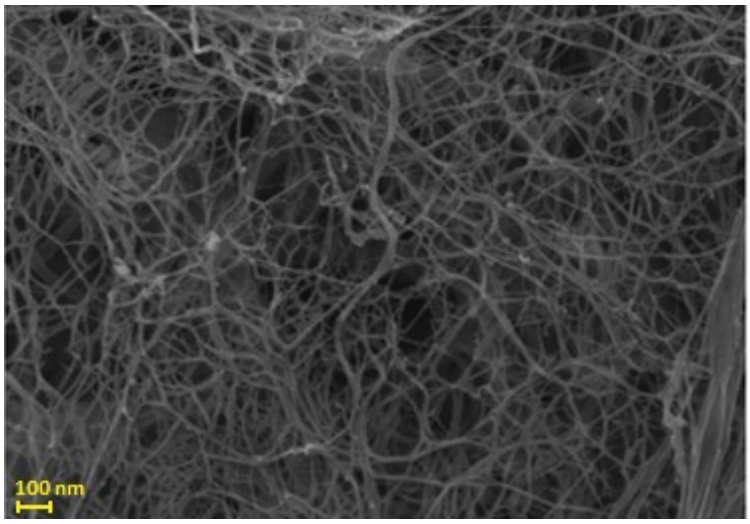

Figure 3. SEM image of cellulose nanofibrils (Modified from Kangas, 2014).

2.2.2 CNF films and nanopaper

Cellulosic micro- and nanofibrils can be used to make films of CNF. When water is removed from CNF, fibrils tend to form organized structures. Thin film of fibrils, a nonwoven structure, can be produced by using vacuum filtration, spraying, pressure filtration, or solvent casting (Guo, 2017; Soledad Peresin et al., 2012). The properties of the CNF films depend on both the used raw materials and production procedures. For example, with the selected production procedure mechanical properties, thickness or optical properties of the films can be altered significantly. In general, CNF films are strong, translucent or transparent (depending from the used CNF grade), smooth, and

they have good thermal stability and chemical reactivity as individual CNFs (Tammelin and Vartiainen, 2014).

Vacuum filtration is a simple film making method that is similar to a method used in traditional papermaking (Yang et al., 2017). This is why the CNF films made by vacuum filtration are often called as nanopapers. In vacuum filtration, a gel layer of CNF is obtained by filtering aqueous suspension of CNF. The CNF gel is then dried into a form of a film. This method is mainly used in a laboratory scale, but CNF films can also be produced in a larger scale. VTT Technical Research Center of Finland has developed a roll-to-roll pilot scale unit, called SutCo, for CNF film manufacturing. This production is based on the solvent casting method. (Soledad Peresin et al., 2012) This method concerns a large-scale preparation of smooth and even CNF films on a surface of plastic support material, like polyethylene or polystyrene. The CNF film is applied and spread directly onto the support in the form of a suspension by rod, blade or roll coating methods. In SutCo, controlled drying and hot pressing can be used to adjust the porosity of the film. In addition, this method provides transparent (depends on the used CNF grade), smooth, strong and uniform films from widely selectable CNF materials (see Figure 4). The drying of the applied suspension is done via controlled evaporation and it is done typically at 25-60 °C so that the hydroxyl groups of CNF can interact at a profitable rate through self-association, leading to even film formation. Upon drying, the necessary adhesion between CNF and the support material prevents the shrinkage of the film. Furthermore, the dried film can be pressed, for example by hot pressing, which leads to a thinner and denser film structure. (Qvintus et al., 2013)

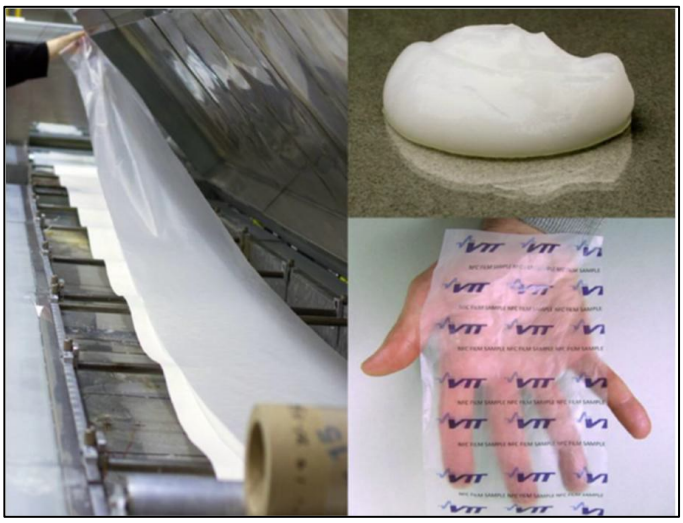

Figure 4. CNF film manufactured from CNF gel by VTT's SutCo line (Kangas, 2014).

2.3 Biosensors and microfluidic devices with cellulosic substrates

Biosensors recognize diseases and physiological conditions by transforming biological responses into a detectable signal. In order to obtain response, biosensors can utilize specific adsorptions of proteins on active surfaces. Usually, a biosensor has probe molecules that are immobilized on a substrate. When a target molecule is bound to the probe molecules, a signal is produced and analytical information can be obtained (Dhruv, 2009). However, the adsorption of proteins can also be non-specific. In general, the non-specific protein adsorption is the biggest problem of biosensors, which disturbs the sensing (Aikio et al., 2006; Masson et al., 2006; Rusmini et al., 2007). It can cause lowering of the sensor signal (Masson et al., 2006). Namely, due to the non-specific binding, target molecules do not always reach the bioactive area of the biosensor, but instead, adsorb to some non-specific sites, where they cannot be recognized.

Recently, cellulosic substrates have gained a lot of interest in the research of diagnostics applications (Orelma et al., 2011). For bioanalytical applications, the surface chemistry of cellulose-based substrates needs to facilitate biosensor immobilization and minimize non-specific adsorption (Pelton, 2009). For example,

bioactive paper has active recognition, functional material and liquid flow capabilities, which make it an interesting material for many applications, including low-cost platforms for diagnostics. (Aikio et al., 2006; Pelton, 2009) In addition, some studies have made use of the porosity of papers to generate paper-based microfluidics devices for biosensors (Pelton, 2009).

Paper-based biosensors can utilize different strategies. For example, dipstick assays, lateral flow assays (LFAs) and microfluidic paper analytical devices (μPADs) with paper substrates have been studied. The dipstick assays are simple papers with stored reagents that react with target molecules, when the sample is blotted onto the paper. The LFAs have also stored reagents in them but, in addition, they incorporate flow of the sample. The liquid flow makes it possible to produce multi-detection designs for the reason that the sample can pass through multiple zones with different reagents. μPADs in turn are made by creating hydrophilic channels with hydrophobic borders. They are cheap, require small amount of sample and can be used in multiplexed, quantitative analysis. (Parolo and Merkoçi, 2013)

Two- and three-dimensional μPADs have been prepared by patterning of paper with various assay designs (Nilghaz et al., 2012). These sensors are made by patterning physical or chemical hydrophobic borders to form microfluidic channels on paper. The channels and barriers can be created on paper by cutting, photolithography, plotting, inkjet etching, plasma etching and wax printing (Martinez et al., 2009). The Figure 5 shows examples of the preparation of microfluidic channels on paper. In addition, the functional molecules required for sensing can be immobilized on paper by physical adsorption, chemical coupling or bioaffinity reactions (Pelton, 2009). For example, the chemical or biological molecules have been immobilized on paper by hand dispersing or inkjet printing (Martinez et al., 2009). μPADs could be used to make for example paper-based enzyme-linked immunosorbent assays (ELISAs). For example, Li et al. (2008) made microfluidic patterns on a paper surface using alkyl ketene dimer (AKD) hydrophobization and plasma treatment by using a metal mask. This method produced well defined hydrophilic channels on the paper. The activity of alkaline phosphatase

enzyme was studied by using BCIP/NBT substrate system, a ready-to-use precipitating substrate system for alkaline phosphatase, to indicate the activity of the enzyme via color change. (Li et al., 2008)

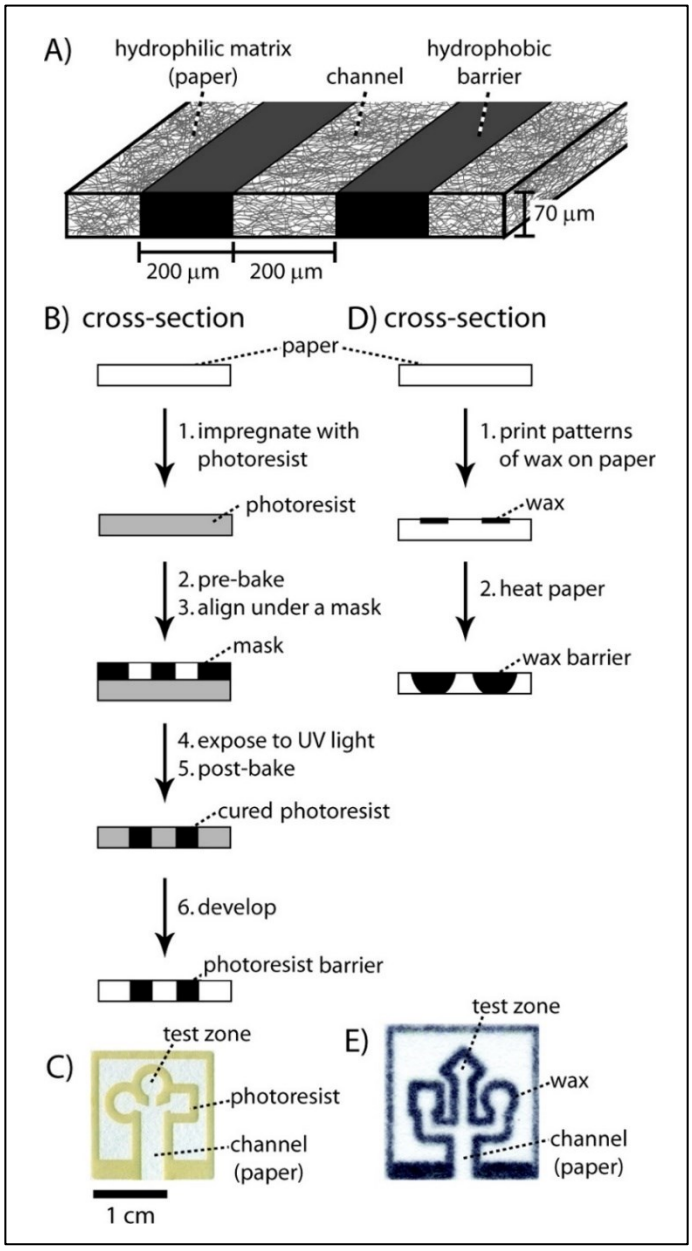

Figure 5. Preparation of microfluidic channels on paper: A) The structure of paper-based microfluidic channel, B) photolithography on paper produces well-defined

hydrophobic barriers and consists multiple steps, C) a device fabricated by photolithography, D) wax printing method requires only two steps but during heating, the lateral spreading of wax lowers the resolution of the pattern and E) a device fabricated by wax printing (Martinez et al., 2009).

2.3.1 Antibodies as recognition elements

Antibodies are widely used recognition elements in biosensors because of the high specificity of the antibody-antigen interaction. (Grieshaber et al., 2008) They are plasma protein molecules that are used by the immune system to identify for example bacteria and viruses. Antibodies recognize specific substances, called antigens, on the invading organism and this induces an immune response. Antibodies can be divided into different classes based on their structure, physical and chemical properties along with their biological activity (Woof and Burton, 2004). There are five antibody classes known as immunoglobulin G (IgG), immunoglobulin A (IgA), immunoglobulin M (IgM), immunoglobulin D (IgD) and immunoglobulin E (IgE) proteins. The main antibody class in human serum is IgG proteins and its structure can be seen in the Figure 6. IgG is used in immunological research and clinical diagnostics because of its abundance and high specificity to antigens. The measurement of IgG can be used as a diagnostic tool and in epidemiological surveys because measured IgG levels indicate immune status to particular pathogens, like measles, hepatitis B and varicella-zoster viruses. (Shors, 2011)

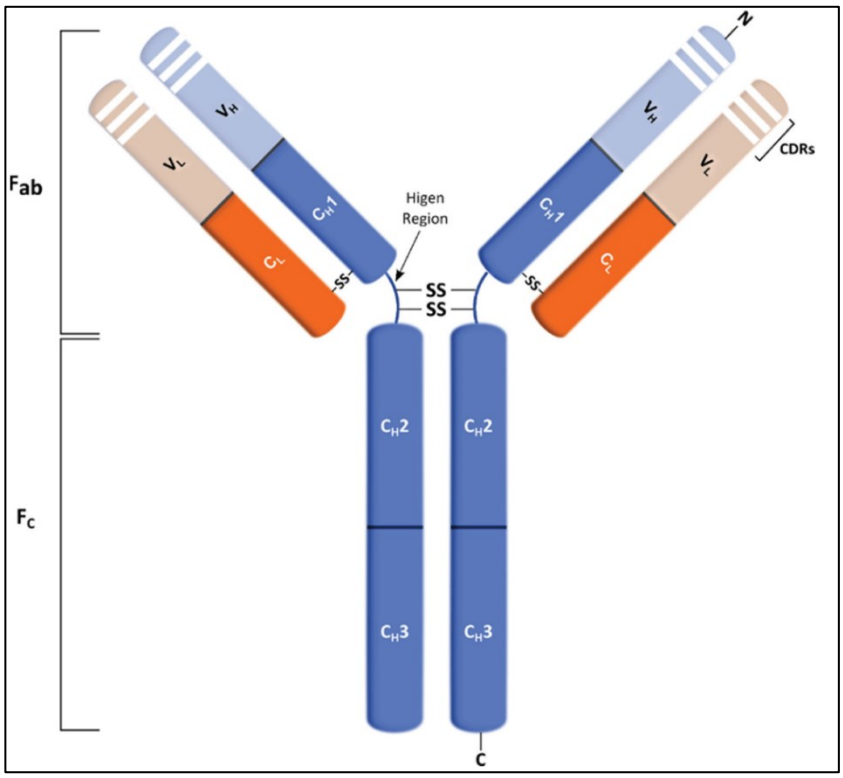

Figure 6. Structure of immunoglobulin G (IgG) composes of the constant (C) and variable (V) domains of the heavy (H) and light (L) chains. The heavy chains have three constant domains (C_H) and one variable domain (V_H). The light chains have one constant domain (C_L) and one variable domain (V_L). IgG can be divided into Fc and Fab regions. Fab regions include complementarity determining regions (CDRs). (Loureiro et al., 2015).

Immunoglobulin (Ig) monomer is the basic functional unit of antibodies. The Ig monomer is a Y-shaped molecule, formed of four polypeptide chains. Two of these chains are called heavy chains and the other two light chains. Light chains have a variable domain and a constant domain, whereas heavy chains have one variable domain and either three or four constant domains. The chains and domains are linked together with disulfide bonds forming functional binding sites for antigens. (Woof and Burton, 2004) An IgG monomer can be divided into Fc and Fab regions (Loureiro et al., 2015). The region that can recognize specific parts of an antigen is called a fragment

antigen-binding region (Fab region). The Fab region is composed of one constant and one variable domain from each heavy and light chain of the antibody. (Putnam et al., 1979) Two Fab regions are linked to a fragment crystallizable region (Fc region) with a flexible hinge region. The Fc region is composed of two heavy chains with two or three constant domains. (Loureiro et al., 2015) This region ensures that each antibody generates an appropriate immune response for a given antigen by interacting with cell surface receptors, called Fc receptors, and with some proteins of the complement system (Larsson, 1988). Part of the Fab region (Fv region) composed of the variable domains of the heavy and light chains form the antigen-binding site, paratope. The paratope is a set of complementarity determining regions (CDRs). The variable domains of both heavy and light chains have three CDRs, and different antibodies have different set of CDRs, which ensures the specificity of the antibody-antigen interactions. (Nguyen, 2012)

Antibody–antigen interaction is based on specific matching of geometric shapes (Shetty, 2005). Antibodies bind antigens specifically with high affinity in a process, where the paratope of an antibody recognizes specific structures on the surface of an antigen called epitope, and interacts with the epitope by spatial complementarity. Usually, a small antigen is bound in a groove of an antibody, locating between the variable domains of heavy and light chains. However, larger antigens cannot fit into these grooves. In this case, the antigen's epitope is recognized at the interface containing the CDRs. (Janeway et al., 2001) The forces that bind antigen and antibody together include electrostatic forces, hydrogen bonding, hydrophobic bonding and van der Waals forces, but the binding between antibody and antigen is reversible. (Shetty, 2005)

Antibodies need to recognize and bind a wide range of molecular structures. However, almost limitless amount of different antigen-binding sites can be produced because of the great difference in the amino acid sequences of the variable domains in different antibodies, especially, in their CDRs (Vuoriluoto, 2017; Madigan et al., 2009). In addition, heavy and light chain variable domains can be folded so that the six CDRs of

the paratope form various sets at the end of the antibody, thus, a profuse amount of unique and specific antigen binding sites can be produced to different antibodies. Antibodies are very efficient to tell apart very similar epitopes. Even a small difference in the orientation of functional groups can be recognized by antibodies, such as glucose and galactose, which differ only with the orientation of a single hydroxyl group. (Vuoriluoto, 2017)

2.4 Surface modification of cellulose and nanocellulose

Modification of cellulosic substrates is required in order to improve its performance in biosensor applications. The surface hydroxyl groups of nanocellulose and its large relative surface area provide reactive sites for modification (Abitbol et al., 2016). In surface modification, new functionalities are introduced to the surface and an increase in reactivity is achieved (Missoum, 2013). The modification methods of cellulose and nanocellulose include direct chemical modifications of the hydroxyl groups, but also, physical adsorption of reactive materials onto the surfaces.

Some biosensor applications require the formation of fluidic channels on the substrate. This means that some areas of the substrate should be hydrophilic and some hydrophobic. Nanocellulose is a hydrophilic material; therefore, the hydrophobic properties need to be introduced to this material separately. This can be done with hydrophobic coatings but also with surface modification methods. The surface modification methods can alter the wettability of nanocellulose by introducing rough structures and low surface energy substances to the nanocellulose surface (Guo, 2017). Hydrophobization methods of nanocellulose include among other things adsorption of hydrophobic compounds, esterification, silane coupling, amine coupling, graft copolymerization and amidification (Missoum, 2013; Khalil et al., 2014). In addition, hydrophobic substances can be coupled to the nanocellulose surface by click chemistry (Guo et al., 2016 and 2018). Furthermore, in order to use cellulosic material as a substrate of a biosensor, the material needs to facilitate biosensing. The sensing activity

can be obtained by immobilizing biological recognition elements, like proteins on cellulose. They can be immobilized on a surface by physical adsorption, chemical coupling or bioaffinity reactions (Pelton, 2009).

2.4.1 Click chemistry reactions

Click chemistry has become a valuable chemical tool during recent years. Click chemistry reactions involve rapid and selective reactions of substances with "clickable" pair of functional groups (Filpponen et al., 2012). For example, thiol-ene and thiol-yne reactions are considered as click chemistry reactions. The thiol-ene reactions occur between terminal alkene and thiol groups and the thiol-yne reactions occur between terminal alkyne and thiol groups. The Figure 7 presents the chemical equations of these reactions. In these reactions, covalent S-H bond is formed across double or triple bonds by free radical or nucleophilic mechanism (Guo, 2017). Both thiol-ene and thiol-yne reactions can be photochemically induced with UV-light. The photochemical reaction enables photolithographic functionalization of surfaces. Therefore, these reactions have been used to make patterns and fluidic channels on cellulosic substrates. For example, Guo et al. (2016 and 2018) reported the use of thiol-ene and thiol-yne click reactions in the preparation of superhydrophobic-superhydrophilic surface patterns and hydrophilic channels with hydrophobic borderlines on filter papers and CNF films.

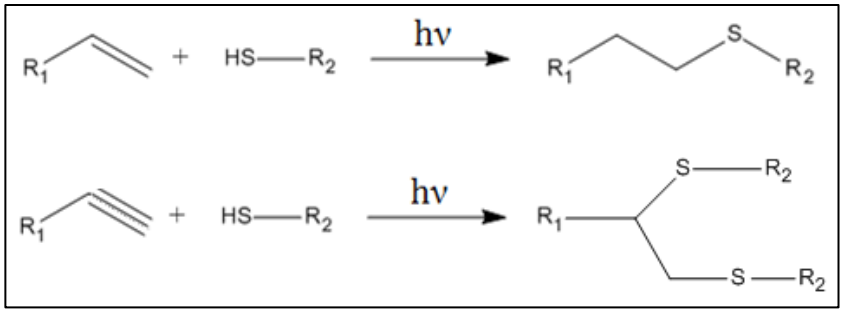

Figure 7. Thiol-ene and thiol-yne click reactions (Adapted from Arsenault et al., 2015).

Thiol-ene reaction

Under UV exposure, thiol-ene reaction proceeds via a typical chain process with initiation, propagation and termination steps (Lowe, 2010). The reaction mechanism of the thiol-ene reaction can be seen in the Figure 8. In the initiation step, a photoinitiator interacts with a thiol and a thiyl radical (RS·) is formed. Next, in the first propagation step, a direct addition of the thiyl radical across the C=C bond of a terminal alkene produces an intermediate carbon-centered radical. Then, chain transfer to a second thiol molecule produces the thiol-ene addition product and a new thiyl radical. Finally, the termination reaction involves typically coupling of two radicals. (Lowe, 2010)

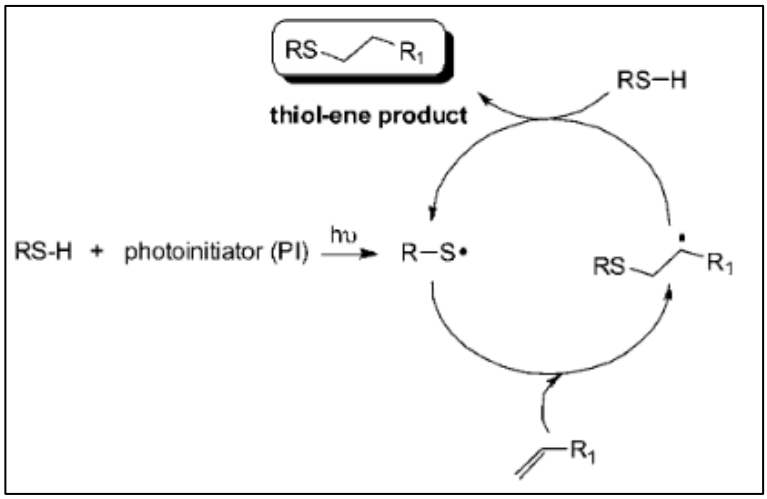

Figure 8. Reaction mechanism of the thiol-ene click reaction (Lowe, 2010).

Thiol-yne reaction

In thiol-yne reaction, the addition of thiols to a terminal C≡C bond can produce six possible products. Monoaddition and dithioacetal adducts are possible but the reaction that leads to a 1,2-bisaddition dithioether product (see Figure 7) is commonly referred as the thiol-yne reaction. This addition reaction contains sequential thiol-yne and thiol-ene reactions. (Lowe, 2014) The mechanism of a double radical hydrothiolation of a

terminal alkyne bond is shown in the Figure 9. In this mechanism, photochemically generated thiyl radicals (R-S·) interact with the C≡C bond of a terminal alkyne resulting in the formation of an intermediate vinylthioether radical. A chain transfer reaction between the intermediate vinylthioether radical with another thiol produces a vinylthioether intermediate. The reaction of this intermediate with a thiyl radical produces an intermediate carbon-centered radical that goes through a second chain transfer reaction, yielding the target 1,2-bisaddition dithioether product. (Lowe, 2014)

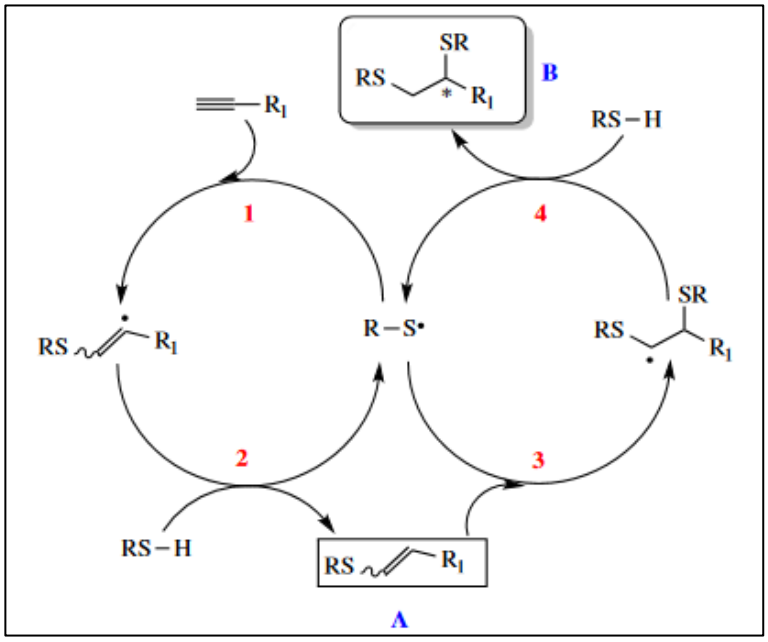

Figure 9. The reaction mechanism of a double radical hydrothiolation in the thiol-yne reaction. Step 1: photochemically generated thiyl radicals (R-S·) interact with the C≡C bond and an intermediate vinylthioether radical is formed. Step 2: a chain transfer to additional thiol gives a vinylthioether intermediate (A). Step 3: the vinylthioether intermediate reacts with R-S· to give an intermediate carbon-centered radical. Step 4: the formed radical undergoes a second chain transfer reaction, in which the target 1,2-bisaddition dithioether product (B) is generated. (Lowe, 2014).

2.4.2 Protein immobilization

Proteins can be immobilized on surfaces mainly by physical, covalent or bioaffinity immobilization. Physical immobilization involves protein adsorption on surfaces by intermolecular forces, like ionic bonds or hydrophobic and polar interactions. The physical adsorption of proteins is simple, often a cheap method and it preserves the original structure of the attached protein (Lin and Dufresne, 2014). Brash and Hove (1993) studied the adsorption of fibrinogen, a blood plasma protein, on regenerated cellulose, but they found that the adsorption rate and extent of adsorption on cellulose were lower than on some hydrophobic surfaces. Among other things, electrostatic interactions between anionic cellulose and cationic parts of proteins act as driving force for protein adsorption onto cellulosic substrate (Jones and O'Melia, 2000). However, proteins are not strongly adsorbed onto unmodified cellulose due to its low charge; therefore, surface modification or other immobilization strategy is usually required in order to immobilize the proteins firmly to the substrate (Pelton, 2009).

In covalent protein immobilization, covalent bonds are formed between accessible functional groups of the exposed amino acids and suitable substrate surfaces. Reactive functional groups of proteins include amino groups from lysine and hydroxylysine, thiol groups from cysteine, carboxylic acid groups from aspartate and glutamate, and hydroxyl groups from serine and threonine (Rusmini et al., 2007). The substrates can be modified so that these functional groups of proteins can react with the surface. For example, in order to immobilize proteins covalently on cellulosic surface, cellulose needs to be functionalized with molecules or polymers so that bioconjugation can be improved. For example, Bora et al. (2006) prepared a photoreactive cellulose membrane by functionalizing the cellulose with 1-fluoro-2-nitro-4-azidobenzene. Under UV exposure, the azido group of the prepared photoreactive membrane transformed into highly reactive nitrene group and immobilization of glucose oxidase (GOD) protein was done. This photoreactive cellulose membrane was successfully used in enzyme-linked immunosorbent assay (ELISA). (Bora et al., 2006) In addition, it has been reported that also nanocellulose surface can be modified to be reactive for

protein immobilization (Orelma et al., 2012a; Orelma et al., 2012b; Vuoriluoto et al., 2016). Chemical conjugation can provide high protein loading and excellent stability of proteins, but the chemistry procedures may be complicated (Lin and Dufresne, 2014). Covalent immobilization creates highly covered surfaces with irreversibly bonded molecules. As a result, covalent immobilization is the most stable immobilization method. (Rusmini et al., 2007)

In bioaffinity immobilization, proteins are immobilized on surfaces by biochemical affinity interactions. In this method, biochemical binding agents adhere spontaneously to each other and make it possible to immobilize proteins to surfaces. One well-known bioaffinity interaction is between avidin and biotin molecules. (Rusmini et al., 2007) For example, avidin-biotin interaction has been used to make bioactive cellulose surfaces. Orelma et al. (2012b) used physical adsorption and chemical conjugation of avidin on carboxylated cellulose and attached biotinylated functionalities on the surface. In addition, cellulose binding domains (CBDs), components of cellulose and hemicellulose degrading enzymes, can be used in bioaffinity immobilization of proteins to cellulose. CBDs have high affinity to cellulose, but they do not have hydrolytic activity. (Cao et al., 2007)

2.5 Protein adsorption

Proteins have surface-active properties so they have natural tendency to aggregate on surfaces (Wilson et al., 2005). The positive adsorption occurs when the protein-surface interactions are more favorable than the protein-liquid interactions. Adsorption occurs spontaneously, when more energy is released than gained according to the Gibbs law of free energy (Lee et al., 2001). Adsorption of proteins can be specific or non-specific. Non-specific interactions occur between many different types of atoms, molecules and surfaces. Specific interactions in turn occur when certain combination of physical forces form a strong non-covalent bond between two molecules. (Leckband and Israelachvili, 2001) As mentioned earlier, specific protein interactions can be utilized

in biosensor applications. However, the non-specific interactions can lower the efficiency of the biosensors and give falls positive results (Rusmini et al., 2007). Specific protein interactions are mainly based on the unique binding sites of protein molecules. The forces affecting specific interactions relate to steric, ionic and directional bonds (Leckband and Israelachvili, 2001). Non-specific protein adsorption is caused by hydrogen bonding, ionic or electrostatic interactions and hydrophobic interactions between proteins and surfaces (Ross and Subramanian, 1981).

2.5.1 Factors affecting protein adsorption

Noteworthy, interactions between proteins and materials are a complex process. The process involves many forces that can act at different sites and times. In other words, different reactions can take place simultaneously or sequentially at different locations on or away from the material surface. (Dhruv, 2009) In addition, proteins do not typically behave like symmetric rigid particles when they approach solid surfaces. In contrast, proteins occur in large range of size and shape and can have varying structural properties. Furthermore, the folding into secondary and tertiary structure, contributes to that proteins contain a specific distribution of charged, hydrophobic and hydrophilic chains. All of these affect greatly the adsorption characteristics of proteins. Moreover, many properties like the folding state or the charges inside proteins can be changed in different conditions by altering pH, ionic strength, or temperature. (Rabe et al., 2015)

In general, protein adsorptions depend on the properties of proteins and material surfaces together with surrounding conditions and adsorption kinetics. Among other things, structure, size, charge distribution and polarity of the protein, charge, roughness and surface energy of the surface plus temperature and pH of the environment affects the adsorption. For example, the adsorption is more probable with larger proteins because they have more sites that can interact with surfaces. In addition, the stability of the protein structure affects adsorption. Increased conformational freedom of peptide

chains caused by protein unfolding can make more sites for interactions and therefore increase adsorption. (Dhruv, 2009)

Hydrophobic interactions

Hydrophobic interactions affect adsorption significantly. Hydration force is attractive between two hydrophobic surfaces or patches on the surfaces, whereas, if both surfaces are hydrophilic, hydration repulsion dominates (Leckband and Israelachvili, 2001; Kanduč and Netz, 2015). It is known that proteins tend to adsorb more likely onto hydrophobic surfaces (Prime and Whitesides, 1991; Sigal et al., 1998). The reason for this is related to entropy and enthalpy changes of protein adsorption system. In aqueous conditions, proteins tend to fold so that their hydrophobic parts are folded inside its hydrophilic parts. This minimizes the energetically unfavorable polar-nonpolar interactions with surrounding water molecules. (Dhruv, 2009) Despite this, some of the hydrophobic amino acids may be available for interaction with hydrophobic substrates and the protein can unfold so that the hydrophobic core turns towards the surface and the hydrophilic parts towards the aqueous environment. (Petersen et al., 2010; Dee et al., 2002) These conformational changes of proteins are favorable because the overall entropy of the system can increase with adsorption. Thus, the entropy gain drives spontaneous adsorption. For example, when a hydrophobic surface is in aqueous environment, the entropy of the system is decreased because water molecules are highly organized on the hydrophobic surface. When proteins are added to the system, adsorption causes displacement of unfavorably organized water molecules and this leads to entropy gain. (Petersen et al., 2010)

Electrostatic interactions

Hydrophilic surfaces can also have protein adsorption. Removal of water from a hydrophilic surface creates a large energy barrier to protein adsorption, but interactive electrostatic interactions and conformational changes can provide favorable energetic

changes that create driving forces for adsorption. (Wilson et al., 2005) Therefore, electrostatic interactions play a big role in the adsorption of proteins on hydrophilic surfaces especially, if the adsorbing protein has a hard structure. To be exact, the hard and stable proteins adsorb on hydrophilic surfaces only in case of electrostatic attraction. Oppositely, soft proteins can adsorb spontaneously on hydrophilic surfaces even under electrostatic repulsion. This is because low structural stability proteins can experience intramolecular structural rearrangements that create driving forces for adsorption that overcome the unfavorable effects of hydrophilic dehydration and electrostatic repulsion. (Norde, 1996)

Amino acids can be charged positively or negatively or be neutral or polar in nature. The net charge of proteins is determined by the sum of the charges of these constituents. Additionally, proteins contain both acidic and basic functional groups and therefore have an isoelectric point (pI). At pH below pI of a protein, it carries a net positive charge and above its pI, it carries a net negative charge (Cleaves, 2011). When the protein is close to a charged surface, electrostatic interactions occur between proteins and the surface. In addition, electrostatic interactions can occur also between proteins and neutral surfaces. This is because biomaterial surfaces adsorb water and ions when exposed to complex environments such as body fluids and formation of water and electric double layers take place near these surfaces (Dhruv, 2009). The stability of dispersions can be estimated with a DLVO theory. When the charges of a protein and surface are same, the DLVO theory states that electrostatic repulsion makes a strong energetic barrier to adsorption. For opposite charges, if the electrostatic attraction overcomes the energy required for displace the hydration shell formed at the near surface, the electrostatic attraction enhances adsorption to the interface. (McUmber et al., 2015) However, the environmental conditions affect the efficiency of the electrical interactions. For example, ionic strength of the surrounding solution determines the Debye length of charged entities. The Debye length determines, how far the net electrostatic effect of a charge carrier influences. Higher the ionic strength, the shorter are the electrostatic interactions between charged entities. Therefore, in high ionic

strength surroundings, the electrostatic repulsion is hindered and the adsorption of charged proteins to similarly charged substrates is enhanced. Oppositely, the adsorption of charged proteins to opposite charged substrates is slowed down. The ionic strength of the surrounding solution, thus, influences the protein adsorption kinetics. (Rabe et al., 2015)

Similarly, as proteins tend to expose hydrophobic patches toward the hydrophobic surfaces, proteins expose oppositely charged regions to charged surfaces. This means that net positively or net negatively charged proteins can adsorb to a like-charged surfaces by unfolding the right charge towards the surface. This explains why adsorption can occur in conditions where the isoelectric point indicates hindered adsorption. (Rabe et al., 2015)

2.6 Controlling non-specific protein binding

In many applications, including biosensors, it is important to reduce non-specific protein adsorption. In order to reduce non-specific adsorption of biomolecules on the substrate, antifouling properties can be introduced to a substrate with protein resistant coatings and blocking agents.

Hydrophilic nature of a material is beneficial when non-specific protein adsorption needs to be minimized. However, typically surfaces are heterogeneous and blocking agents are usually required in order to eliminate non-specific binding completely. (Charles et al., 2009) For example, bovine serum albumin (BSA), polyethylene glycol (PEG), block and random copolymers and casein have been used to reduce non-specific protein adsorption (Dhruv, 2009; Vikholm-Lundin, 2005; Vuoriluoto et al., 2016).

In general, protein inert surfaces should be hydrophilic, should contain hydrogen bond acceptor groups and its total electric charge should be neutral (Ostuni et al., 2001). Biomimetic materials, proteins and synthetic polymers have been studied for antifouling applications. For example, phosphorycholines (PC) have been used in

polymers that are made to improve protein resistance. In biological systems, PC inhibits non-specific protein adsorption for example in cell membranes. The PC-based polymers contain hydrophilic phospholipid head group, and when water adsorbs on the head group, a low energy interface is produced and protein adsorption is decreased. In addition, PC has a neutral charge that reduces electrostatic attraction between proteins and surfaces. (Lewis, 2000)

In addition, bovine serum albumin (BSA) is a common protein-blocking agent used to reduce non-specific interactions (Dhruv, 2009). BSA is an albumin protein found in blood serum. It is a small, hard, stable and relatively non-reactive protein; hence, it is used as a protein-blocking agent. (Goodsell, 2013) BSA binds to sites, which may be available for non-specific binding and prevents further adsorption of proteins. In addition, it is a common blocker used to reduce non-specific hydrophobic binding. (Xiao and Isaacs, 2012)

Synthetic polymers, such as polyacrylates and PEG-based block copolymers have also been used to make antifouling coatings. PEG has been found to be effective polymer in reducing of non-specific adsorption. The non-specific protein resistance of PEG is mainly based on physical steric repulsion and hydration forces. Hydration of the flexible PEG chains causes repulsive interaction between the protein and the swollen polymer brush, thus, causing steric repulsion. In addition, the interaction between water and PEG is very strong and proteins cannot easily remove water molecules from the PEG chains. (Dhruv, 2009)

Modification of cellulose fibers is often required in order to prevent non-specific protein adsorption on cellulosic surfaces. Vuoriluoto et al. (2016) contolled hIgG adsorption on TEMPO-oxidized CNF by introducing block and random copolymers of poly(2-(dimethylamino)ethyl methacrylate) (PDMAEMA) and poly(oligo(ethylene glycol) methyl ether methacrylate) (POEGMA) to the surface (see Figure 10). Results showed that these copolymers were highly effective in preventing non-specific interactions with hIgG. (Vuoriluoto et al., 2016) It is believed that the cationic

PDMAEMA-block anchors the POEGMA onto CNF. The POEGMA in turn provides surface passivation towards non-specific hIgG adsorption, because it is highly hydrophilic and it takes an extended conformation in an aqueous media. (Vuoriluoto et al., 2015) In addition, Orelma et al. (2011) used carboxymethylated cellulose (CMC) to control non-specific protein binding on cellulose. It was hypothesized that CMC prevents non-specific protein interactions because it forms hydrogel-like layers. They studied adsorptions of BSA and hIgG on CMC-cellulose surfaces and found that the pH of the surroundings affected the protein binding significantly. The CMC decreased protein adsorption in basic conditions but in acidic conditions, adsorption was increased. (Orelma et al., 2011)

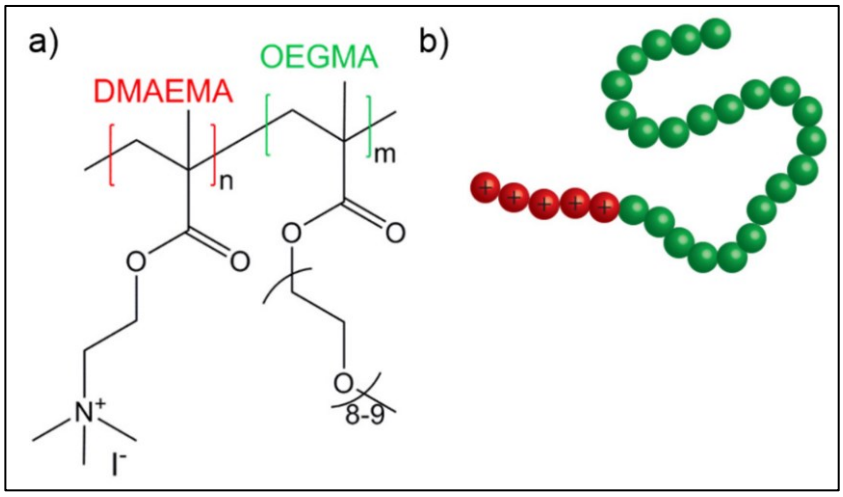

Figure 10. PDMAEMA-block-POEGMA copolymer: a) molecular structure and b) representative structure (Adapted from Vuoriluoto, 2017).

3. Experimental

3.1 Materials

3.1.1 Nanocellulose substrates

Two nanocellulose substrates with different thicknesses and transparencies were used in this study (see Figures 11 and 12). The 24 μm thick CNF films were provided by VTT Technical Research Centre of Finland and they were prepared with a pilot scale SutCo unit. These films were prepared from birch kraft pulp (treated twice in Masuko grinder and seven passes through a Microfluidics fluidizer). Another substrate, CNF nanopaper (thickness 50 μm), was prepared from 2 % CNF suspension of bleached sulfite birch fibers (six passes through a M110P fluidizer (Microfluidics corp.)) by vacuum filtration.

In addition, ultrathin model films of CNF were prepared for protein adsorption measurements. These films were made of 1.48 % CNF suspension of bleached sulfite birch fibers (12 passes through a M110P fluidizer (Microfluidics corp.)) by spin coating.

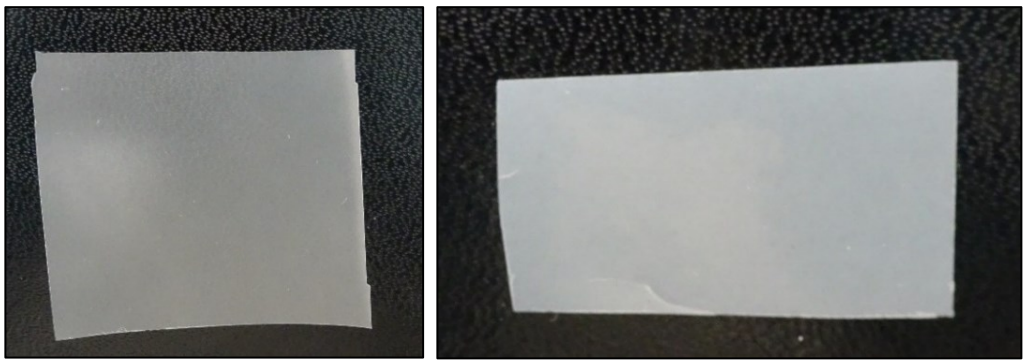

Figure 11. Used substrates: CNF film provided by VTT (left) and CNF nanopaper prepared by vacuum filtration (right).

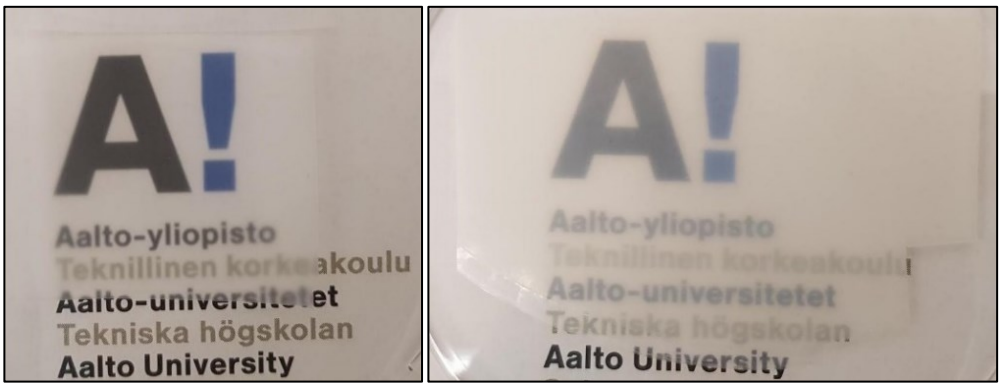

Figure 12. Transparencies of the used substrates: CNF film provided by VTT (left) was more transparent than the CNF nanopaper prepared by vacuum filtration (right).

3.1.2 Protein blocking agents

Protein blocking materials; bovine serum albumin (BSA) (≥98 %) and fibrinogen from human plasma (50-70 % protein) were purchased from Sigma-Aldrich.

Raft copolymerized poly(2-(dimethylamino)ethyl methacrylate) (PDMAEMA) and poly(oligo(ethylene glycol) methyl ether methacrylate) (POEGMA) protein blockers were studied (see Figure 10). PDMAEMA-block-POEGMA copolymers with sample codes of D33-EGMA-110, D33-EGMA-137 and D58-EGMA-118 were provided by Dr. Baolei Zhu (DWI, Leibniz-Institute for Interactive Materials Research, Germany). The sample codes are explained in the Table 1, in which information about the relation of the cationic PDMAEMA-block and the hydrophilic POEGMA-block is provided.

Table 1. PDMAEMA-block-POEGMA copolymer samples.

	Polymerization degree	
Sample code	DMAEMA	OEGMA
D33-EGMA-110	33	110
D33-EGMA-137	33	137
D58-EGMA-118	58	118

3.1.3 Other chemicals

Toluene (99.9 %) and acetone (100 %) were purchased from VWR Chemicals. Ethanol (99,5 %) from Altia. Ethyl acetate (≥99,5 %) and dimethyl sulfoxide (DMSO) (≥99,9 %) from Merck. Fluorescein 5(6)-isothiocyanate (FITC) (≥90 %) from Fluka. Poly(ethyleneimine) 30 % aqueous solution (PEI) (M_w 50 000-100 000) from Polysciences Inc.

All other chemicals were purchased from Sigma-Aldrich (Finland): trichlorovinylsilane (TCVS) (97 %), 1H,1H,2H,2H-perfluorodecanethiol (97 %), cysteamine hydrochloride (≥98 %), 2-mercaptoethanol (99 %), poly(ethylene glycol) methyl ether thiol (PEG-SH) (average M_n 6000), 1,2-dichloroethane (≥99.0 %) 4-pentynoic acid (95 %), 4-(dimethylamino)pyridine (DMAP) (≥99 %), N,N'-diisopropylcarbodiimide (DIC) (≥98.0 %), tetraethyl orthosilicate (TEOS) (99.99 %), octyltrichlorosilane (OCTS) (97 %), immunoglobulin G from human serum (hIgG) (≥95 %) and polystyrene (average M_w 192 000).

All water used in this study was purified with a Millipore Synergy UV unit (MilliQ).

3.2 Methods

3.2.1 Preparation of CNF nanopaper by vacuum filtration

The vacuum filtrated CNF films were prepared from CNF suspension. In the produced CNF nanopapers, the diameter was 150 mm and the thickness 50 μm. The film was prepared by first, diluting a 2 % CNF suspension to 0.1 %. This diluted suspension was agitated for 12 h. Then, sonication of the suspension was done for 15 min with 35 % amplitude. The CNF suspension was poured inside a filtering apparatus on top of filter papers. The system was closed and a vacuum was pumped to the system for 1.5 h. When all water was removed from the system, the filtration was completed. Next, hot pressing between metal plates and layers of different absorbing sheets was done at 100

°C and 1500 kg/cm^2 pressure for 50 min. Finally, the CNF nanopaper was cooled for 20 min.

3.2.2 Preparation of model CNF films by spin coating

Spin coating was used to produce ultrathin films of CNF to flat substrates. Spin coating is a deposition procedure, where a drop of coating material is applied on a static surface, which is then rotated at a high speed. The centrifugal force removes the excess fluid from the surface and only a thin layer of the solution remains on the surface. Then, the residual solvent evaporates forming a thin layer of the coated material. (Hall et al., 1998)

In this work, ultrathin films of CNF were prepared by spin coating (Model WS-650SX-6NPP, Laurell Technologies). Prior spin coating, silicon dioxide or gold substrate surfaces were treated with polyethyleneimine (PEI). PEI was used to create positive charge on the surface, which improved the deposition of negatively charged fibrils on the substrate. First, the silicon dioxide or gold substrates were cleaned with nitrogen gas and placed in an ozonizer for 15 min. A thin layer of PEI was adsorbed on the substrates by placing cleaned substrates in 0.33 % PEI solution for 60 min. Then, 0.148 % CNF suspension was prepared by diluting stock CNF with MilliQ-water. This suspension was mixed by hand and defibrillation was done with a tip sonicator for 10 min (amplitude 25 %). The ultrasonicated CNF solution was centrifuged at 10 400 rpm for 45 min. Then, 5 ml of the supernatant was collected and used for spin coating CNF thin films at 3000 rpm with 90 s spinning time. Finally, spin coated substrates were cured in an 80 °C oven for 10 min.

3.2.3 Photo-induced click reactions on CNF substrates

Hydrophilic and hydrophobic CNF substrates were prepared with click chemistry. Prior click reactions, surface modifications of CNF substrates needed to be done so that the

reactive functional groups were obtained on the surfaces. Functionalization was done following the methods by Guo et al. (2016 and 2018). In order to introduce vinyl groups to CNF substrates, functional silicone nanofilaments were grown on CNF substrates. First, a piece of CNF substrate was dried in a vacuum oven for 2 h. Then, 8 µl of MilliQ-water was added to 40 ml of dried toluene in a falcon tube and sonication of this solution was done at 50 °C for 40 min. Next, 50 µl of trichlorovinylsilane (TCVS) was added to the mixture and the sample piece was placed horizontally inside the falcon tube. After reaction time of 24 h, the substrate was washed with ethanol and dried with nitrogen gas. Functional CNF substrates with alkyl groups were also prepared. First, vacuum oven dried CNF substrates were immersed in 50 ml of dichloroethane. Then, 150 mg of 4-pentynoic acid, 20 mg of 4-(dimethylamino)pyridine (DMAP) and 500 µl of N,N'-diisopropylcarbodiimide (DIC) were added. The reaction was left to happen for 1.5-2 days under stirring. Then, the substrates were washed with acetone and dried with nitrogen gas.

Next, photo-induced thiol-ene and thiol-yne click reactions were done in order to couple hydrophobic and hydrophilic substances to the CNF surface. Hydrophilic substrates were made with a cysteamine hydrochloride solution (20 w%, in ethanol) or 2-mercaptoethanol solution (20 vol% in ethanol). One piece of a substrate with vinyl or alkyl groups was placed on a glass slide, wetted with cysteamine hydrochloride (or 2-mercaptoethanol) and covered with a quartz slide. Exposure to UV light (254 nm, 10 $mW \cdot cm^{-2}$) was done for 5 min. After UV exposure, the substrate was washed with ethanol in the dark and dried with nitrogen gas. The hydrophobic substrates were in turn made by using 1H,1H,2H,2H-perfluorodecanethiol solution (20 vol%, in ethyl acetate). Substrate with vinyl or alkyl groups was placed on a glass slide, wetted with 1H,1H,2H,2H-perfluorodecanethiol and covered with a quartz slide. Exposure to UV light (254 nm, 10 $mW \cdot cm^{-2}$) was done again for 5 min. After this, the substrate was washed with acetone in the dark and dried with nitrogen gas.

In addition, another hydrophilic CNF substrate was prepared by introducing poly(ethylene glycol) methyl ether thiol (PEG-SH) to CNF substrates with alkyl

groups. First, PEG-SH was adsorbed on reactive CNF substrate for 15 min. Then, UV activation (254 nm, 10 mW·cm^{-2}) was done for 60 min. Finally, the substrate was washed in ethanol.

3.2.4 Patterning of CNF substrates

Hydrophobic-hydrophilic patterns were done on CNF substrates in order to produce fluidic channels. In this work, simple straight 3x20 mm channels were produced with two methods by using click chemistry and polymer patterning. Figure 13 presents the structures of the prepared patterns. The pattern A was made with click chemistry or by polymer patterning. The pattern B was made by polymer patterning only. In addition, in order to practice the click chemistry method, also simple hydrophilic rectangle shapes with hydrophobic borders were produced (see Figure 14).

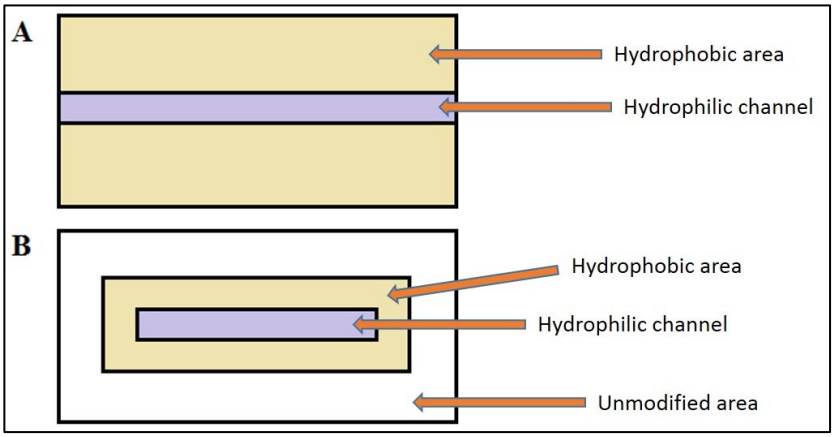

Figure 13. Fluidic channels patterned on CNF substrates.

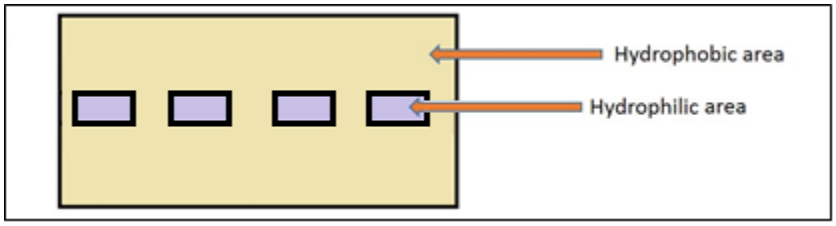

Figure 14. Hydrophilic-hydrophobic pattern on CNF substrates.

First, hydrophobic-hydrophilic patterns were done by using click chemistry with the methods by Guo et al. (2016 and 2018). A schematic illustration of these methods can be seen in the Figure 15. Before patterning, CNF substrates with reactive functional groups on the surface were prepared with the same methods explained in the chapter 3.2.3. Then, a substrate with the vinyl or alkyl groups was placed on a glass slide, wetted with cysteamine hydrochloride solution (20 w%, in ethanol) and covered with a photomask. Exposure to UV light (254 nm, 10 $mW \cdot cm^{-2}$) was done for 20 min. After UV exposure, the substrate was washed completely with ethanol in the dark and dried with nitrogen gas. This step created the hydrophilic channel on the substrate. Then, 1H,1H,2H,2H-perfluorodecanethiol solution (20 vol%, in ethyl acetate) was used to make the hydrophobic area. The substrate was placed on a glass slide, wetted with 1H,1H,2H,2H-perfluorodecanethiol and covered with a quartz slide. Exposure to UV light (254 nm, 10 $mW \cdot cm^{-2}$) was done again for 2 min. After this, the substrate was washed completely with acetone in the dark and dried with nitrogen gas.

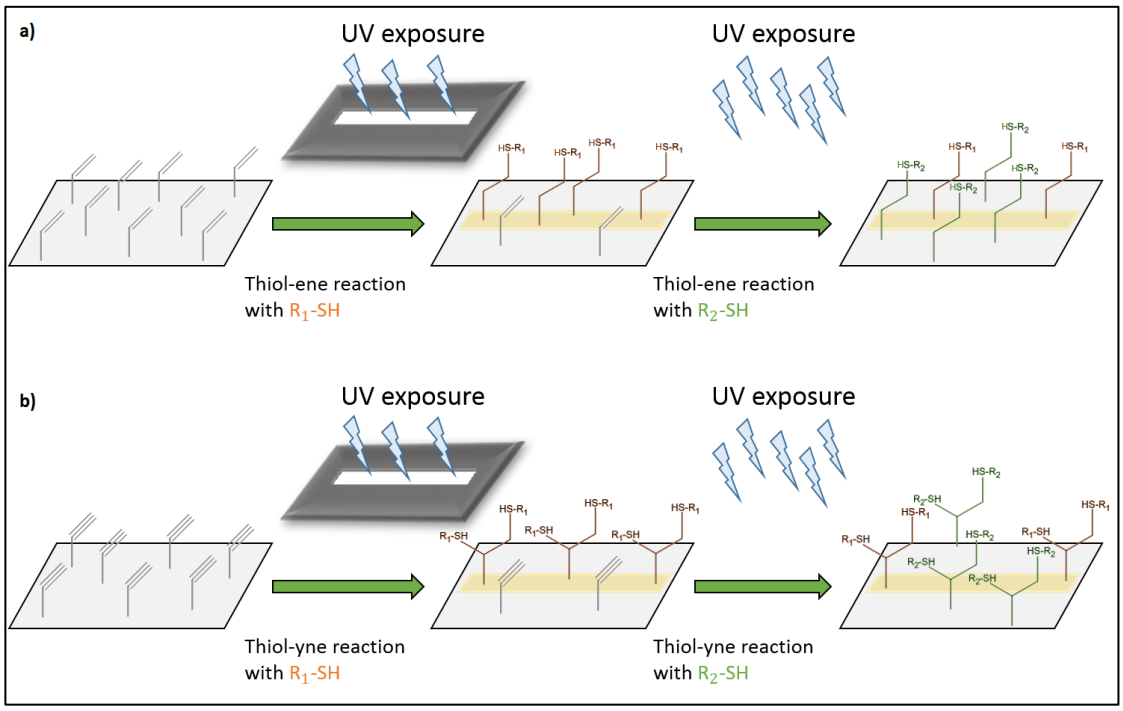

Figure 15. Schematic illustration of patterning with a) thiol-ene reactions and b) thiol-yne reactions. In this work, R_1-SH was cysteamine hydrochloride and R_2-SH was 1H,1H,2H,2H-perfluorodecanethiol (Adapted from Guo et al., 2016 and 2018).

The second method used to create hydrophobic-hydrophilic patterns was patterning with hydrophobic polymer solutions. In this method, fluidic channels were created by using solutions of polystyrene in toluene and p-xylene. First, a 10 g/l polystyrene solution was done by dissolving polystyrene into toluene. Then, this solution was sprayed with a pipet on CNF substrates to create hydrophobic edges of the 3x20 mm channels. A glass plate was used to make straight channels on substrates. Also, in order to improve the flow in the channels, the backside of the sample was treated with the polystyrene solution. In addition, inkjet printing of a polystyrene solution was also tested. 5 w% polystyrene solution (in p-xylene, with 0.1 w% Sudan Red G color) was printed on substrates with a Dimatix Materials Printer (DMP-2800, Fujifilm) to create rectangle shaped channels. 3x20 mm channels with 1 mm and 2 mm edges were printed

with drop spacing of 30 μm, 40 μm and 50 μm. In addition, printing of two layers was tested.

3.2.5 Controlling non-specific protein adsorption

The protein attachment on CNF substrates were studied with surface-sensitive techniques, including SPR and QCM-D. The blocking efficiencies of different blocking agents were studied. Human immunoglobulin G (hIgG) was used as a model protein in the tests of non-specific adsorption. The adsorption tests were performed at physiological pH 7.4. First, the non-specific adsorption was studied on model CNF films prepared by spin coating and later adsorption tests were performed on CNF films and studied with CLSM.

Quartz Crystal Microbalance with Dissipation (QCM-D)

Quartz Crystal Microbalance with Dissipation monitoring (QCM-D) was used to measure interactions between proteins and CNF surfaces. QCM-D is a technique for analyzing nanoscale surface phenomena. In this method, the samples are deposited on specific QCM sensors. The QCM sensor comprises a thin quartz disc that is sandwiched in between a pair of electrodes. This crystal experiences piezoelectric effect when alternating voltage is applied across the sensor electrodes. This effect causes oscillation of the sensor at its resonance frequency, which depends on the total oscillating mass. (Höök et al., 1998) The mass changes are observed with the changing frequency. For example, when mass is adsorbed on the sensor, the frequency decreases. If the adsorbed layer is thin and rigid, the frequency decrease is proportional to the mass of the layer. QCM-D can be used to observe the mass changes and the kinetics of structural changes simultaneously. QCM-D measures the frequency shift and the damping of the freely oscillating sensor. (Dixon, 2008) The viscoelastic properties of the adsorbed layer can be analyzed with energy dissipation. The decaying of the oscillation amplitude is dependent on the softness of the adsorbed layer and it is observed when the voltage of

the system is switched off. Rigid layers have longer decaying times and lower dissipation values but soft layers do not follow the sensor oscillation perfectly. The deformation of viscous layers causes friction, energy loss and therefore higher dissipation values. (Vuoriluoto et al., 2017) The Figure 16 shows, how rigid and soft materials affect the frequency and dissipation signals of QCM-D.

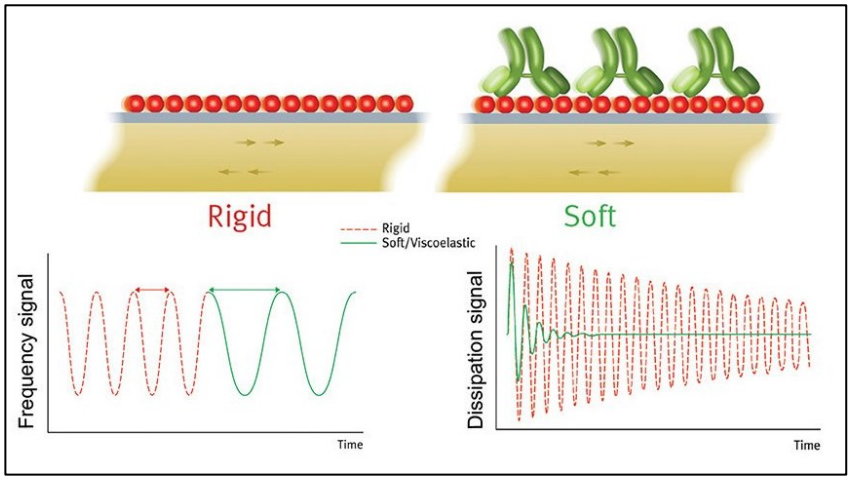

Figure 16. Effects of material rigidity on the frequency and dissipation signals. On left: the frequency changes of the oscillating sensor crystal when the mass is increased by adsorbing a rigid (red) and a soft (green) molecular layer. On right: the difference in dissipation signal generated by a rigid (red) and soft (green) molecular layer on the sensor crystal. (Anonymous, 2018).

In this work, the QCM-D measurements were conducted using a Q-Sense E4 instrument. The frequency and dissipation changes were measured at a fundamental resonance frequency of 5 MHz and its overtones. The 3^{rd}, 5^{th}, 7^{th}, 9^{th}, 11^{th} and 13^{th} overtones were used. Before measurements, the CNF films were prepared with spin coating (see chapter 3.2.2) and these films were stabilized in a phosphate buffer overnight. Samples were placed inside the QCM-D measurement chambers and the films were stabilized in a continuous flow of phosphate buffer (pH 7.4) until a stable baseline was observed. Adsorption of hIgG (0.1 g/l at pH 7.4) was tested on CNF and

blocked CNF substrates. Blocking efficiency of BSA, fibrinogen and copolymers (D33-EGMA-137 and D58-EGMA-118) were studied. The concentrations of each blocking agent solutions were 0.1 g/l and the adsorption was measured at pH 7.4. All QCM-D measurements were performed at least twice at 23 °C under constant flow of 100 µl/min.

The masses of the adsorbed layers were determined with the Sauerbrey equation (equation 1):

$$\Delta m = -C_{QCM-D}\frac{\Delta f}{n} \quad (1)$$

where Δm is the adsorbed mass, C_{QCM-D} is 17,7 $\frac{ng}{Hz \times cm^2}$ for 5 MHz crystal (provided by the manufacturer), Δf is the change in frequency and n is the overtone number. (Sauerbrey, 1959; Vuoriluoto et al., 2017)

Noteworthy, the Sauerbrey equation underestimates the adsorbed mass if the layer is not uniformly spread on the crystal or the adsorbed layer is not rigid, the adsorbed mass is much larger than the mass of the crystal (Höök et al., 1998). Therefore, the Voigt viscoelastic model (Q-Tools software, version 2.1 Q-Sense) was used to estimate the mass changes. The fluid density was approximated to be 1000 kg/m^3, the fluid viscosity 0.001 m^3/kg and the density of the adsorbed layer 1200 kg/m^3 (Vuoriluoto et al., 2017).

Surface Plasmon Resonance (SPR)

Surface Plasmon Resonance (SPR) was used to monitor protein adsorption onto CNF substrates. SPR is an optical method for the analysis of biomolecular interactions. It is based on the surface plasmon resonance phenomenon. (Schasfoort, 2017) For the measurement, samples are deposited on specific SPR sensors. The SPR sensor has a thin metal coating, for example made of gold, on top of a transparent optical substrate such as glass. When a stream of light passes from a high refractive index material (for example glass) into a low refractive index material (for example water), a fraction of

light is reflected from the interface. Total internal reflection occurs when the angle of the light beam is greater than the critical angle and the light is completely reflected. When the glass substrate is coated with a gold film (or some other noble metal), the reflection is not total, but instead, some of the light is coupled with the electrons of the metal film. Photons from the light interact with the free electrons of the gold film, causing resonance of the electrons and a propagating surface plasmon wave is created. This coupling of light consumes energy, and thus, a decrease in reflectivity and a drop in the measured intensity is observed. The angle, at which the intensity of the reflected light reaches the minimum value, is called as the surface plasmon resonance angle. The SPR instrument detects small changes of the surface plasmon resonance angle. The resonant frequency of the surface plasmon wave and, in consequence, the surface plasmon resonance angle depend on the refractive index of the medium. For example, proteins have higher refractive indexes than aqueous buffers. Thus, when proteins adsorb on the SPR sensor surface, an increase in refractive index occurs and the surface plasmon resonance angle changes. (Van Der Merwe, 2001) The Figure 17 presents a schematic illustration of the SPR apparatus.

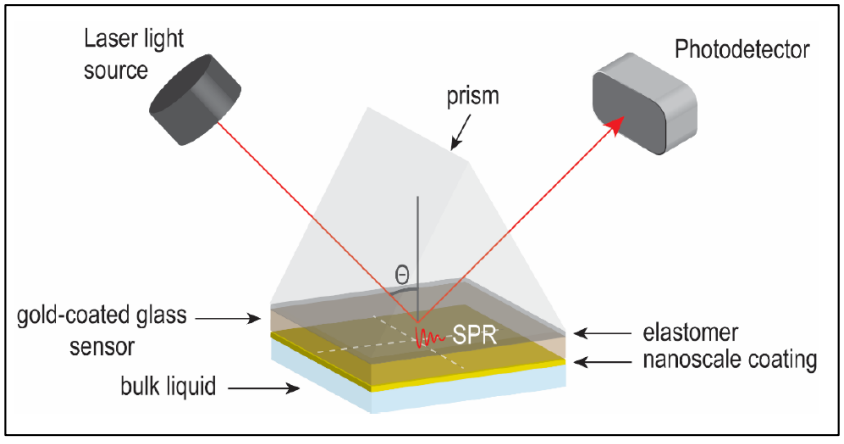

Figure 17. The working mechanism of SPR (Vuoriluoto, 2017).

The SPR measurements in this work were performed with a multiparametric SPR instrument (MP-SPR Model Navi 200, Oy BioNavis Ltd.). Before measurements, the CNF films were prepared with spin coating (see chapter 3.2.2) and these films were stabilized in a phosphate buffer overnight. Samples were placed inside the SPR module and the films were stabilized in a continuous flow of phosphate buffer (pH 7.4) until a stable baseline was observed. Adsorptions of hIgG (0.1 g/l at pH 7.4) were tested on CNF and hydrophilized CNF surfaces. The hydrophilized CNF substrates were obtained by cysteamine hydrochloride, 2-mercaptoethanol or PEG-SH treatments of CNF substrates with thiol-ene and thiol-yne click reactions (see chapter 3.2.3). In addition, hIgG was adsorbed onto blocked CNF surfaces. Protein blocking efficiency of BSA, fibrinogen and copolymers (D33-EGMA-110 and D33-EGMA-137) were studied (see Table 2). The blocking agents were first adsorbed on CNF. Then, washing with a buffer was done and the adsorption of hIgG (0.1 g/l at pH 7.4) followed. All SPR measurements were performed at least twice at 20 °C under constant flow of 100 µl/min.

Table 2. Tested blocking agents.

Blocking agent	**Concentration**	**Preparation procedure**
BSA	0.1 g/l	Dissolution in phosphate buffer (pH 7.4)
Fibrinogen	0.1 g/l	Dissolution in phosphate buffer (pH 7.4)
D33-EGMA-110 (1)	0.1 g/l	Dissolution in phosphate buffer (pH 7.4)
D33-EGMA-137 (1)	0.1 g/l	Dissolution in phosphate buffer (pH 7.4)
D33-EGMA-110 (2)	0.5 g/l	Dissolution in phosphate buffer (pH 7.4), sonication
D33-EGMA-137 (2)	0.5 g/l	Dissolution in phosphate buffer (pH 7.4), sonication

The thickness of the adsorbed layer was determined with an equation 2:

$$d = \frac{l_d}{2} \frac{\Delta_{angle}}{m(n_a - n_0)} \qquad (2)$$

where d is the thickness, l_d is the characteristic evanescent electromagnetic field decay length (estimated as 0.37 of the light wavelength 240 nm), Δ_{angle} is the change in the SPR angle, m is the sensitivity factor for the sensor (109.94 °/RIU, obtained after calibration), n_0 is the refractive index of the bulk solution (1.334 RIU) and n_a is the refractive index of the adsorbed substance (for proteins 1.57). (Jung et al., 1998; Vuoriluoto et al., 2017)

The mass of the adsorbed layer per unit area was determined with an equation 3:

$$\Delta m = d \times \rho \quad (3)$$

where Δm is the adsorbed mass, d is the thickness and ρ is the packing density of the proteins (estimated to be 1.3 g/cm^3). (Campbell and Kim, 2007; Vuoriluoto et al. 2017)

Fluorescent hIgG adsorption tests on CNF films

Antifouling properties were introduced to real CNF films and non-specific protein adsorption tests were performed by using fluorescent-stained hIgG (hIgG-FITC) and confocal laser scanning microscopy (CLSM). CNF films were blocked with BSA (0.1 g/l pH 7.4) and D33-EGMA-137 copolymer (0.5 g/l, pH 7.4) by adsorbing these blockers for 20 min onto the CNF films. Then, washing with a phosphate buffer (pH 7.4) was done for 10 min. Next, fluorescent hIgG-FITC proteins (100 µg/ml) were introduced to unmodified CNF films and blocked CNF films. These films were imaged with CLSM. In addition, a reference sample, unmodified CNF film without adsorbed hIgG-FITC, was also imaged. The methods of the preparation of hIgG-FITC and CLSM are described in the chapter 3.2.7.

3.2.6 Surface flow tests

The flow efficiencies of prepared fluidic channels were tested by dropping 30 µl of water onto the channels. The drop was applied few millimeters from the edge of the

channel and the fluid was colored with a green food coloring so that the flow was easier to observe. The Figure 18 presents the schematic illustration of the flow test. The flowing of the fluid was recorded with a camera (Sony DSC-HX90V) attached 15 cm above the channel. A 2 min recording time was used. Advancing of the frontline of the flowing fluid was analyzed from the frames of the recorded video.

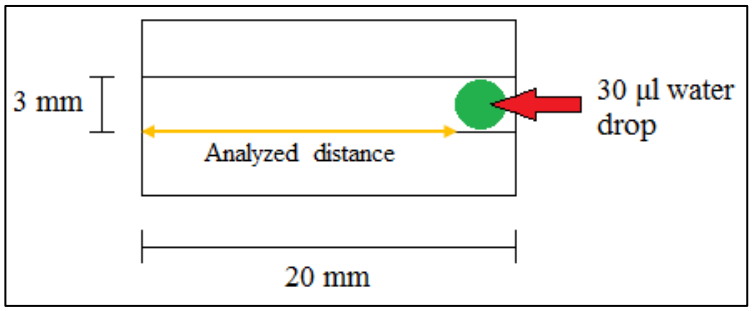

Figure 18. A schematic illustration of the flow test.

In addition, flow tests with fluids containing fluorescent hIgG-FITC were also performed. These tests were done in order to see how much hIgG adsorbs onto the channels. The hIgG-FITC solution was introduced to unmodified channel, BSA- and D33-EGMA-137 copolymer-blocked channels and to a channel with a hydrophobic line in the middle. The tested channels were twice printed channels (40 µm drop spacing) with 2 mm polystyrene edges. The blocked channels were prepared by adsorbing BSA (0.1 g/l pH 7.4) and D33-EGMA-137 copolymer (0.5 g/l, pH 7.4) onto channels for 20 min. Then, washing with a phosphate buffer (pH 7.4) was done for 10 min. The channel with a hydrophobic line was prepared by placing a drop of a hydrophobic solution onto the middle of the channel with a pipette. The hydrophobic solution was done by mixing 6 ml of tetraethyl orthosilicate (TEOS), 3ml of octyltrichlorosilane (OCTS), 73 ml of ethanol, 12.4 ml of MilliQ-water and 0.5 ml of 1 M hydrochloric acid at room temperature for 24 h.

The flow tests were performed by dropping a 30 µl drop of hIgG-FITC solution (100 µg/ml) onto the channels. The drop was applied few millimeters from the edge of the channels. These channels with hIgG-FITC were imaged with confocal laser scanning microscopy (CLSM), described in the next chapter 3.2.7.

3.2.7 Additional methods

Atomic Force Microscopy (AFM)

Atomic Force Microscopy (AFM) was used to study the morphology of the different CNF substrates. AFM is a high-resolution scanning probe microscopy technique (SPM). In the AFM technique, the sample is scanned by a sharp probe connected to a flexible cantilever. (Binnig et al., 1986) The movement of the tip is followed by a quadrant photodiode that detects the reflected laser beam from the cantilever. When the probe scans the sample surface either in direct or close contact, the forces between probe and surface cause deflection of the cantilever. The interactions of the probe with the surface leads to a change in reflected laser position. Thus, the laser beam is detected at different points of the quadrant photodiode with respect to the surface topography. This way an image of the surface is obtained. The AFM can be used in tapping, contact, or non-contact modes. (Eaton and West, 2010) The tapping mode is appropriate for the soft materials like nanocellulose (Magnov, 1997; Vuoriluoto, 2017). The tapping mode is based on the oscillation of the probe at constant frequency. The amplitude of the probe changes when the tip comes close to the surface and the interaction forces affects the cantilever. The amplitude is measured and kept constant by controlling the height of the cantilever. (Eaton and West, 2010)

In this work, MultiMode 8 Scanning Probe Microscope (Bruker AXS Inc.) was used to analyze the surface topography of the CNF substrates. CNF films and modified CNF films were imaged. In addition, the effects of protein adsorption on the topographical characteristics of CNF substrates were also studied. Tapping mode in air and silicon cantilevers (NSC15/AIBS, MicroMasch) were used to scan 5x5 μm^2 surface areas.

Three different spots on each sample were imaged. In addition, flattening was used in the image processing.

Scanning Electron Microscopy (SEM)

Scanning Electron Microscope (SEM) was used to image different CNF samples. SEM is an electron microscope that produces a magnified image of a sample surface with a focused beam of electrons. SEM consists of an electron source, electromagnetic lenses and an electron detector. The electron source accelerates an electron beam, which is focused on the sample by the lenses. When the electron beam hits the sample, interactions of the electron beam and atoms of the sample take place. Excitation of atoms causes them to emit secondary electrons which can be collected by the electron detector. The variations of the sample surface topography affect, how many electrons are emitted. Thus, a surface topography image can be produced by scanning the electron beam and detecting the variation of the number of emitted electrons. Before imaging, non-conductive samples, such as cellulose, must be coated with an ultrathin coating of electrically conductive material. This is because non-conductive materials collect charge when scanned by the electron beam and this causes scanning faults. (Stokes, 2008)

SEM images of the unmodified and modified CNF films were taken with a field emission microscope (Zeiss Sigma VP) at 2 kV. Images of the unmodified CNF films, alkyne-modified CNF films, thiol-yne modified CNF films and polystyrene coated CNF films were taken. Several magnification images were taken for each sample. Before imaging, the samples were sputtered with palladium or silver alloy using a glow discharge apparatus (Emitech K100X) at 30 mA for 1-2 min depending on the thickness of the sample.

Water Contact Angle measurements

The wettability of different CNF substrates was studied by measuring the water contact angle (WCA) of the samples. The WCA of a surface can be measured with an optical contact angle meter. The higher the contact angle of a surface, the higher the hydrophobicity of the surface. Surfaces with a contact angle less than 90° are considered as hydrophilic and surfaces with an angle higher than 90° are considered as hydrophobic. (Nosonovsky and Bhushan, 2007) The adhesion forces between the surface and the fluid cause wetting of a surface. The completion of the wetting depends on the structure of the surface and the fluid tension of the droplet. (Yuan and Lee, 2013) When the surface is hydrophilic, the adhesion forces between water and the surface are greater than the cohesive forces in the bulk liquid water; therefore, the liquid spreads evenly over the surface. Oppositely, in hydrophobic surfaces, water droplets are formed on the surface because the cohesive forces in bulk water are greater than the adhesion forces between water and the surface. (Begat et al., 2004) The WCA measurement device uses drop shape analysis for determining the static or dynamic contact angles on different substrates. The contact angles can be obtained after fitting the images with methods such as curve fitting the drop profile to Young-Laplace equation. (Pesonen-Leinonen et al., 2006; Roero, 2006)

The wetting properties of the CNF films and surface modified CNF films were studied with CAM200 optical contact angle meter (KSV INSTRUMENTS Ltd.). 7 µl of water was dropped on the sample surfaces for 20 s and the contact angle measurement was performed. The Young-Laplace drop shape analysis was used to calculate the contact angles.

Preparation of fluorescent hIgG-FITC

To modify human immunoglobulin G (hIgG) antibodies with a fluorescent probe, a general protocol for immunoglobulin modification by Hermanson (2008) was used with few alterations. First, a 2 mg/ml protein solution was prepared in 0.1 M sodium

carbonate buffer (pH 9.0). Then, in a darkened lab, fluorescein 5(6)-isothiocyanate (FITC) was dissolved in dry DMSO in a glass bottle to obtain a 1 mg/ml FITC solution. This solution was protected from light by wrapping the glass bottle in aluminum foil. Next, 100 µl of the FITC solution was slowly added to each ml of hIgG solution in the darkened lab. The protein solution was gently mixed while the FITC solution was added. The reaction was left to happen at 4 °C in the dark for over 8 hours.

To purify the obtained hIgG-FITC solution from unreacted FITC molecules, the solution was centrifuged at 4000 rpm for 30 min by using centrifugal filter units (Amicon Ultra-15, MWCO 30 kDa). The centrifugation step was repeated four times.

Confocal Laser Scanning Microscopy (CLSM)

Confocal laser scanning microscope (CLSM) was used to image fluorescent CNF samples. CLSM is a type of a fluorescence microscope. This microscope consists of magnifying lenses, multiple dichroic mirrors and filters. In addition, two pinhole apertures are positioned at confocal positions. A laser beam is positioned on a sample and the first filter selects the light, which excites the fluorophores of the sample. The laser beam is focused by the first pinhole on only a small part of the sample. When the fluorophores in the sample are illuminated with the proper wavelength, they emit a fluorescent light of another wavelength. The dichroic mirror and a second filter select only this fluorescent light emitted by the sample. The second pinhole positioned in the focal plane selects only the light coming from the targeted point of the sample. The surface of the sample is scanned by moving the sample or the laser beam. The image of the sample is reconstructed by collecting the emitted photons from the fluorophores of the sample. (Guthoff et al., 2006)

In this work, CLSM images were taken of the CNF film and channel samples with a laser scanning spectral confocal microscope (Leica TCS SP2). Images were recorded using 488 nm laser wavelength and 727 V laser with constant imaging conditions. The images were taken of untreated and blocked CNF samples that were exposed to FITC-

stained human IgG (hIgG-FITC). BSA and D33-EGMA-137 copolymer blocking agents were used. In addition, reference samples without adsorbed hIgG-FITC were imaged. Before measurement, hIgG-FITC was adsorbed on the samples for 20 min. After adsorption, washing with a sodium carbonate buffer (pH 9) was done.

Digital microscopy imaging

A digital microscope was used to study the printing quality of the polystyrene printed fluidic channels on CNF films. The digital microscope combines a traditional optical microscope and a digital camera to output a digital image to a computer monitor. The optical microscope uses a system of lenses and visible light in order to magnify objects. The digital microscopy can be used to improve resolution and sample contrast. It also allows a wider analysis of a microscope image, for example the measurements of distances can be obtained with the digital microscopy.

Microscopy images of the printed channels were taken with a high definition digital microscope camera (Leica ICC50 HD Camera). Magnification of 300X was used.

4. Results and discussion

4.1 Patterning with click chemistry

The thiol-ene and thiol-yne patterns were first practiced by producing simple rectangle shapes on CNF films. These patterns can be seen in the Figure 19. The hydrophilic rectangle shapes can be distinguished from the CNF films, but the patterns on CNF nanopaper could not be seen with the naked eye. Thiol-yne click reactions produced patterns with higher consistency and the edges of the patterns were clearer if compared to the patterns produced with thiol-ene reactions.

Figure 19. Hydrophilic-hydrophobic patterns on CNF substrates. From left to right: thiol-yne pattern on CNF film, thiol-ene pattern on CNF film and thiol-yne pattern on CNF nanopaper.

The wetting properties of unmodified CNF, hydrophilized CNF, hydrophobized CNF and patterned CNF substrates were studied by water contact angle measurements. The Figure 20 presents the thiol-ene reaction results and the Figure 21 the thiol-yne reaction results. The measurements of the unmodified substrates showed that both CNF film and nanopaper were hydrophilic materials. However, the water contact angle (WCA) of the CNF film was 31° lower than the WCA of the CNF nanopaper. This difference in hydrophilicity can be explained with the fact that the CNF film was smoother than the nanopaper and contained sorbitol, which was used as a plasticizer. To be exact, hydrophobicity is known to be enhanced with surface roughness (Wenzel, 1936; Cassie

and Baxter, 1944). In addition, it is also known that the hydrophobicity is increased when the surface energy of the sample is minimized (Jin et al., 2011). Thus, when surface modifications were done, changes in WCAs could be observed due to changes in the surface roughness and surface energies. In these modifications, the introduction of vinyl and alkyl groups to the CNF surfaces increased nanoscale roughness and decreased the amount of exposed hydroxyl groups that could interact with water. In addition, clicking of the different thiol compounds changed the surface energies of the samples so that adhesion forces between the surface and water were changed, therefore, an increased hydrophobicity or hydrophilicity could be observed.

	CNF Nanofilm	Nanopaper
Unmodified	22° 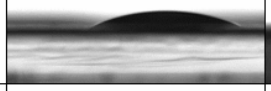	53° 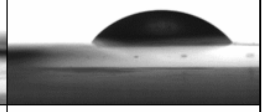
Hydrophobized	121° 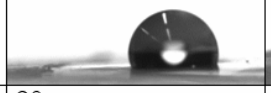	122° 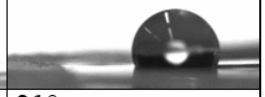
Hydrophilized	9° 	21° 
Patterning, hydrophobic parts	119° 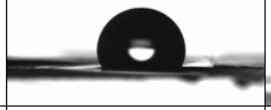	120° 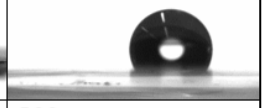
Patterning, hydrophilic parts	31° 	50° 

Figure 20. The WCA results of the unmodified substrates and thiol-ene click modified substrates.

	CNF Nanofilm	Nanopaper
Unmodified	22° 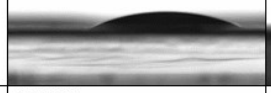	53° 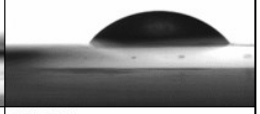
Hydrophobized	122° 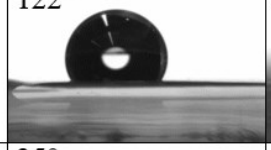	113° 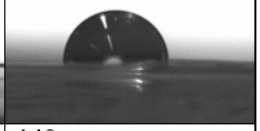
Hydrophilized	35° 	44° 
Patterning, hydrophobic parts	122° 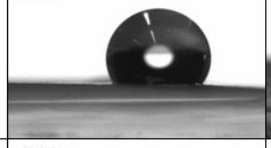	102° 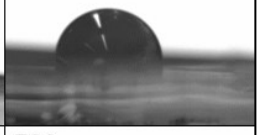
Patterning, hydrophilic parts	44° 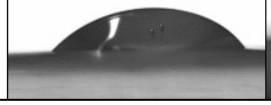	72° 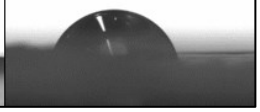

Figure 21. The WCA results of the unmodified substrates and thiol-yne click modified substrates.

In this work, 1H,1H,2H,2H-perfluorodecanethiol was used as the hydrophobic thiol compound. The hydrophobizations with this fluoroalkyl molecule by thiol-ene reactions increased the WCAs of the both CNF substrates to above 120°. Therefore, a significant increase in WCA was observed after hydrophobizations and the water droplets seemed to show the Wenzel's pinning state. The hydrophobizations with the same chemical by thiol-yne reactions increased the WCA up to 122° in the CNF film but the WCA of the nanopaper was smaller. The reason why nanopaper obtained lower hydrophobicity is unclear. One would expect that the WCA would be higher in the nanopaper because the initial roughness was higher than the roughness of the other substrate.

The hydrophilic thiol compound used in this work was cysteamine hydrochloride. The thiol-ene click reactions with cysteamine hydrochloride improved the hydrophilicities of both CNF substrates. The WCAs decreased to 9° in the CNF film and to 21° in the nanopaper. This means that the cysteamine hydrochloride modified CNF film was superhydrophilic. However, similar results were not obtained with thiol-yne click reactions. The hydrophilizations with cysteamine hydrochloride by thiol-yne reactions created hydrophilic surfaces but the WCAs were higher than the ones obtained with the thiol-ene click reactions. In fact, the WCA of the thiol-yne hydrophilized CNF film was even 13° higher than the WCA of the unmodified film. It may be that the introduction of alkyl groups created higher roughness than the introduction of vinyl groups and the cysteamine hydrochloride was not hydrophilic enough to overcome the roughness effect of the alkyl groups. On the other hand, the obtained thiol-yne results were similar as previously reported results by Guo et al. (2018). Better hydrophilicity could probably be achieved by introducing carboxyl groups to the surface by using for example 3-mercaptopropionic acid instead of cysteamine hydrochloride (Guo et al., 2018).

Then, the WCA results of the patterned films showed varying success. The hydrophobic parts of the pattern had similar contact angles than the just hydrophobized films (around 120°). The exception was the hydrophobic pattern part in the CNF nanopaper done by thiol-yne reaction. The WCA of this sample was only 102°. The reason for this could be that some of the unreacted hydrophilic thiol compound remained on the nanopaper even after washing and reacted in the second UV treatment. In addition, the hydrophilic parts of the patterns done with both thiol-ene and thiol-yne reactions did not reach equally good hydrophilicity than the just hydrophilized films. It is possible that some of the vinyl/alkyl groups on the substrate surface did not react with the cysteamine hydrochloride on the desired area, but instead, these groups reacted with the hydrophobic thiol in the second UV treatment. In addition, it can be that some of the unreacted 1H,1H,2H,2H-perfluorodecanethiol stayed on the film even after washing and in this way increased the WCAs of the hydrophilic parts. Noteworthy,

during the experiments it was noted that longer washing times improved the patterning results, which indicates that at least the latter explanation could be the reason for the problem.

Despite that the thiol-ene reactions created areas with better hydrophilicity, the production of patterns by thiol-yne reaction was more consistent. Furthermore, both click chemistry modifications were quite complex and time consuming, but the thiol-yne reaction was simpler, so that is why the thiol-yne reaction was chosen for the production of the fluidic channels. In addition, because better results were obtained by using the CNF films, these substrates were chosen for further investigation. An image of a fluidic channel made with thiol-yne click reaction on CNF film is presented in the Figure 22. It can be seen that there are some defects in the pattern but 3x20 mm channels with hydrophobic and hydrophilic areas were successfully produced with thiol-yne click reactions.

Figure 22. 3x20 mm hydrophobic-hydrophilic channel produced with thiol-yne click reactions onto CNF film.

The hydrophilic-hydrophobic patterns on CNF films were further characterized with SEM and AFM imaging methods. The SEM images of the unmodified and modified CNF films can be seen in the Figure 23. It can be seen that the surface of the unmodified CNF film was very smooth (Figure 23.a). The CNF fibers were packed tightly and there were no pores. However, after modifications, the surface topography of the films was changed. From the Figures 23.c and 23.d, it can be seen that the alkyne-modified film

contained some aggregations and some darker spots formed around the fibers. Therefore, the roughness of the sample seemed to be higher due to the introduced alkyl groups. The Figures 23.e and 23.f present the surface images of the hydrophilic sample. In this sample, the CNF fibers can be seen more clearly, because higher amount of darker spots were found around the fibers. Then, in the Figures 23.g and 23.h one can see the surface of the hydrophobic sample. The hydrophobic sample differed from the other samples significantly. One can see that the hydrophobic thiol compound covered the surface well and the roughness of the substrate was increased. In addition, after hydrophobization, the fibers can be seen only with the higher magnification (see Figure 23.h). Noteworthy, not all effects to the surface topography caused by modifications of the samples can be seen with SEM. That is why also AFM imaging was performed.

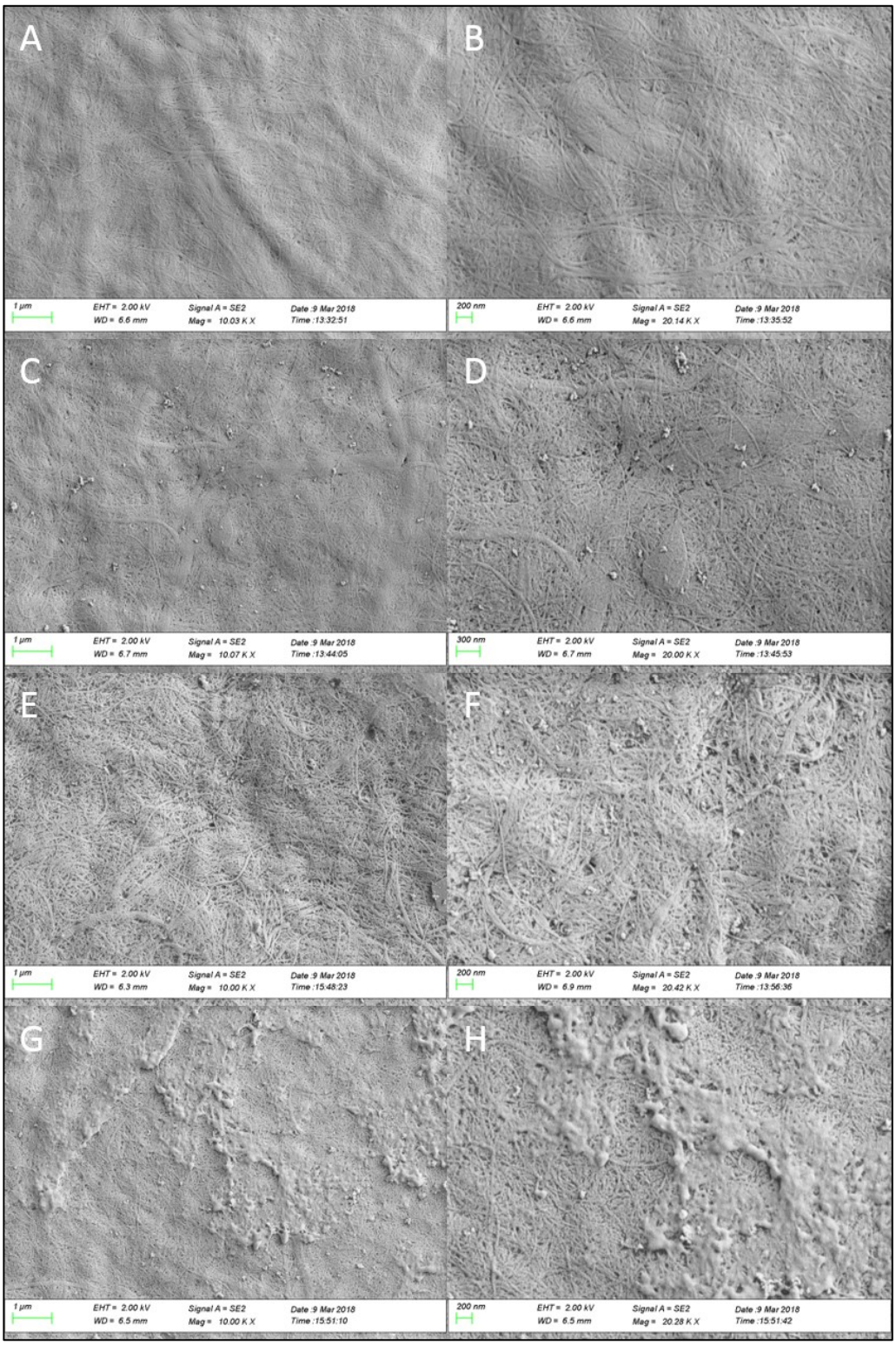

Figure 23. The SEM images of A) unmodified CNF film (magnification x10k), B) unmodified CNF film (magnification x20k), C) alkyne-modified CNF film

(magnification x10k), D) alkyne-modified CNF film (magnification x20k), E) hydrophilic part of thiol-yne patterned CNF film (magnification x10k), F) hydrophilic part of thiol-yne patterned CNF film (magnification x20k), G) hydrophobic part of thiol-yne patterned CNF film (magnification x10k) and H) hydrophobic part of thiol-yne patterned CNF film (magnification x20k). The scale bars for the lower magnification images are 1 μm and 200 nm for the higher magnification images.

The AFM images were taken of the unmodified and modified CNF films. These images can be seen in the Figure 24. It can be seen that the modifications changed the surface morphology in a way that the imaging with the AFM became harder and the images of the modified samples became blurred. The CNF fibers can be observed from the unmodified films, but after modification, the fibers were undetectable. This indicates that the modifications created a well-covering coating on top of the CNF films. In addition, the surface roughness increased with modifications, which was seen as increased blurriness of the images and increased amount of grain structures. Moreover, the grain size was biggest in the hydrophobized sample, which indicates that this sample had the roughest surface. This roughness could also be seen in the SEM images (Figure 23.g and 23.h). Additionally, if the surface of a sample is sticky and soft, the AFM tip can get stuck to the surface and the obtained image is blurred. This is to say that the obtained blurred images may indicate that the surface modifications changed the structural properties of the CNF film surface to more soft structure.

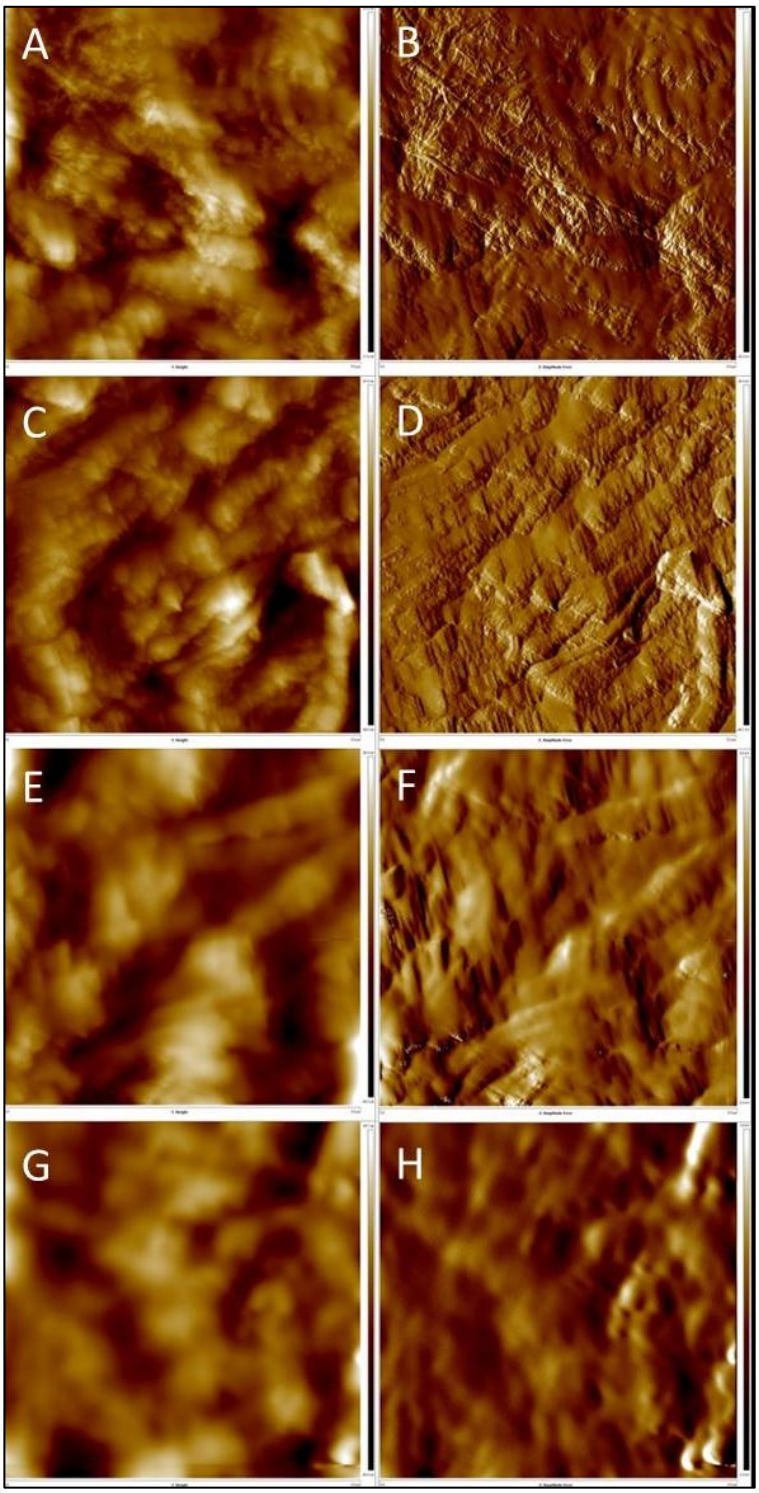

Figure 24. AFM height and amplitude error images of A) and B) unmodified CNF film, C) and D) alkyne-modified CNF film, E) and F) hydrophilic CNF film, and G) and H) hydrophobic CNF film.

4.2 Patterning with polystyrene

Polymer patterning method was also used to prepare fluidic channels. In this method, polystyrene solutions were used to create hydrophobic edges to the channels. The patterning was done in the beginning by hand. This method was a very simple and fast but the production of patterns with exact size was somewhat challenging. An image of a handmade polystyrene channel is presented in the Figure 25.

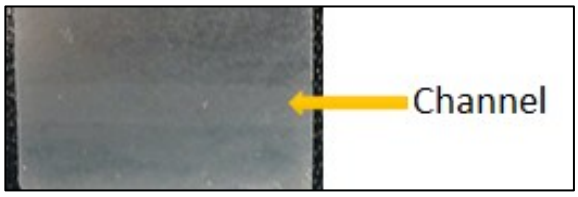

Figure 25. 3x20 mm channel with polystyrene edges on CNF film.

Next, the polymer patterning was performed by inkjet printing. The printing of the polystyrene solution made it easy to make well-defined patterns. In addition, multiple channels could be produced at the same time. By changing the printing parameters, different printing results were obtained. The Figure 26 presents images of the prepared printed channels. The thickness of the printed layer affects the channels ability to hold fluid; therefore, different drop spacing values were tested. From the Figure 26, it can be seen that the 50 µm and 40 µm drop spacing values created thin polystyrene layers on top of the films but a thicker print layer was obtained with the 30 µm drop spacing. However, the drop spacing affected also the quality of the printed pattern. If the drop spacing was too small, the ink drops spread on top of each other causing a smeared pattern. On the other hand, too large drop spacing caused uneven ink spreading and empty spaces to the print. It can be seen that the 40 µm drop spacing (Figures 26.c and 26.d) created the clearest patterns, whereas the higher and lower drop spacing values created uneven patterns. The printing of two polystyrene layers with 40 µm drop spacing created the clearest pattern with a thick polystyrene layer.

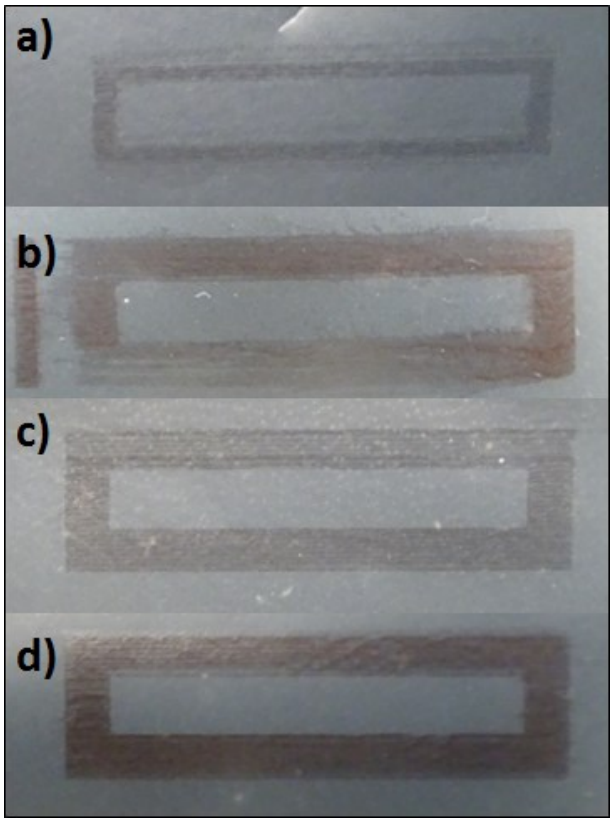

Figure 26. Printed 3x20 mm channels with polystyrene edges: a) channel with 1 mm edges, 50 µm drop spacing, b) channel with 2 mm edges, 30 µm drop spacing, c) channel with 2 mm edges, 40 µm drop spacing and d) channel with 2 mm edges, 40 µm drop spacing and two print layers.

To view the printed patterns more carefully, microscopy images of the printed channels were taken. The Figure 27 shows the microscopy images of the printed channels with 2 mm polystyrene edges. The same observations can be made from the microscopy images that the channels with 50 µm and 40 µm drop spacing were made of a thin polystyrene layer but the channel with 30 µm drop spacing and the twice printed channel with 40 µm drop spacing had thicker print layers. The most defined channel edges were created to the twice printed channel with 40 µm drop spacing.

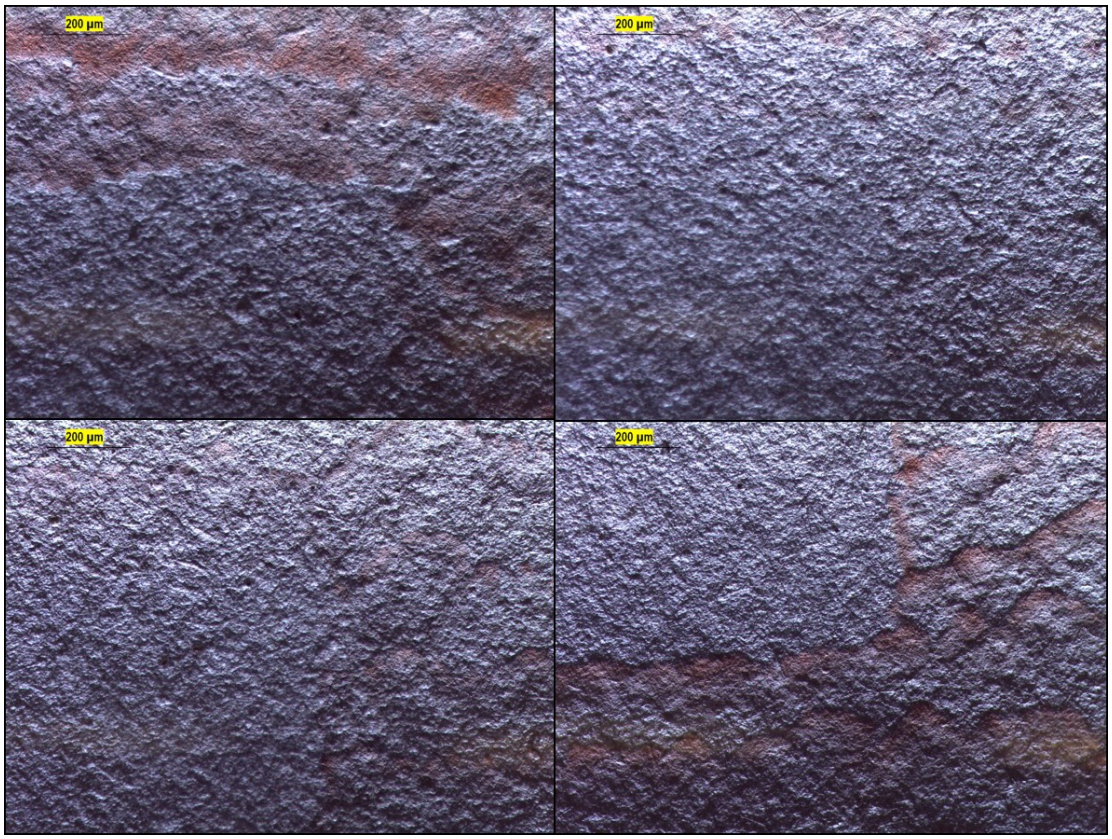

Figure 27. Microscopy images of printed channels with 2 mm edges. Channel with 30 µm drop spacing (top left), channel with 50 µm drop spacing (top right), channel with 40 µm drop spacing (bottom left) and channel with two print layers and 40 µm drop spacing (bottom right). Value of the scale bars is 200 µm.

The wetting properties of the polystyrene patterned CNF substrates were studied with WCA measurements. The contact angle results of the polystyrene patterns can be seen in the Figure 28. The polystyrene coating on the CNF film had the WCA of 94° and 96° on the CNF nanopaper. This means that the polystyrene coatings were mildly hydrophobic.

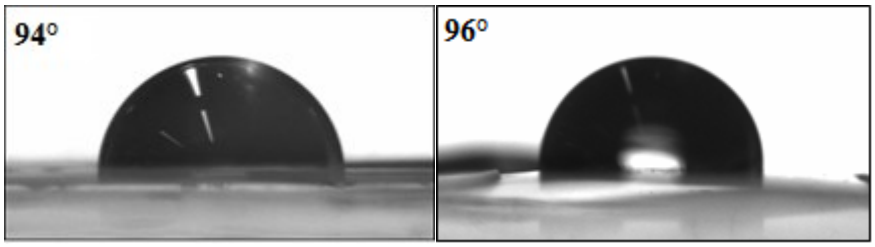

Figure 28. WCA results of the polystyrene coated CNF film (left) and CNF nanopaper (right).

Next, the surface topography of the polystyrene-coated films was characterized with SEM and AFM. The Figure 29 presents the SEM image of the polystyrene coated film and the Figure 30 presents the AFM images of the polystyrene coated films. The SEM image showed that the surface of sample was very smooth and the polystyrene coating was evenly distributed onto the surface. No fibers could be seen. Then, the AFM images (Figure 30) show that the polystyrene coated film consisted blurred grain structures and again no fibers could be seen. The grain structures indicates that the surface had some roughness. In addition, the blurred height image point to that the polystyrene coating was soft and the AFM tip stuck to the surface in some extent during the imaging.

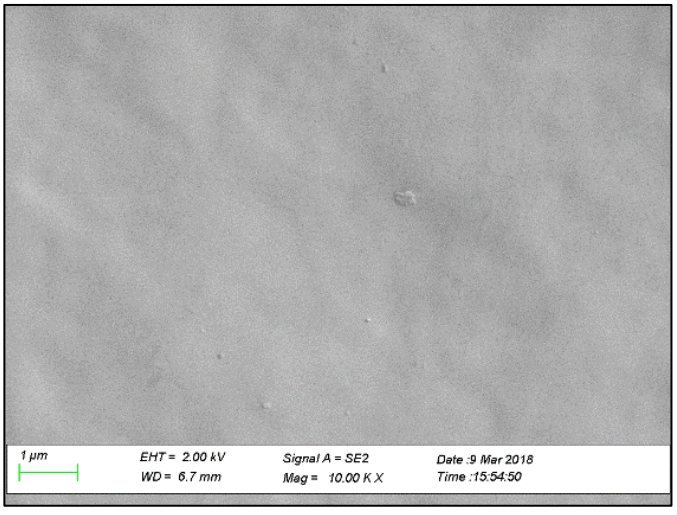

Figure 29. SEM image of polystyrene-coated CNF film.

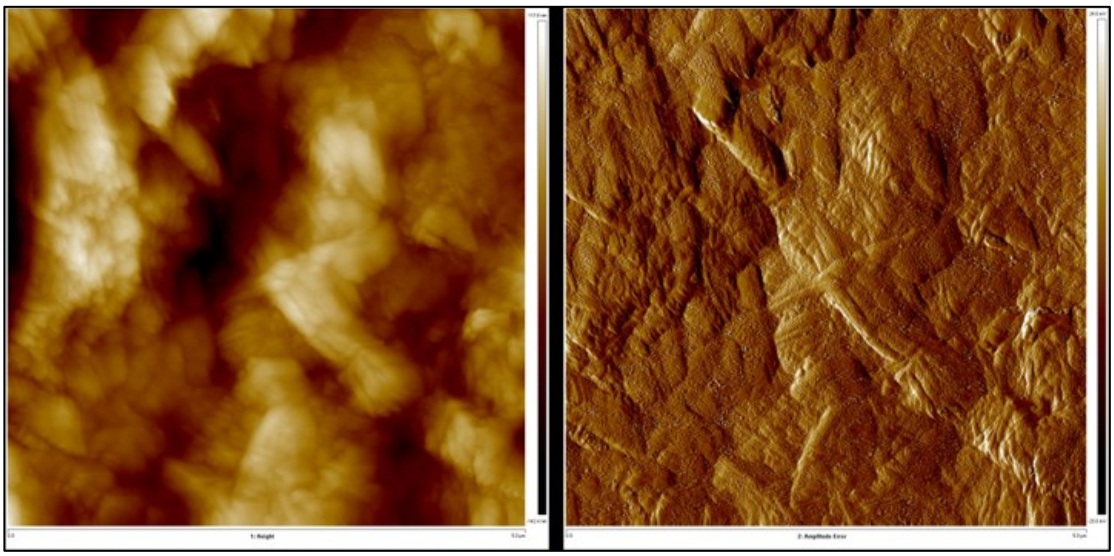

Figure 30. AFM height and amplitude error images of the CNF film with polystyrene coating.

4.3 Controlling non-specific protein adsorption

4.3.1 QCM-D and SPR results

The protein attachment on CNF substrates was studied with QCM-D. The Figure 31.a shows hIgG adsorption to an unmodified CNF film surface, which was studied as a reference surface. The decreasing frequency of the QCM sensor during measurement indicated that the mass of the sensor was increased, and in other words, the hIgG adsorbed to the surface. The hIgG adsorption was fast in the beginning, but after a while, the surface became covered with the protein molecules, adsorption slowed down and the frequency curve started to level off. After washing with the buffer, some of the proteins desorbed from the surface, which could be seen in the increasing frequency. The adsorption of hIgG can be explained at least in some extent by electrostatic interactions. The isoelectric point (pI) of hIgG is around 8 (Hamilton, 1987). At the testing conditions (pH 7.4) the hIgG was net positively charged, which made it electrostatically attracted to anionic CNF.

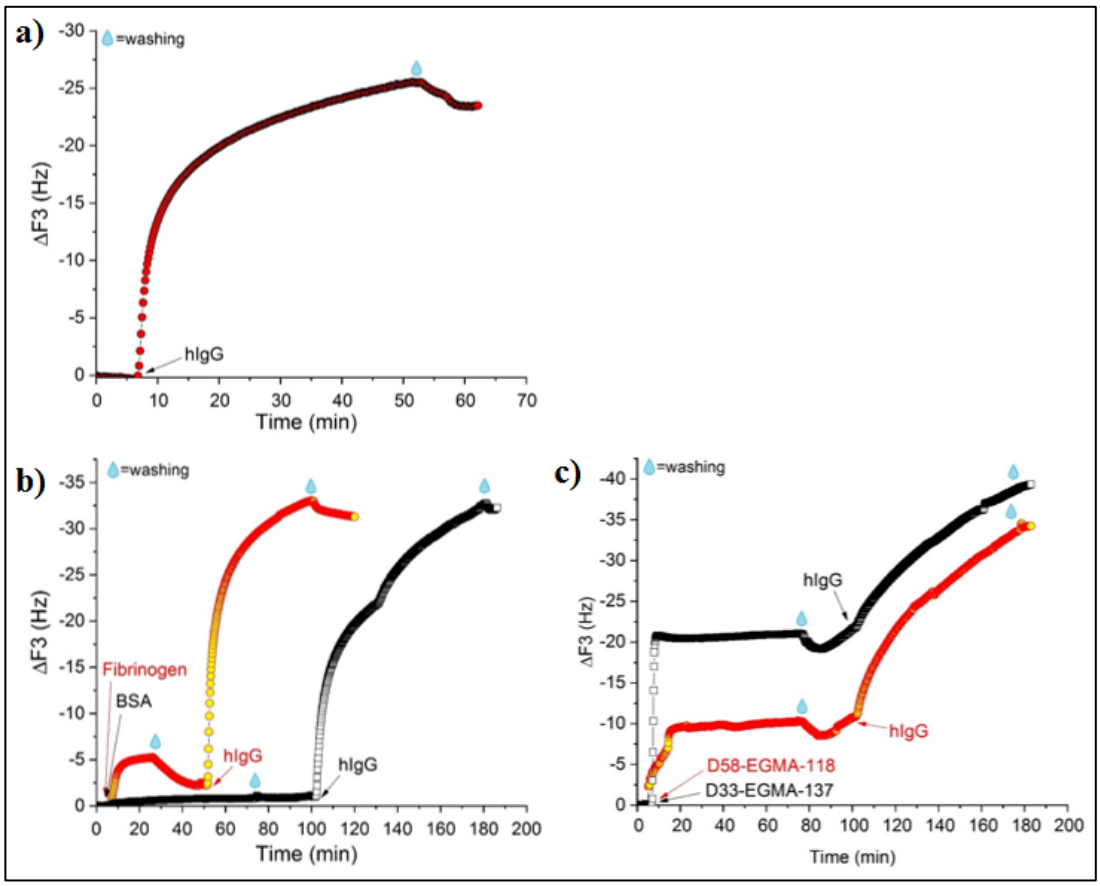

Figure 31. Frequency changes as a function of time: a) hIgG adsorption on CNF, b) fibrinogen and BSA adsorptions on CNF followed by hIgG adsorptions, c) block copolymer adsorptions and hIgG adsorptions on CNF.

The red curve in the Figure 31.b shows fibrinogen adsorption to CNF followed by washing with a buffer and hIgG adsorption. The black curve shows BSA adsorption to CNF film followed by washing with a buffer and hIgG adsorption. It can be seen that the adsorption of fibrinogen caused only a small change in frequency and after washing, the most of the fibrinogen proteins detached from the surface and the blocking efficiency was not very good. Namely, after introduction of the hIgG, a large frequency change can be observed. The pI of fibrinogen is 5.8, so it is negatively charged under physiological conditions (pH 7.4) (Protopopova et al., 2015). This means that at the testing conditions, the adsorption of fibrinogen was electrostatically unfavorable to

CNF. However, adsorption occurs despite the electrostatic repulsion because other interactions, such as hydrophobic interactions and van der Waals forces as well as the stability of the protein affect the adsorption. Nonetheless, the weak attachment and desorption of fibrinogen molecules could be explained with the poor electrostatic interactions. Additionally, the hIgG adsorption occurs, because it is electrostatically attracted to the negatively charged surface. In the case of BSA adsorption, the introduction of BSA to the CNF surface caused a very small decrease in frequency, which indicates that only a small amount of BSA is adsorbed to the surface. However, after washing, this small amount remained at the surface. Furthermore, similarly as in the fibrinogen-blocked surface, the BSA did not block the surface and a large frequency change was observed after hIgG was introduced to the surface. BSA has a pI of 5 (Orelma et al., 2011). Therefore, the same conclusions about the electrostatic interactions can be reasoned as in the case of fibrinogen adsorption.

The Figure 31.c shows the copolymer adsorptions to CNF surfaces followed by washings with buffers and hIgG adsorptions. The red curve shows the adsorption of a copolymer with a longer cationic block (D58-EGMA-118) and the black curve shows the adsorption of a copolymer with a longer hydrophilic block (D33-EGMA-137). From these graphs, we can see that the adsorption of the copolymers was fast, especially the adsorption of the D33-EGMA-137 copolymer. This can be explained by the effect of electrostatic interactions. The adsorbed copolymers have a cationic block, which makes it electrostatically attracted to the anionic CNF surface. After washing, some of the adsorbed or coupled copolymer molecules detached from the surface. In addition, hIgG adsorption was observed from the decreased frequency. The adsorbed amount was, however, smaller than the adsorption to the reference surface. The adsorption of hIgG was decreased because the POEGMA-block of the copolymers is highly hydrophilic and it takes an extended conformation in an aqueous media (Vuoriluoto et al., 2015). This caused steric repulsion between the surface and proteins, which decreased the adsorption of hIgG.

When material layers are adsorbed to the QCM sensors, in some cases water molecules can couple to the adsorbed material by direct hydration. In QCM-D, the resonance frequency of the oscillating sensor depends on the total oscillating mass of the system, including the masses of the sensor, surface adhering layers and hydrodynamically coupled water. That is to say, adsorbed masses obtained by QCM-D frequency response can be larger than expected. Therefore, the analysis of the dissipation signal was also conducted. By measuring the dissipation, the viscoelastic properties of the adsorbed films were determined. The data obtained in QCM-D measurements of different CNF surfaces can be seen in the Figure 32. This figure shows the frequency and dissipation graphs of the adsorption measurements. The frequency changes (ΔF) are shown in black on the left axis, and the dissipation changes (ΔD) are shown in red on the right axis.

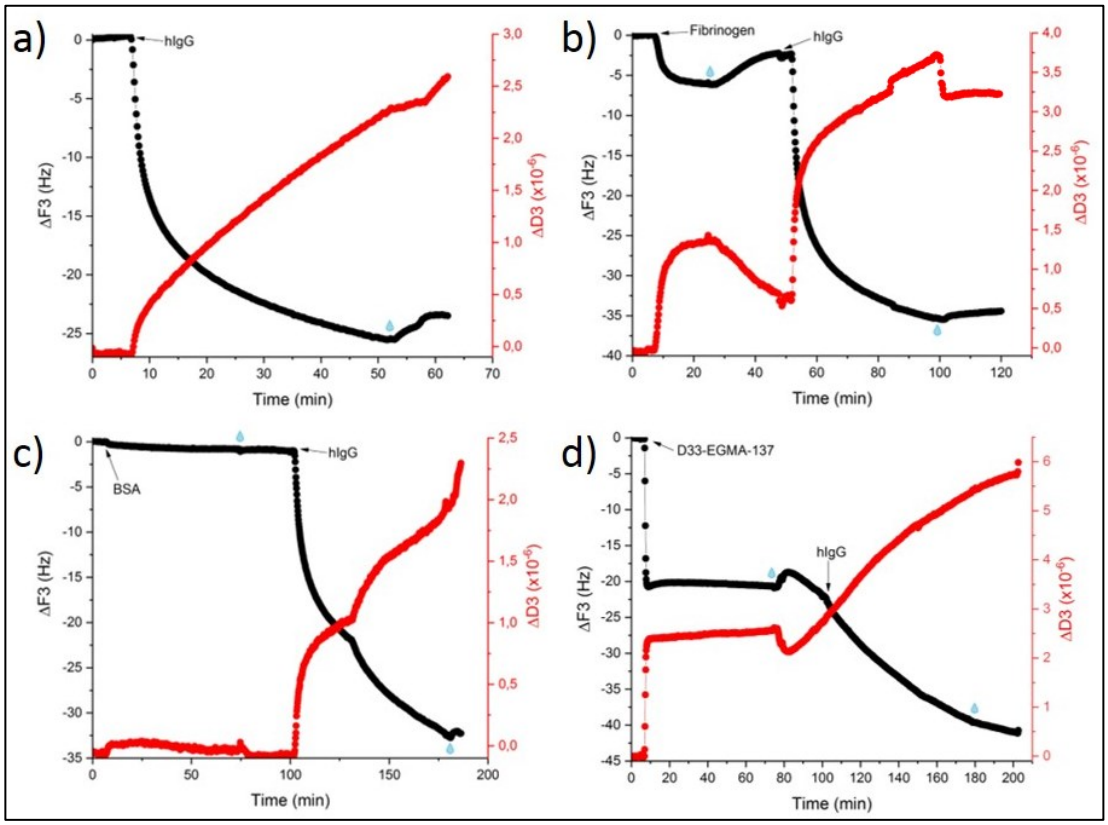

Figure 32. Frequency and dissipation changes as a function of time: a) hIgG adsorption

on CNF, b) fibrinogen and hIgG adsorption on CNF, c) BSA and hIgG adsorption on CNF and d) copolymer and hIgG adsorption on CNF.

In the Figure 32.a, one can see the viscoelastic behavior of the adsorbed hIgG layer on the reference CNF surface. The dissipation change increased almost linearly after hIgG was introduced to the surface. This means that the softness of the adsorbed layer was increased when the amount of adsorbed hIgG was increased. It is known that the formation of soft layers increases dissipation and if elongated molecules adsorb standing up to the surface, water molecules couple to the film and create higher dissipation change (Dixon, 2008). The hIgG is a small protein but its Y-shaped structure causes that it is often adsorbed to a surface in stand-up position. Therefore, when hIgG is adsorbed on top CNF surface, a soft viscoelastic layer is created.

The Figure 32.b presents viscoelastic behaviors of the adsorbed fibrinogen and hIgG layers on CNF. When fibrinogen was adsorbed to the surface, a large dissipation change occurred. This can be explained by the size and shape of the fibrinogen. Fibrinogen has an elongated shape with dimensions of 45nm×9nm×6nm, which makes it a quite large protein (Dolatshahi-Pirouz et al., 2009). As a result, the adsorbed fibrinogen proteins were most likely hydrated and water was trapped in the pores of the protein film. In addition, it is possible that some of the fibrinogen molecules were coupled to the protein layer, which increased the elongation of the adsorbed layer and increased viscoelasticity. After washing, the dissipation change dropped back to a value that indicated more rigid layer structure. The adsorption of hIgG increased again the viscoelastic properties of the adsorbed layer.

In the Figure 32.c, one can see the effect of BSA and hIgG on the rigidity of the adsorbed layer. The small frequency and dissipation changes after BSA adsorption indicate that the adsorbed BSA layer was rigid. BSA is a small and stable protein, which explains this (Goodsell, 2013). The softness of the adsorbed layer was increased when the elongated hIgG molecules were attached to the surface.

Finally, the Figure 32.d shows the effect of copolymer and hIgG adsorptions on frequency and dissipation signals. From the graph d), we can see that large frequency and dissipation changes occurred after copolymer introduction to the system. This indicates that both mass and viscoelastic characteristics of the adsorbed layer were increased due to the incorporation of water. Water couples to the layer because the used PDMAEMA-block-POEGMA copolymer contains a very hydrophilic block (Vuoriluoto et al., 2015). After adsorption of hIgG, the dissipation change increased further. From the high dissipation change value, it can be concluded that the adsorbed layer had most likely an elongated structure and a large amount of coupled water.

The Figures 33 and 34 summarize the QCM-D adsorption result of hIgG on CNF and blocked CNF surfaces. It can be seen that fibrinogen and BSA did not block hIgG adsorption, but instead increased it. On the other hand, the copolymers decreased hIgG adsorption. The best result, 26 % reduction in adsorption, was obtained with the D33-EGMA-137 copolymer. In addition, comparison of the dissipation and frequency graphs shows that the adsorbed layers most likely contained some coupled water that affects the results. Especially, the adsorbed layer with D33-EGMA-137 copolymer and hIgG seemed to be very soft and probably contained the highest amount of coupled water.

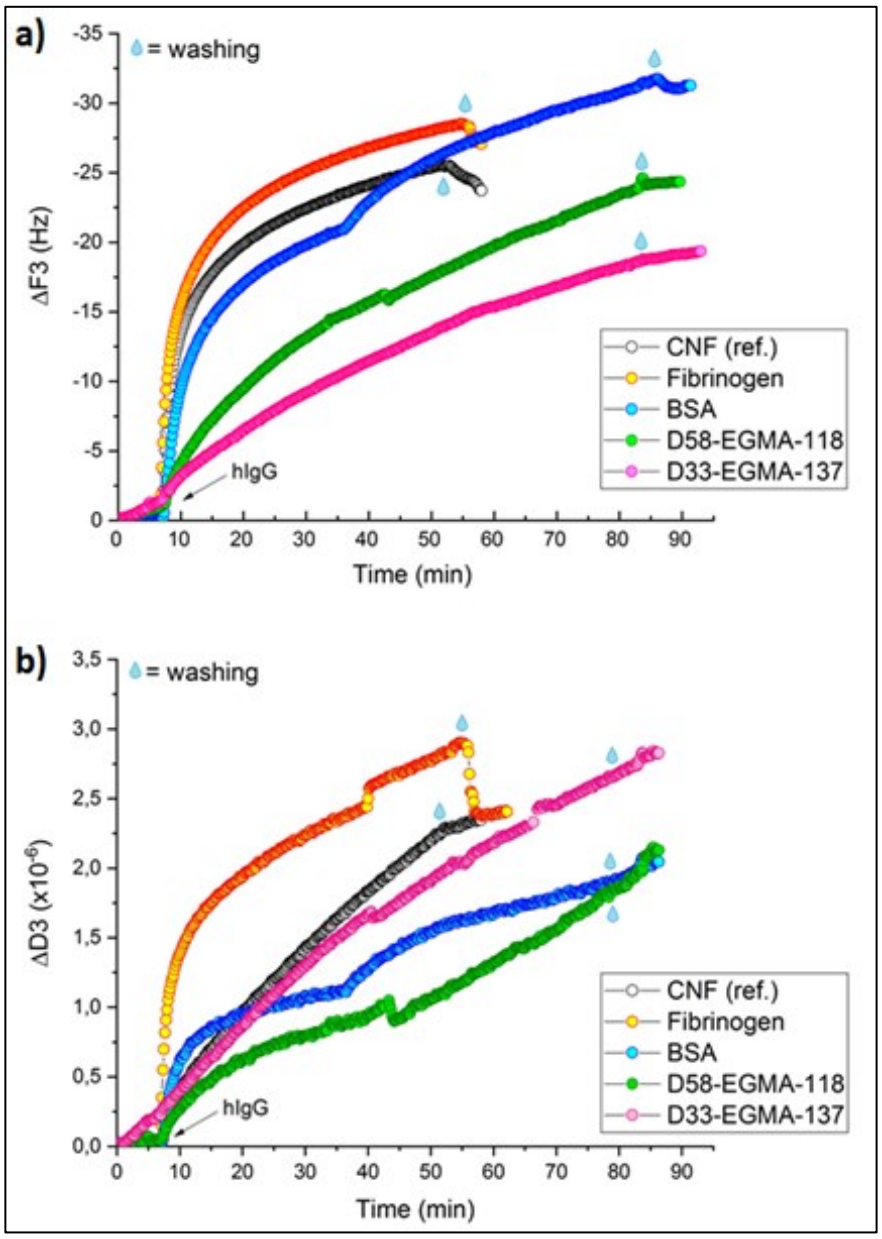

Figure 33. Adsorption of hIgG on CNF and blocked CNF surfaces: a) frequency change, b) dissipation change.

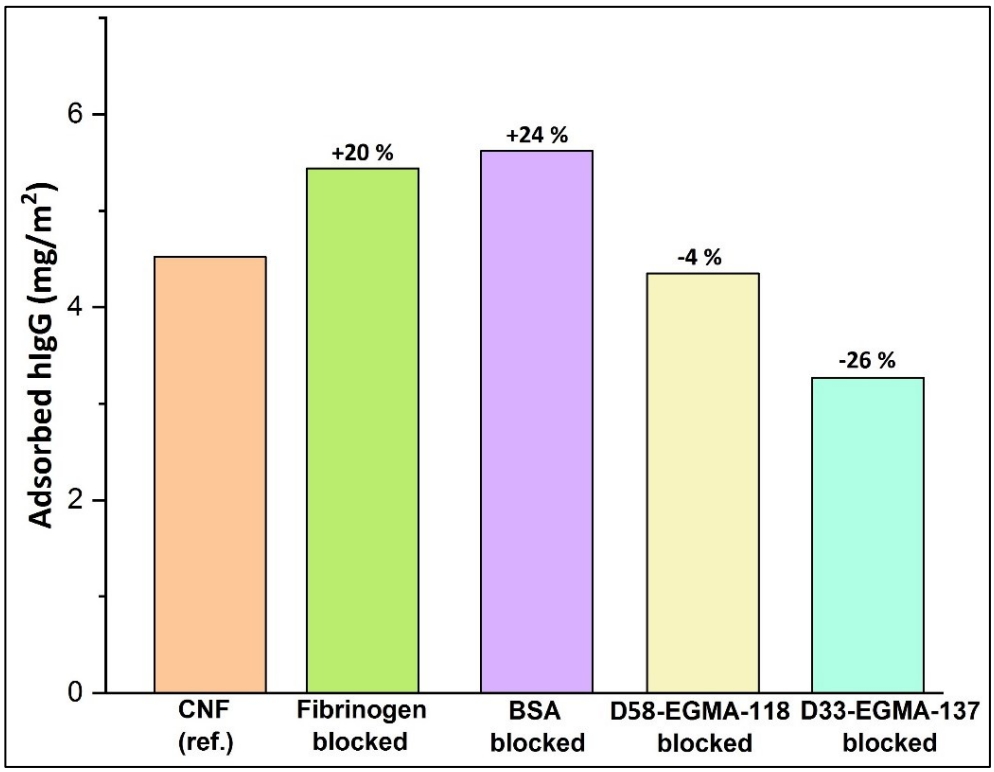

Figure 34. Adsorbed masses on CNF and blocked CNF surfaces. Masses were obtained with the Sauerbrey equation (equation 1).

In addition, the Voigt viscoelastic model was used to estimate the mass changes of the soft adsorbed layers. The plot fits of the adsorption results can be seen in the Appendices 1-5. All samples showed quite good fitting and these fittings were used to calculate adsorbed masses. The Figure 35 presents the adsorbed masses on CNF and blocked CNF surfaces obtained with the Voigt viscoelastic model. The adsorbed masses were quite similar as the masses obtained with the Sauerbrey equation.

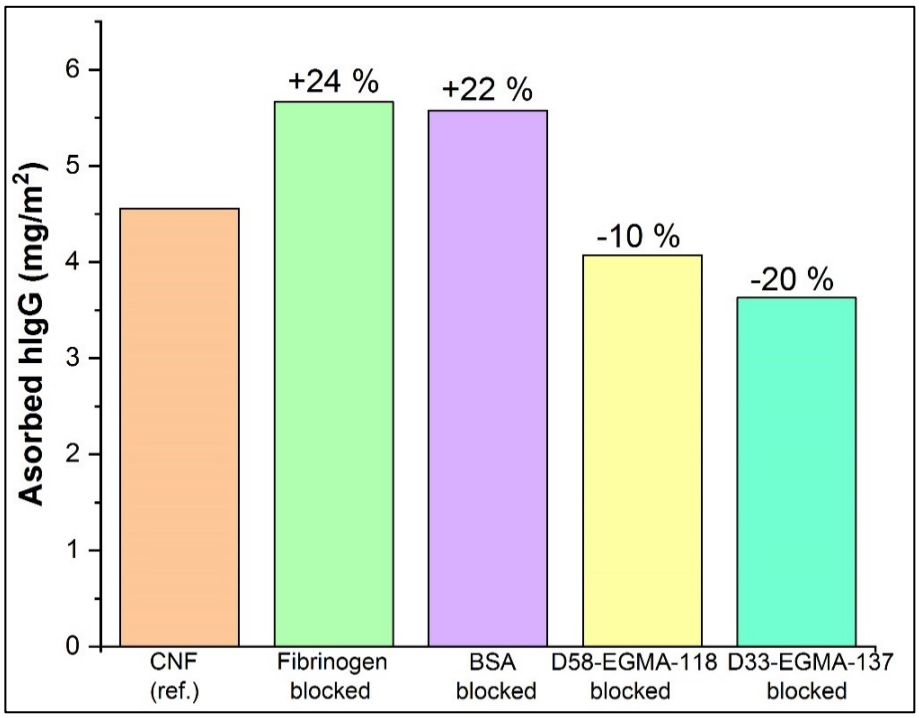

Figure 35. Adsorbed masses on CNF and blocked CNF surfaces. Masses were obtained with the Voigt viscoelastic model.

Protein adsorption studies were also performed in SPR. The SPR method is an optical method that measures the refractive index near the SPR sensor surface. Therefore, coupled water of the adsorbed layer does not affect the SPR results as it affects the QCM-D results. First, adsorptions onto unmodified CNF films and hydrophilized CNF films were measured with SPR. The Figure 36 shows results of hIgG adsorption onto CNF and hydrophilic CNF surfaces. Similarly, as seen in QCM-D, the hIgG adsorbed steadily to the CNF surface and after a while, the surface became covered with protein molecules, adsorption slowed down and leveling off the SPR angle curve could be observed. After washing with the buffer, some of the proteins desorbed from the surface, which can be seen in the decreasing SPR angle. From the Figure 36.b, it can be seen that higher changes in SPR angle were obtained when measuring the hydrophilic samples. This means that more hIgG adsorbed onto hydrophilic surfaces than on reference surface. Especially, the PEG-SH surface adsorbed much hIgG. High

hydrophilicity is in theory beneficial for the reduction of non-specific adsorption but blocking agents are usually required in order to eliminate the non-specific binding completely (Charles et al., 2009). The hydrophilic surfaces were analyzed further in order to understand the higher protein adsorption.

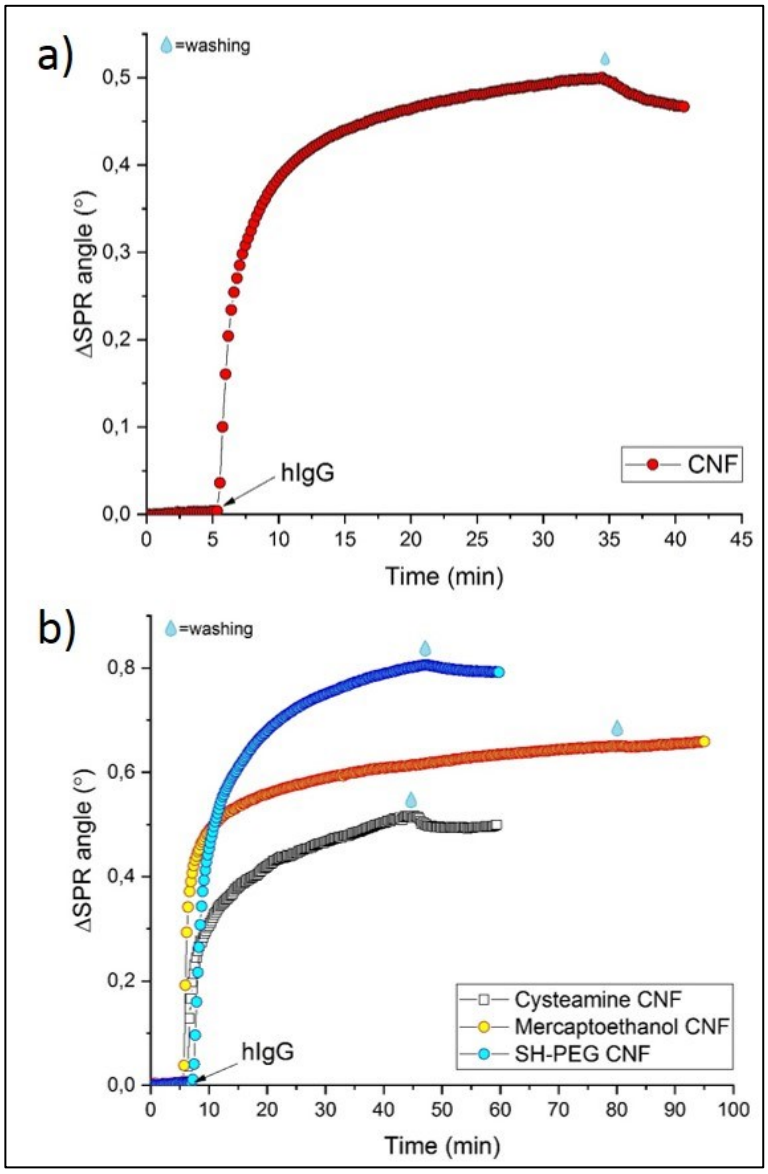

Figure 36. hIgG adsorption on a) CNF and b) hydrophilic CNF.

The CNF model film and the hydrophilic samples were imaged with SEM in order to see their surface structures. The images of the unmodified CNF film can be seen in the Figure 37. The unmodified film was very smooth and a high magnification needed to be used in order to see the nanofibrils. The cysteamine hydrochloride and 2-mercaptoethanol modified CNF films can be seen in the Figure 38. It can be seen that modifications caused formation of aggregations to the surfaces. The aggregations were much larger than the CNF fibrils, therefore, they cannot be seen in these SEM images. Probably, upon drying of the samples the hydrophilic molecules precipitated and formed aggregations on the sample surfaces due to capillary forces. These aggregations formed porous structures on the surface and this explains why the hIgG adsorbed more on these surfaces than the unmodified surface. Namely, proteins tend to adsorb more to porous structures because they have higher surface areas for interactions.

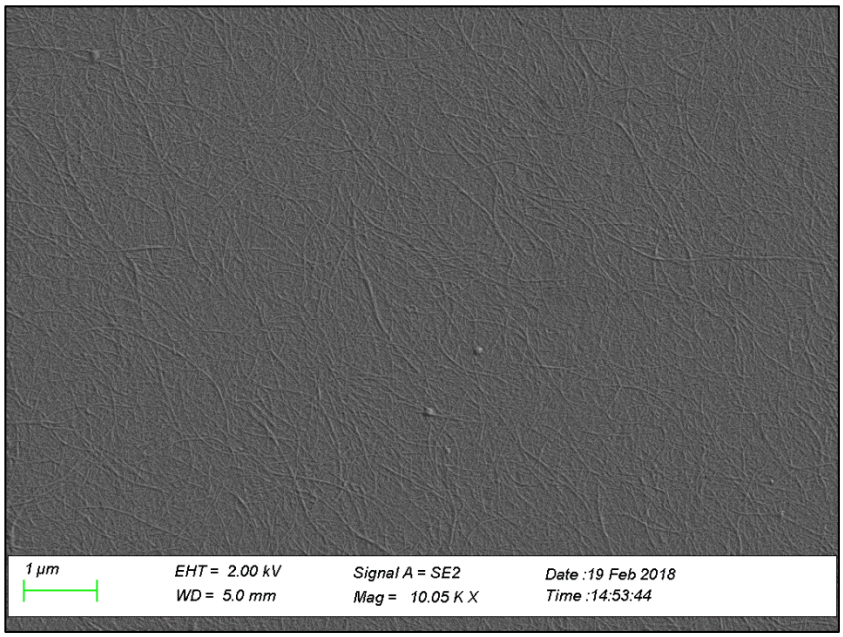

Figure 37. A SEM image of a thin model film of CNF, magnification x10k. The film was prepared by spin coating.

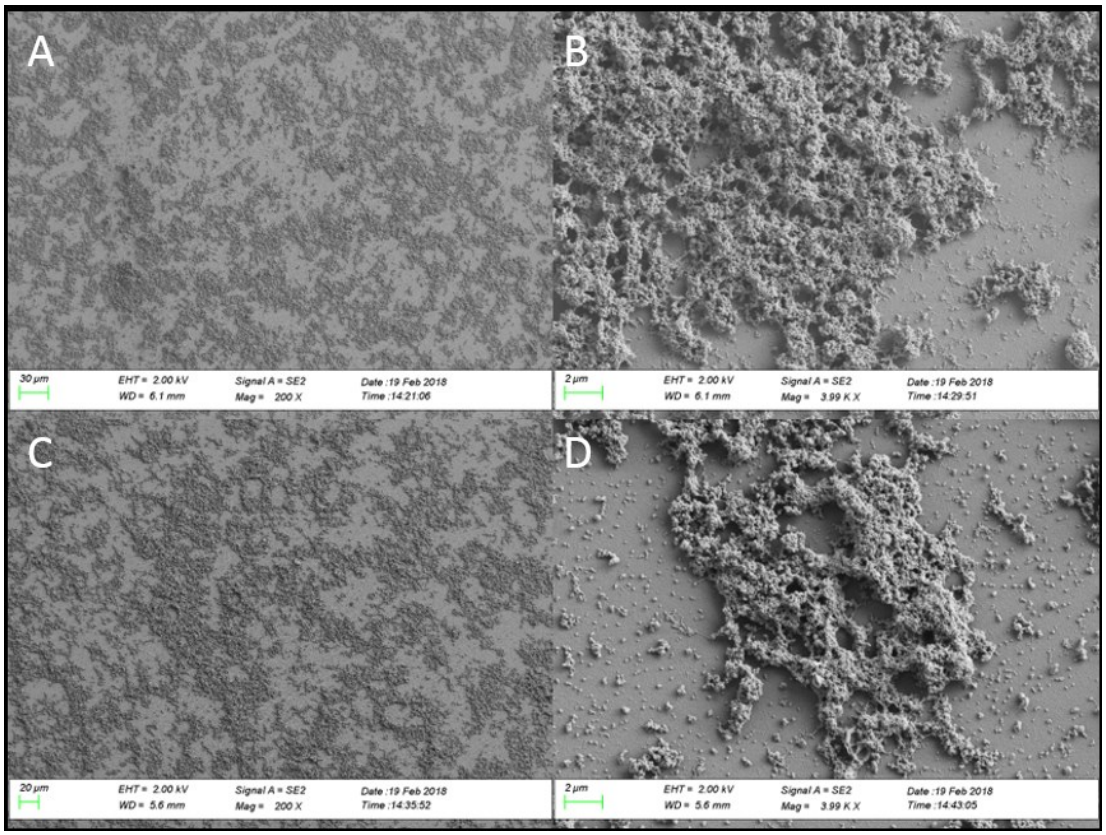

Figure 38. The SEM images of hydrophilic CNF samples: A) cysteamine hydrochloride modified CNF film, magnification x200, B) cysteamine hydrochloride modified CNF film, magnification x4k, C) 2-mercaptoethanol modified CNF film, magnification x200 and D) 2-mercaptoethanol modified CNF film, magnification x4k. The scale bars of the images are 30 µm, 2 µm, 20 µm and 2 µm respectively.

In addition, AFM images were taken from the unmodified CNF film and cysteamine hydrochloride and 2-mercaptoethanol modified CNF films. These images can be seen in the Appendix 6. Same conclusion can be made from these images that the introduction of hydrophilic molecules produced aggregated structures, which were much larger than the nanofibrils.

Furthermore, protein blocker adsorptions followed by hIgG adsorptions were performed in SPR. The Figure 39 shows SPR results of these measurements. In the

Figure 39.a, adsorption of fibrinogen can be seen in the red curve and BSA adsorption in the black curve. After both blocker adsorptions, samples were washed with a buffer and hIgG was introduced to the blocked surfaces. It can be seen that the adsorption of fibrinogen caused larger SPR angle change than the adsorption of BSA. After washing, only a small amount of protein is detached from the surfaces. However, the blocking efficiencies of both BSA and fibrinogen were not very good. After introduction of hIgG, a large SPR angle change was observed. However, fibrinogen blocked hIgG adsorption better than BSA. Then, in the Figure 39.b, adsorptions of the block copolymers in two concentrations can be seen. Adsorptions and blocking efficiencies of D33-EGMA-110 and D33-EGMA-137 copolymers were studied. The red and green curves in the Figure 39.b show the adsorption of D33-EGMA-110. The black and blue curves show the adsorption of D33-EGMA-137. From these graphs, we can see that the adsorption of the copolymers was fast. This is due to the electrostatic interactions. In addition, the adsorbed amounts of the copolymers were quite high. The completely dispersed copolymers introduced to the surface in higher concentrations adsorbed in higher amounts to the surface. Thus, the completely dispersed copolymers produced better covering layer on the CNF surface. After washing, some of the adsorbed or coupled copolymer chains detached from the surface. In addition, after hIgG was introduced to the surface, some adsorption could be observed but the adsorbed amount was very small. Thus, the passivation of the CNF surface was successful after introduction of the block copolymer. This is because the copolymer has a hydrophilic POEGMA-block that causes steric repulsion between the surface and proteins. The adsorption was smallest to the surfaces, which were blocked with the completely dispersed copolymers.

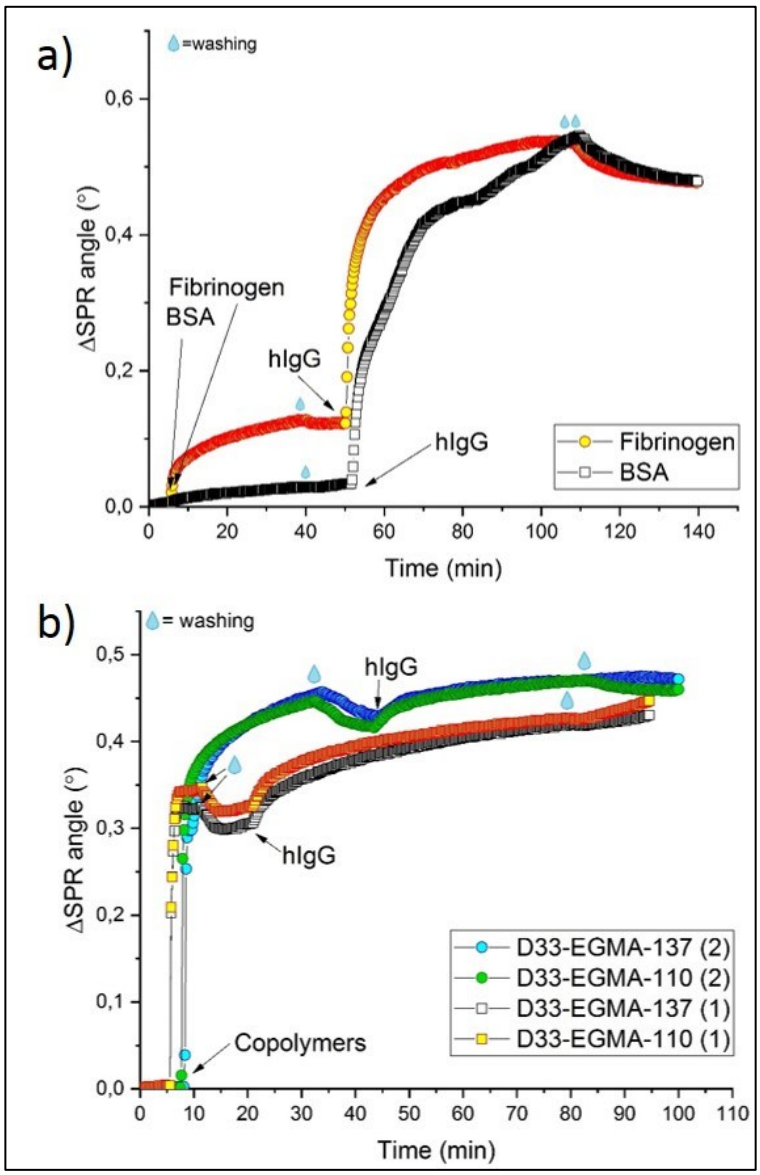

Figure 39. Adsorptions of protein blockers and hIgG on CNF: a) fibrinogen and BSA adsorptions on CNF followed by hIgG adsorptions, b) block copolymer adsorptions followed by hIgG adsorptions ((1) samples prepared to concentration of 0.1 g/l and (2) samples prepared to 0.5 g/l concentration and sonication was used to disperse undissolved parts).

The Figures 40 and 41 summarize the SPR results of the hIgG adsorption on the CNF, hydrophilic CNF and blocked CNF surfaces. It can be seen that the hydrophilic samples

had higher adsorption of hIgG than the reference surface, which was explained by the porous surface structures of the hydrophilic samples. In addition, it can be seen that BSA did not block the hIgG adsorption but fibrinogen and copolymers decreased the hIgG adsorption. Fibrinogen decreased adsorption 17 % but the copolymers decreased adsorption significantly by reducing the adsorption over 90 %. The best result, 95 % reduction in adsorption, was obtained with the D33-EGMA-137 copolymer.

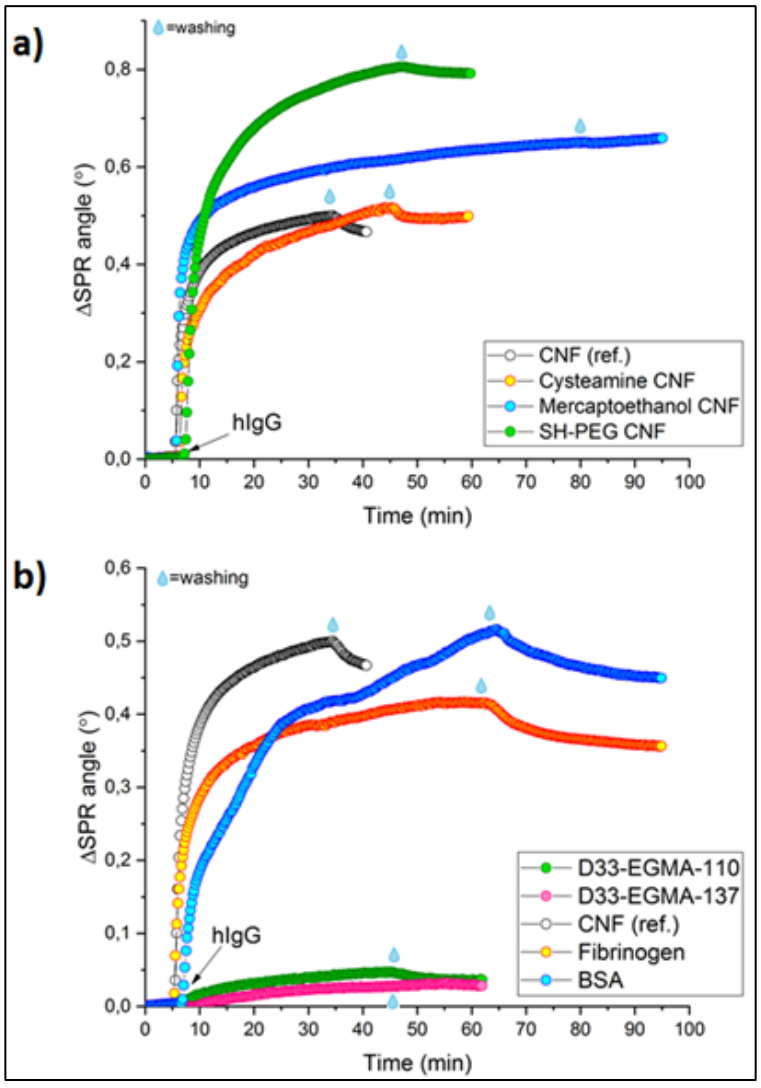

Figure 40. hIgG adsorption on CNF, hydrophilic CNF surfaces and blocked CNF surfaces: a) adsorption on hydrophilic samples and b) adsorption on blocked samples.

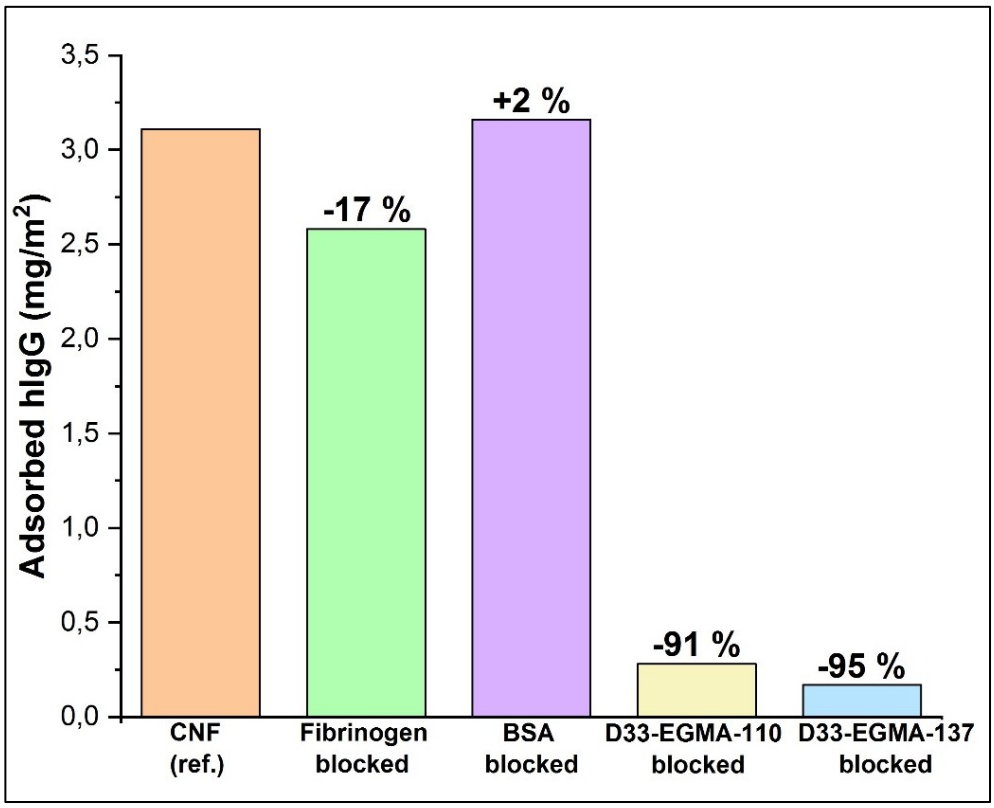

Figure 41. Adsorbed masses on CNF and blocked CNF surfaces. Masses were obtained with equations 2 and 3.

If compared with the QCM-D results, it can be seen that there is a huge difference in the adsorption results. Notably, the amount of coupled water on blocked surfaces, especially on the copolymer blocked surfaces, affects the QCM-D results and higher adsorbed masses were obtained than in the SPR. Therefore, the SPR results are considered more reliable when determining the blocking efficiencies of the different blockers. The most efficient protein blocker for CNF was found to be the hydrophilic D33-EGMA-137 copolymer.

4.3.2 Further analysis

In order to see the topographies of the non-blocked and blocked samples with and without hIgG, AFM images were taken of unblocked CNF, BSA blocked and D33-EGMA-137 copolymer blocked CNF samples with and without hIgG (see the Figure 42). It can be seen that the image of a pure CNF contained only CNF fibers but after introduction of hIgG to the surface (Figure 42.b), some spots appeared to the image and it became blurred. These spots and the blurriness of the image indicate that antibody adsorbed to the surface. In the Figure 42.c, the D33-EGMA-137 copolymer can be seen as small spots around the CNF fibrils. The surface coverage of the copolymer seemed to be good. After introduction of hIgG, the AFM image was blurred and darker spots could be seen. This indicates that some hIgG was adsorbed to the surface despite the blocker. However, in the Figure pair 42.e and 42.f, which present the BSA blocked samples with and without hIgG, a clear difference between images can be seen. The BSA protein can be seen as darker spots in the image. Then, the adsorbed hIgG proteins can be seen as increased amount of white spots in the Figure 42.f. Based on these images; it seems that the highest adsorbed amount of hIgG occurred on the BSA blocked sample. On the other hand, the amount of adsorbed hIgG is difficult to estimate from the AFM images and more accurate conclusion from these images would be that all samples, including the blocked samples, adsorbed some hIgG.

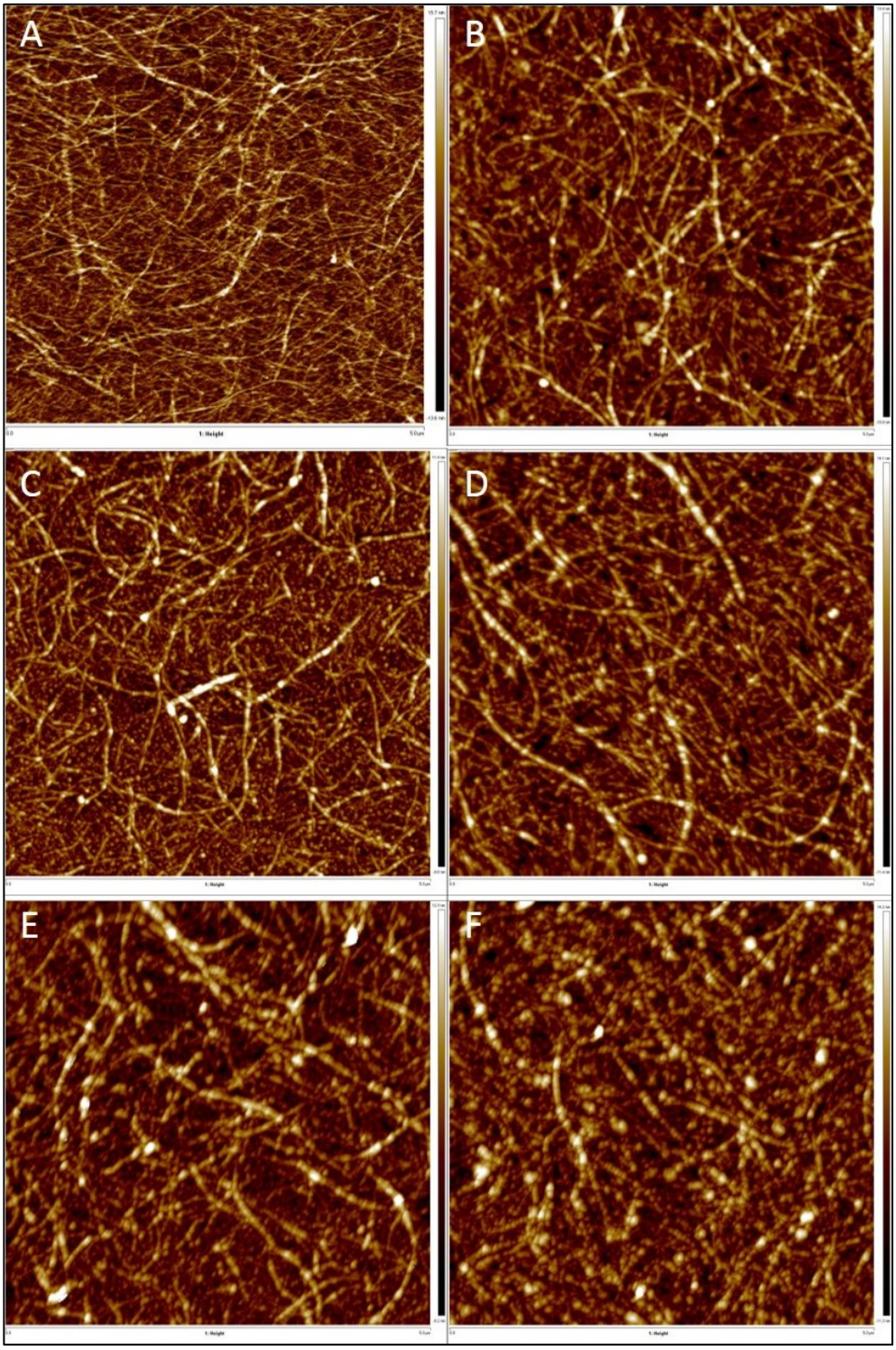

Figure 42. AFM height images of A) CNF, B) CNF with hIgG, C) D33-EGMA-137 copolymer blocked CNF, D) D33-EGMA-137 copolymer blocked CNF with hIgG, E) BSA blocked CNF and F) BSA blocked CNF with hIgG.

In addition to testing of protein adsorption on the model CNF films, the non-specific hIgG adsorption study was performed also on real CNF films. In order to see, how hIgG adsorbs to the films, hIgG molecules were reacted with a fluorescent probe. The fluorescent hIgG molecules were then adsorbed on CNF films and blocked CNF films. These samples were imaged with a CLSM and these images can be seen in the Figure 43. The reference sample (Figure 43.a) contained no fluorescent hIgG, therefore, it is completely black. The unmodified CNF film (Figure 43.b) adsorbed a high amount of hIgG-FITC and this can be seen from the strong green color of this sample. The, intensity of the green color was decreased when BSA was introduced to the film surface. However, some aggregations of the protein can be seen in the Figure 43.c. The copolymer-blocked sample (Figure 43.d) had the lowest intensity of the green color and this intensity was significantly lower than the color intensity of the unmodified sample. This indicates that the copolymer blocked the surface quite well. However, some adsorption of the hIgG-FITC occurred, because a pale green color can be seen in the copolymer-blocked sample. These CLSM results are, thus, similar as the results obtained with model CNF surfaces with SPR. Noteworthy, the BSA seemed to block films surfaces better than the model surfaces. However, it can be concluded that the blockers have similar effect on the thicker CNF films as on the thinner model CNF films.

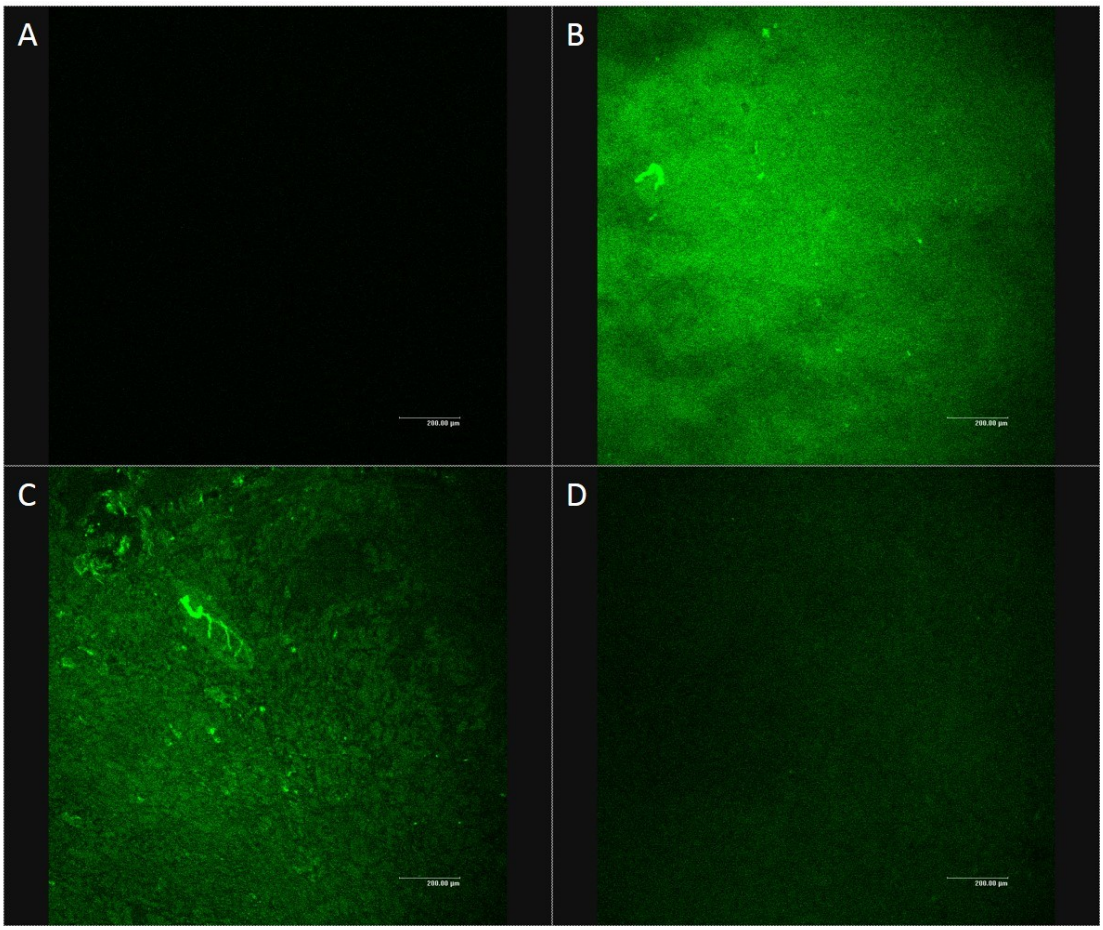

Figure 43. Confocal microscopy images of untreated and blocked CNF samples. A) unmodified CNF film (reference), B) unmodified CNF film with adsorbed FITC-stained human IgG (hIgG-FITC). C) BSA blocked CNF film with adsorbed hIgG-FITC and D) D33-EGMA-137 copolymer blocked CNF film with adsorbed hIgG-FITC. Images were recorded using 727 V laser with constant imaging conditions. Scale bars: 200.00 µm.

4.4 Flow test results

The functionalities of the prepared fluidic channels were studied by testing flowing of water in these channels. The tests showed that water flowed on top of the CNF films and did not penetrate into the films significantly. This is because CNF substrates have quite high density and there are only little amount of pores in which the fluid can go

to. For this reason, no lateral flow was observed during the tests. The driving force for the flow was concluded to be the pressure of the fluid and the capillary effect had only a minor role in this.

The summary of the flow test results can be seen in the Figure 44. The channels patterned with click chemistry (Figure 44.a) did not hold the fluid and the flow was very slow. Even after 2 minutes, the flowing of the fluid was minimal. Better results were obtained with the polystyrene patterned channels. The handmade polystyrene channels (Figure 44.b) held the fluid well and the fluid flowed well in the channel. However, 30 µl of water did not flow to the end of the channel. Then, the printed channels with 1 mm edges and 50 µm drop spacing (Figure 44.c) had a slow flow in them but the fluid flowed slightly over the edges. The printed channels with 2 mm edges and 30 µm drop spacing (Figure 44.d) did not hold the fluid well but flow was observed before spreading. The printed channels with 2 mm edges and 40 µm drop spacing (Figure 44.e) held fluid quite well and the flow of the fluid was fast. The channels with twice printed 2 mm edges and 40 µm drop spacing (Figure 44.f) held the fluid well and had the fastest flow.

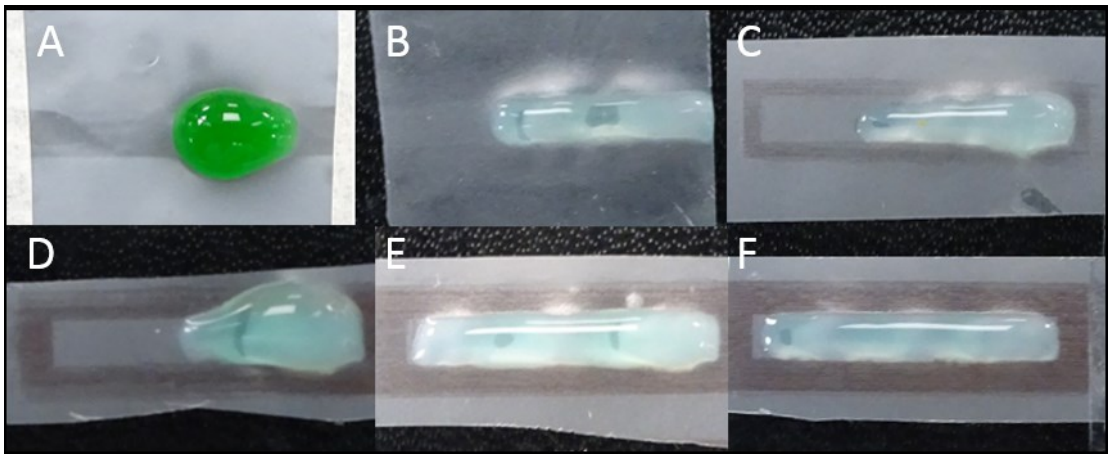

Figure 44. Flow test results. A) Thiol-yne hydrophobic-hydrophilic patterned channel, B) handmade polystyrene channel, C) printed channel with 1 mm edges and 50 µm drop spacing, D) printed channel with 2 mm edges and 30 µm drop spacing, E) printed

channel with 2 mm edges and 40 μm drop spacing and F) printed channel with 2 mm edges and 40 μm drop spacing (two layers).

It was notable, that the polystyrene channel held fluid better than the click chemistry channel. This was despite that the WCA difference between the channel and the hydrophobic edges was higher in the click chemistry patterned channel than in the polystyrene channel. The reason for this is that the polystyrene formed a clear three-dimensional structured barrier on the channel edge, which helped in the holding of the fluid. Then again, the channel patterned with click chemistry had a surface tension difference but no three-dimensional edges in the channel that would prevent the fluid flow over the edges. Namely, the required water pressure for flow was so high that the surface tension barrier was not able to hold the fluid. The click reactions have been reported to work on filter paper and most likely, these methods produce more efficient channels in materials with higher porosity (Guo et al., 2018). In addition, it was clear that the thicker polystyrene edges held fluid better than the thinner edges. The handmade polystyrene channel and the twice-printed polystyrene channel with 2 mm edges and 40 μm drop spacing showed best results in the holding of the fluid.

The handmade channel and the printed channel with two layers (2 mm edges, 40 μm drop spacing) were analyzed further. The Figure 45 presents the flow distances of these samples as a function of time. In addition, the Figure 46 shows the position of the fluid front line in handmade and printed channels after 0, 1, 3, 9 and 30 seconds from the addition of the water droplets. These figures show that water flowed faster in the printed channel and the applied fluid reached the end of the channel. Oppositely, the applied fluid did not reach the end of the handmade channel and the front line of the fluid passed only by little the half way of this channel. This flow rate difference can be seen clearly 3 seconds after the water droplets were applied on the channels. Additionally, already after 9 seconds from the addition of the water droplets, the fluid in the printed channel had almost reached the end but in the handmade channel, the fluid flow was significantly slowed down and only a halfway of the channel was

reached. The reason for this flow rate difference was probably that the edges of the handmade channel were not as even and sharp as the edges of the printed channels. The water molecules attached to the uneven edges of the handmade channel and this hindered the flow of the fluid. In addition, it can be concluded that a smaller water pressure drove the flow in the printed channels than in the handmade channels.

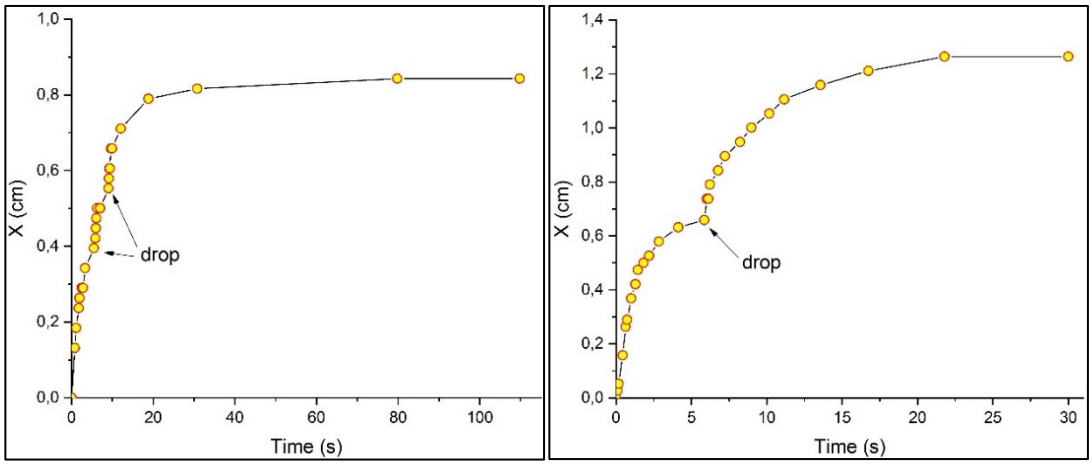

Figure 45. The flow distances as a function of time. On left: the flow in the handmade polystyrene channel and on right: the flow in the twice printed polystyrene channel with 2 mm edges and 40 µm drop spacing.

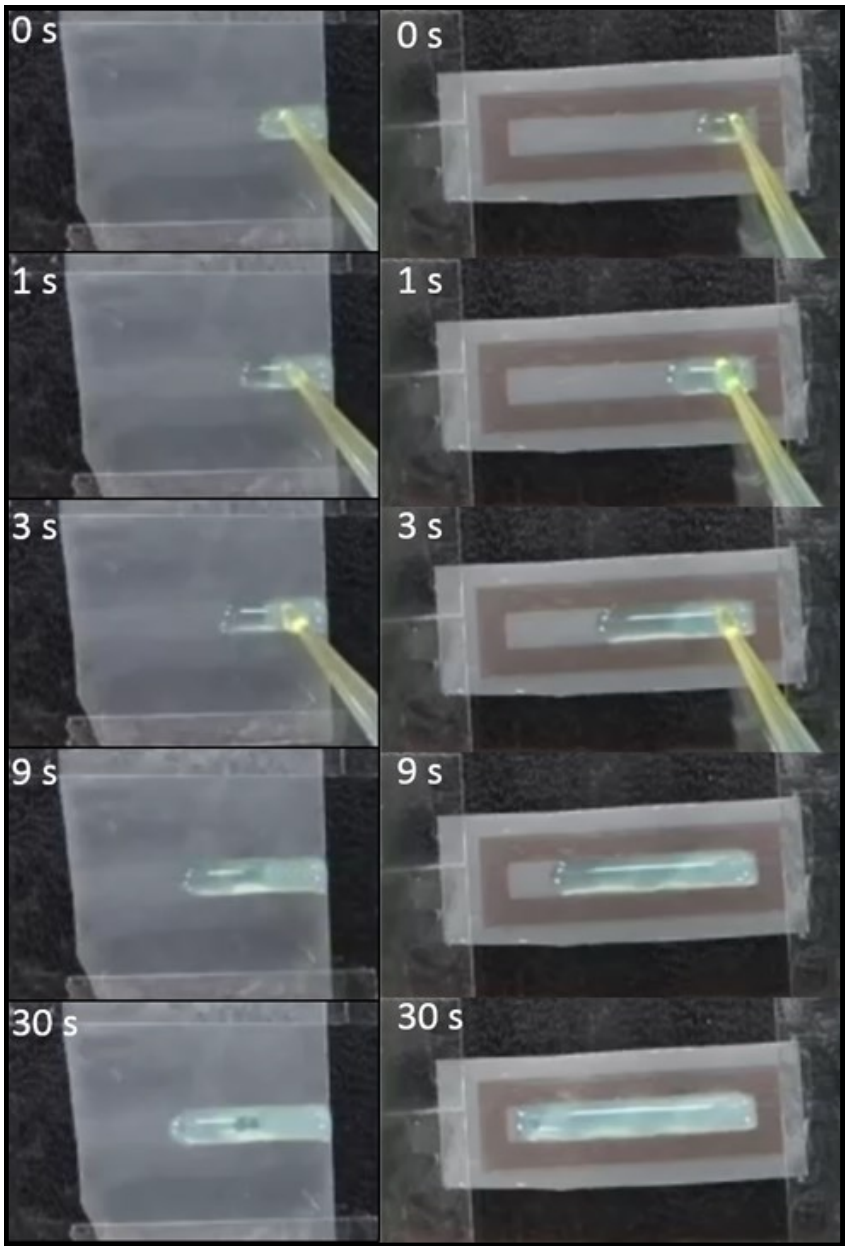

Figure 46. Propagation of fluid in handmade polystyrene channel (left) and in printed polystyrene channel (2 mm edges, 40 μm drop spacing and two layers) (right).

In biosensors, it is important the target molecule reaches the bioactive area of the biosensor and does not adsorb to some non-specific sites. Therefore, the non-specific adsorption of proteins should be minimized in the fluidic channels. In order to see how

much hIgG is adsorbed in the channels and does the introduction of the blocking agents reduce this adsorption, flow tests with fluorescent stained hIgG antibodies were also performed. The CLSM was used to detect the adsorbed proteins.

The CLSM images of the tested channels can be seen in the Figure 47. CLSM images were taken along the length of the channels, therefore, one can see how adsorption changes at different parts of the channels. In the Figure 47, on the left of each channel is the point where the hIgG-FITC solution was dropped and on the right, one can see the end of the channel. In addition, the green color in the images indicates hIgG adsorption. It can be seen that the unmodified channel had the highest amount of adsorbed hIgG. The green color can be seen along the whole length of the channel. Then, the blocked channels had significantly less green areas than the unmodified channel. However, the BSA-blocked channel had some aggregations of adsorbed hIgG. The observed aggregations formed, when the drying of the residual antibody solution caused precipitation due to capillary forces. The lowest amount of hIgG was adsorbed on the copolymer-blocked channel, in which only pale spots of green can be seen in the beginning of the channel. This was the spot where the hIgG-FITC solution was dropped. Thus, the blocking agents passivated the surface from the adsorption of hIgG quite efficiently. Surprisingly, if compared to the SPR results and previous CLSM image (Figure 43.c) the BSA prevented hIgG adsorption better in the channels than in the plain films. Furthermore, the Figure 47 shows that the hIgG adsorbed more on the early part of the channel. This can be seen especially in the BSA blocked channel, where the amount of green spots is reduced along the length of the channel. The adsorption was probably higher in the beginning because at this spot hIgG-FITC solution was applied on the channel and this spot had the highest hIgG concentration and fluid pressure. High fluid pressure caused antibodies to be pressed against the surface and stick to it. The bright green lines at the end of channels indicate that the hIgG reached the end of the channel and the adsorption was high again at the end.

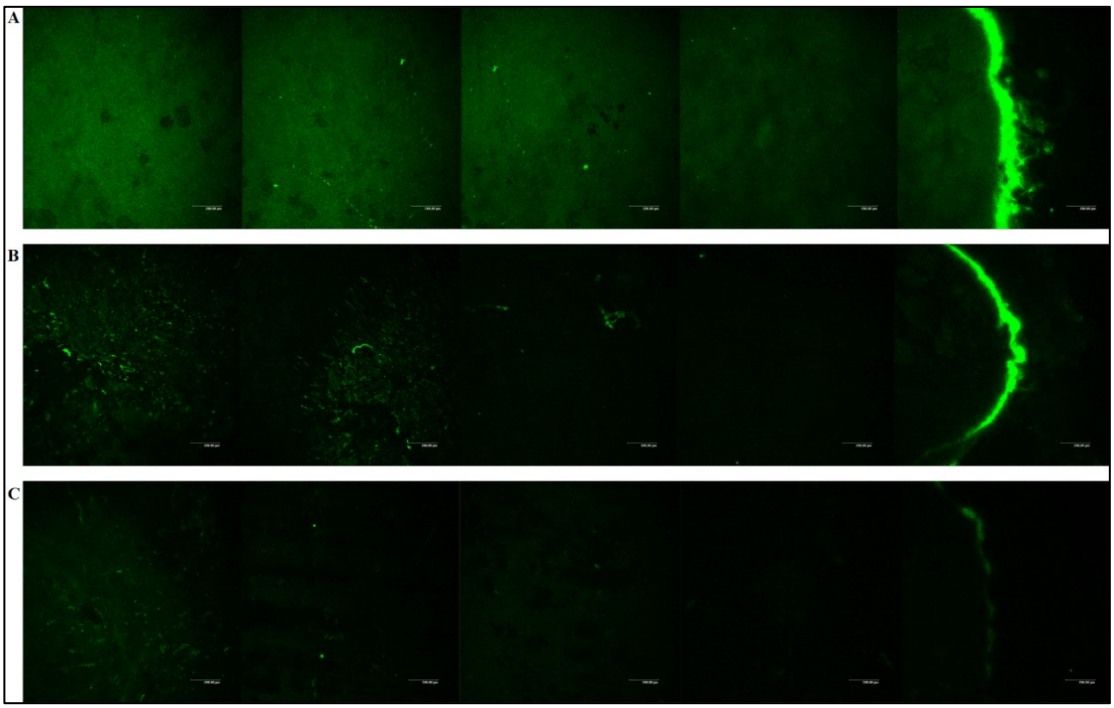

Figure 47. CLSM images of unmodified and blocked channels that were introduced with a fluorescent hIgG solution. Images are taken along the length of A) unmodified channel, B) BSA-blocked channel and C) D33-EGMA-137 copolymer blocked channel.

Based on the bright green lines at the end of the channels (see Figure 47) it can be concluded that the hIgG adsorbed mostly on the edges of the channels. This phenomenon was investigated further and images of the corners and edges of the different channels were taken. The Figure 48 shows these CLSM images. It can be seen that indeed the most of the adsorbed hIgG located at the edges of the channels. Especially, the borders of the unmodified channel adsorbed antibodies. It is known that proteins tend to adsorb more on hydrophobic and rough surfaces (Prime and Whitesides, 1991; Sigal et al., 1998). The borders of these channels are both hydrophobic and rough, which explains the high adsorption of hIgG. Namely, the roughness increases surface area of interactions and proteins tend to stick to the small grooves of the edges. The introduction of the antifouling properties reduced the overall

adsorption including the adsorption to the edges. In the copolymer-blocked channel, the adsorbed amount was decreased significantly and only some parts of the edges had adsorbed hIgG. It seems that during the introduction of the blocking agents, some of the blockers adsorbed also to the edges and the edges obtained antifouling properties. Therefore, no separate procedure was needed to prevent protein adsorption to the edges.

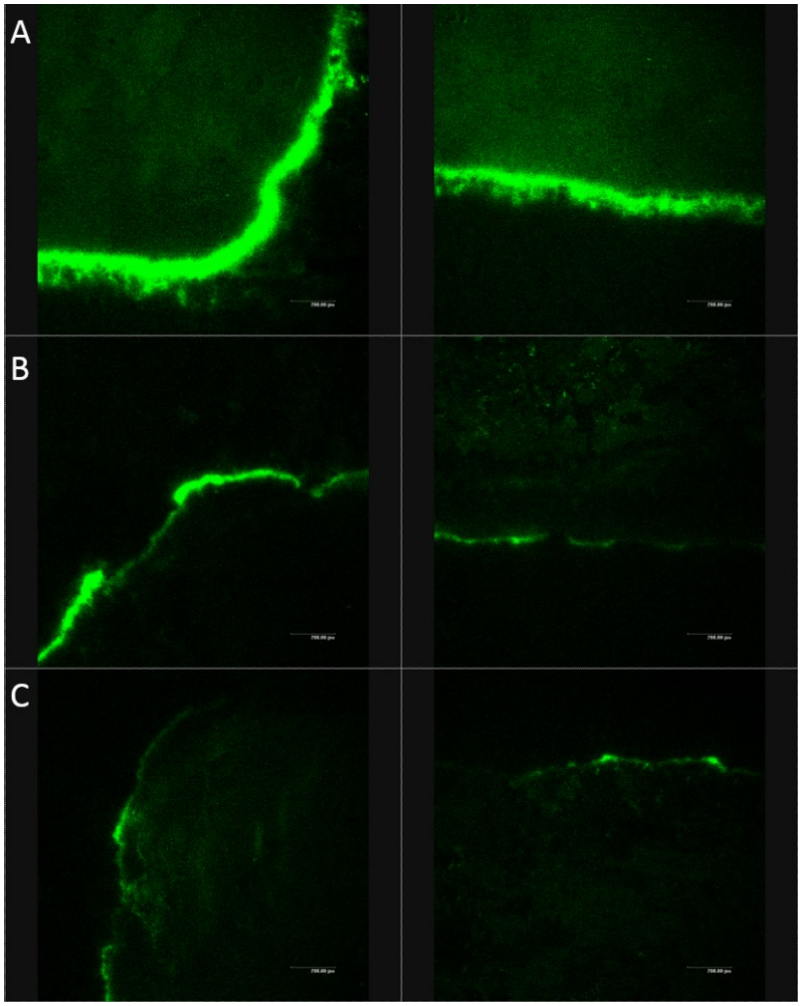

Figure 48. Edges and corners of the fluidic channels with adsorbed hIgG-FITC: A) unmodified channel, B) BSA blocked channel and C) D33-EGMA-137 copolymer blocked channel.

In addition, in order to see how protein adsorption differs in hydrophilic and hydrophobic surfaces, flow test was done with a channel containing a hydrophobic area. The Figure 49 shows the CLSM images of this channel. The tested channel was unmodified and that is why hIgG adsorbed in all parts of the channel. However, the hydrophobic area can clearly be seen in the middle of this figure, which indicates that the hIgG adsorbed more to this hydrophobic area.

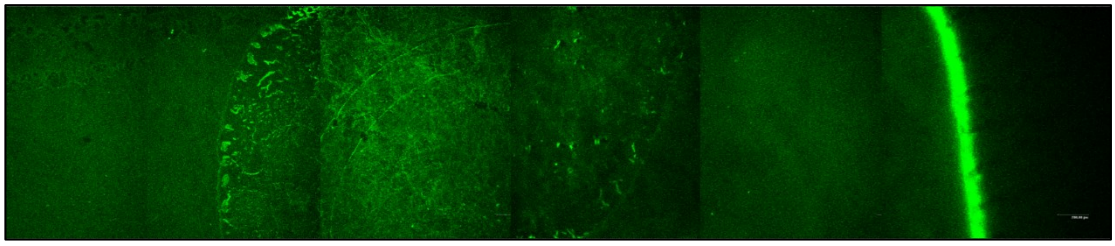

Figure 49. hIgG-FITC adsorbed on a channel with a hydrophobic area in the middle. The figure was obtained by combining five CLSM images.

5. Conclusions

The objective of this thesis was to produce fluidic channels on CNF films by creating hydrophilic-hydrophobic patterns. An additional goal was to study non-specific adsorption of proteins on CNF and to find a suitable antifouling agent for the CNF films. Thiol-ene and thiol-yne click chemistries and polymer patterning were utilized to produce fluidic channels. These channels were characterized with SEM, AFM, contact angle measurements and flow tests. Additionally, non-specific protein adsorption was studied on model CNF films with QCM-D, SPR and AFM by using hIgG as a model protein. In addition, the adsorption of fluorescent hIgG was studied on CNF films and channels with CLSM. The protein blocking ability of BSA, fibrinogen and PDMAEMA-block-POEGMA copolymers were studied.

The click chemistry methods did not produce efficient fluidic channels on CNF films. These channels produced retarded flow and they did not hold the fluid well. These methods are probably more suitable for materials with higher porosity. In addition, the click reactions were complicated and time-consuming and that is why they would not be optimal if a high throughput production of fluidic channels is required. On the other hand, inkjet printing of polystyrene on CNF films produced well-defined designs. Printing two layers of polystyrene with 40 μm drop spacing produced the most efficient channel system. The optimal channel edge thickness was 2 mm. These channels displayed fast flow and held the fluid well. The printing method was easy, fast and it was possible to create multiple channels at the same time. These characteristics make this method very efficient.

Antifouling properties were introduced to the channels successfully. The best blocking agent for CNF was D33-EGMA-137 block copolymer, which decreased adsorption of hIgG up to 95 %. This copolymer has a short cationic PDMAEMA-block and longer hydrophilic POEGMA-block. Most likely, the cationic block attached the copolymer efficiently to the CNF surface and the end block formed a hydrated layer on the CNF surface. The blocking efficiency of this hydrated layer was good since, water molecules

could not be removed from this layer by the protein. This is from the steric repulsion that was created between the surface and hIgG proteins.

The successful blocking of the channels and efficient fluid flow point out that these channels could be developed further and can possibly be used in future biosensor applications. However, more research is needed in order to develop the full potential of the CNF films as working biosensor substrates. For example, addition of the bioactive sensing area and testing of its functionality should be studied more deeply. In addition, the mechanical properties of the CNF film need to be adjusted for the applications and especially the wet-strength of the substrates should be investigated.

References

Abitbol, T., Rivkin, A., Cao, Y., Nevo, Y., Abraham, E., Ben-Shalom, T., Lapidot, S. and Shoseyov, O. (2016). Nanocellulose, a tiny fiber with huge applications. *Current opinion in biotechnology*, 39, 76-88.

Aikio, S., Grönqvist, S., Hakola, L., Hurme, E., Jussila, S., Kaukoniemi, O.-V., Kopola, H., Känsäkoski, M., Leinonen, M., Lippo, S., Mahlberg, R., Peltonen, S., Qvintus-Leino, P., Rajamäki, T., Ritschkoff, A.-C., Smolander, M., Vartiainen, J., Viikari, L. and Vilkman, M. (2006). Bioactive paper and fibre products, patent and literary survey. *VTT Working Papers 51*, 1-84. ISBN 951-38-6603-3.

Anonymous, Biolin Scientific. Measurements: QCM-D. Available: https://www.biolinscientific.com/measurements/qcm-d, [Accessed 11.4.2018].

Arseneault, M., Wafer, C. and Morin, J.F. (2015). Recent advances in click chemistry applied to dendrimer synthesis. *Molecules*, 20(5), 9263-9294.

Begat, P., Morton, D.A., Staniforth, J.N. and Price, R. (2004). The cohesive-adhesive balances in dry powder inhaler formulations I: Direct quantification by atomic force microscopy. *Pharmaceutical research*, 21(9), 1591-1597.

Binnig, G., Quate, C.F. and Gerber, C. (1986). Atomic force microscope. *Physical review letters*, 56(9), 930-933.

Bora, U., Sharma, P., Kannan, K. and Nahar, P. (2006). Photoreactive cellulose membrane - A novel matrix for covalent immobilization of biomolecules. *Journal of biotechnology*, 126(2), 220-229.

Brash, J.L. and Hove, T.P. (1993). Protein adsorption studies on 'standard' polymeric materials. *Journal of Biomaterials Science, Polymer Edition*, 4(6), 591-599.

Brinchi, L., Cotana, F., Fortunati, E. and Kenny, J.M. (2013). Production of nanocrystalline cellulose from lignocellulosic biomass: technology and applications. *Carbohydrate Polymers*, 94(1), 154-169.

Campbell, C.T. and Kim, G. (2007). SPR microscopy and its applications to high-throughput analyses of biomolecular binding events and their kinetics. *Biomaterials*, 28(15), 2380-2392.

Cao, Y., Zhang, Q., Wang, C., Zhu, Y. and Bai, G. (2007). Preparation of novel immunomagnetic cellulose microspheres via cellulose binding domain-protein A linkage and its use for the isolation of interferon α-2b. *Journal of Chromatography A*, 1149(2), 228-235.

Cassie, A.B.D. and Baxter, S. (1944). Wettability of porous surfaces. *Transactions of the Faraday society*, 40, 546-551.

Charles, P.T., Stubbs, V.R., Soto, C.M., Martin, B.D., White, B.J. and Taitt, C.R. (2009). Reduction of non-specific protein adsorption using poly(ethylene) glycol (PEG) modified polyacrylate hydrogels in immunoassays for staphylococcal enterotoxin B detection. *Sensors*, 9(1), 645-655.

Cleaves H.J. (2011) Isoelectric Point. In: *Encyclopedia of Astrobiology.* Berlin, Germany: Springer-Verlag Berlin Heidelberg, 858. ISBN: 9783642112713.

Dee, K.C., Puleo, D.A. and Bizios, R., (2002). Chapter 3: Protein-Surface Interactions, In: *An introduction to tissue-biomaterial interactions*. New Jersey, USA: John Wiley & Sons, 37-51. ISBN: 978-0-471-25394-5.

Dhruv, H.D. (2009). Controlling nonspecific adsorption of proteins at bio-interfaces for biosensor and biomedical applications. Doctoral dissertation, Utah State University, Logan, Utah. 19.

Dixon, M.C. (2008). Quartz crystal microbalance with dissipation monitoring: enabling real-time characterization of biological materials and their interactions. *Journal of biomolecular techniques: JBT*, 19(3), 151-158.

Dolatshahi-Pirouz, A., Skeldal, S., Hovgaard, M.B., Jensen, T., Foss, M., Chevallier, J. and Besenbacher, F. (2009). Influence of nanoroughness and detailed surface morphology on structural properties and water-coupling capabilities of surface-bound fibrinogen films. *The Journal of Physical Chemistry C*, 113(11), 4406-4412.

Eaton, P. and West, P. (2010). *Atomic force microscopy*. New York, USA: Oxford University Press. 1-64.

Edwards, J.V., Prevost, N., French, A., Concha, M., DeLucca, A. and Wu, Q. (2013). Nanocellulose-based biosensors: design, preparation, and activity of peptide-linked cotton cellulose nanocrystals having fluorimetric and colorimetric elastase detection sensitivity. *Engineering*, 5(9), 20.

Fenton, E.M., Mascarenas, M.R., López, G. P. and Sibbett, S.S. (2008). Multiplex lateral-flow test strips fabricated by two-dimensional shaping. *ACS applied materials & interfaces*, 1(1), 124-129.

Filpponen, I., Kontturi, E., Nummelin, S., Rosilo, H., Kolehmainen, E., Ikkala, O., Laine, J. (2012). Generic method for modular surface modification of cellulosic materials in aqueous medium by sequential “click” reaction and adsorption. *Biomacromolecules*, 13(3), 736–742.

Fujisawa, S., Saito, T., Kimura, S., Iwata, T. and Isogai, A. (2013). Surface engineering of ultrafine cellulose nanofibrils toward polymer nanocomposite materials. *Biomacromolecules*, *14*(5), 1541-1546.

Fukuoka, A. and Dhepe, P.L. (2006). Catalytic conversion of cellulose into sugar alcohols. *Angewandte Chemie International Edition*, 45(31), 5161-5163.

Ge, L., Yan, J., Song, X., Yan, M., Ge, S. and Yu, J. (2012). Three-dimensional paper-based electrochemiluminescence immunodevice for multiplexed measurement of biomarkers and point-of-care testing. *Biomaterials*, *33*(4), 1024-1031.

Ge, X., Asiri, A. M., Du, D., Wen, W., Wang, S. and Lin, Y. (2014). Nanomaterial-enhanced paper-based biosensors. *TrAC Trends in Analytical Chemistry*, 58, 31-39.

Goodsell, D.S. (2013). Featured System Serum Albumins and Allergies. *Protein Structure Initiative Structural Genomics Knowledgebase*. doi:10.3942/psi_sgkb/fm_2013_10.

Grieshaber, D., MacKenzie, R., Voeroes, J. and Reimhult, E. (2008). Electrochemical biosensors-sensor principles and architectures. *Sensors*, 8(3), 1400-1458.

Guo, J., Fang, W., Welle, A., Feng, W., Filpponen, I., Rojas, O.J. and Levkin, P.A. (2016). Superhydrophobic and Slippery Lubricant-Infused Flexible Transparent Nanocellulose Films by Photoinduced Thiol–Ene Functionalization. *ACS applied materials & interfaces*, 8(49), 34115-34122.

Guo, J. (2017). Covalent Modification of Nanocellulose Towards Advanced Functional Materials. Doctoral dissertation, Aalto University, School of Chemical Engineering, Department of Bioproducts and Biosystems, Espoo. 4-60. ISBN 978-952-60-7490-0.

Guo, J., Filpponen, I., Johansson, L.-S., Heiβler, S., Li, L., Levkin, P. and Rojas, O.J. (2018). Micro-patterns on nanocellulose films and paper by photo-induced thiol–yne click coupling: a facile method toward wetting with spatial resolution. *Cellulose*, 25(1), 367-375.

Guthoff, R.F., Baudouin, C. and Stave, J. (2006). Chapter 2 Principles of Confocal In Vivo Microscopy, In: *Atlas of Confocal Laser Scanning In-vivo Microscopy in Ophthalmology*. New York, USA: Springer-Verlag Berlin Heidelberg, 3-16. ISBN 354032707X.

Hall, D.B., Underhill, P. and Torkelson, J.M. (1998). Spin coating of thin and ultrathin polymer films. *Polymer Engineering & Science*, 38(12), 2039-2045.

Hamilton, R.G. (1987). Human IgG subclass measurements in the clinical laboratory. *Clinical Chemistry*, 33(10), 1707-1725.

Hermanson, G.T. (2008). Chapter 9 Fluorescent Probes, In: *Bioconjugate techniques*. 2nd edition, New York, USA: Academic Press, 403.

Hu, J., Wang, S., Wang, L., Li, F., Pingguan-Murphy, B., Lu, T. J. and Xu, F. (2014). Advances in paper-based point-of-care diagnostics. *Biosensors and Bioelectronics*, *54*, 585-597.

Höök, F., Rodahl, M., Brzezinski, P. and Kasemo, B. (1998). Energy dissipation kinetics for protein and antibody−antigen adsorption under shear oscillation on a quartz crystal microbalance. *Langmuir*, 14(4), 729-734.

Janeway, C.A., Travers, J.P. Walport, M. and Shlomchik, M.J. (2001). Chapter 3: The interaction of the antibody molecule with specific antigen, In: *Immunobiology: The Immune System in Health and Disease*. 5th edition. New York, USA: Garland Publishing, 123-125.

Jarujamrus, P., Tian, J., Li, X., Siripinyanond, A., Shiowatana, J. and Shen, W. (2012). Mechanisms of red blood cells agglutination in antibody-treated paper. *Analyst*, 137(9), 2205-2210.

Jin, H., Kettunen, M., Laiho, A., Pynnönen, H., Paltakari, J., Marmur, A., Ikkala, O. and Ras, R.H. (2011). Superhydrophobic and superoleophobic nanocellulose aerogel membranes as bioinspired cargo carriers on water and oil. *Langmuir*, 27(5), 1930-1934.

Jones, K.L. and O'Melia, C.R. (2000). Protein and humic acid adsorption onto hydrophilic membrane surfaces: effects of pH and ionic strength. *Journal of Membrane Science*, 165(1), 31-46.

Jung, L.S., Campbell, C.T., Chinowsky, T.M., Mar, M.N. and Yee, S.S., (1998). Quantitative interpretation of the response of surface plasmon resonance sensors to adsorbed films. *Langmuir*, 14(19), 5636-5648.

Kanduč, M. and Netz, R.R. (2015). From hydration repulsion to dry adhesion between asymmetric hydrophilic and hydrophobic surfaces. *Proceedings of the National Academy of Sciences*, 112(40), 12338-12343.

Kangas, H. (2014). Opas selluloosa-nanomateriaaleihin. *VTT Technology*, *199*, 6-40. ISBN 978-951-38-8194-8.

McKendry, P. (2002). Energy production from biomass (part 1): overview of biomass. *Bioresource technology*, 83(1), 37-46.

Khalil, H.A., Davoudpour, Y., Islam, M.N., Mustapha, A., Sudesh, K., Dungani, R. and Jawaid, M. (2014). Production and modification of nanofibrillated cellulose using various mechanical processes: a review. *Carbohydrate polymers*, 99, 649-665.

Klemm, D., Philipp, B., Heinze, T., Heinze, U. and Wagenknecht, W. (1998). *Comprehensive Cellulose Chemistry. Volume 1. Fundamentals and Analytical Methods.* Weinheim, Germany: Wiley, 260. ISBN 3-527-29413-9.

Lamas-Ardisana, P.J., Martínez-Paredes, G., Añorga, L. and Grande, H.J. (2018). Glucose biosensor based on disposable electrochemical paper-based transducers fully fabricated by screen-printing. *Biosensors and Bioelectronics*, 109, 8-12.

Larsson, L.I. (1988). Chapter 1: Antibodies and Antisera. In: *Immunocytochemistry: Theory and Practice*. Florida, USA: CRC press, Inc., 1-2.

Lasseuguette, E. (2008). Grafting onto microfibrils of native cellulose. *Cellulose*, 15(4), 571-580.

Leckband, D. and Israelachvili, J. (2001). Intermolecular forces in biology. *Quarterly reviews of biophysics*, 34(2), 105-267.

Lee, J.H., Li, T. and Park, K. (2001). Chapter 5: Solvation Interactions for Protein Adsorption to Biomaterial Surfaces. In: *Water in Biomaterials Surface Science.* West Sussex, UK: John Wiley & Sons, 128. ISBN 0471490415.

Lequin, R.M. (2005). Enzyme immunoassay (EIA)/enzyme-linked immunosorbent assay (ELISA). *Clinical chemistry*, 51(12), 2415-2418.

Lewis, A.L. (2000). Phosphorylcholine-based polymers and their use in the prevention of biofouling. *Colloids and Surfaces B: Biointerfaces*, 18(3-4), 261-275.

Li, X., Tian, J., Nguyen, T. and Shen, W. (2008). Paper-based microfluidic devices by plasma treatment. *Analytical chemistry*, 80(23), 9131-9134.

Li, X., Tian, J. and Shen, W. (2010). Progress in patterned paper sizing for fabrication of paper-based microfluidic sensors. *Cellulose*, 17(3), 649-659.

Lin, N. and Dufresne, A. (2014). Nanocellulose in biomedicine: current status and future prospect. *European Polymer Journal*, 59, 302–325.

Loureiro, L.R., Carrascal, M.A., Barbas, A., Ramalho, J.S., Novo, C., Delannoy, P. and Videira, P.A. (2015). Challenges in antibody development against Tn and Sialyl-Tn antigens. *Biomolecules*, 5(3), 1783-1809.

Lowe, A.B. (2010). Thiol-ene "click" reactions and recent applications in polymer and materials synthesis. *Polymer Chemistry*, 1(1), 17-36.

Lowe, A.B. (2014). Thiol-yne 'click'/coupling chemistry and recent applications in polymer and materials synthesis and modification. *Polymer*, 55(22), 5517-5549.

Madigan, M.D., Martinko, J.M., Dunlap, P.V. and Clark, D.P. (2009). Chapter 29. Essentials of Immunology. In: *Brock Biology of Microorganisms,* 12th edition. San Francisco, USA: Pearson Education inc., 839-864.

Magonov, S., Elings, V. and Whangbo, M. (1997). Phase imaging and stiffness in tapping-mode atomic force microscopy. *Surface Science*, 375(2-3), L385-L391.

Masson, J. F., Battaglia, T. M., Cramer, J., Beaudoin, S., Sierks, M. and Booksh, K. S. (2006). Reduction of nonspecific protein binding on surface plasmon resonance biosensors. *Analytical and bioanalytical chemistry*, 386(7-8), 1951-1959.

McUmber, A.C., Randolph, T.W. and Schwartz, D.K. (2015). Electrostatic interactions influence protein adsorption (but not desorption) at the silica–aqueous interface. *The journal of physical chemistry letters*, 6(13), 2583-2587.

Missoum, K., Belgacem, M.N. and Bras, J. (2013). Nanofibrillated cellulose surface modification: a review. *Materials,* 6(5), 1745–1766.

Moon, R. J., Martini, A., Nairn, J., Simonsen, J. and Youngblood, J. (2011). Cellulose nanomaterials review: structure, properties and nanocomposites. *Chemical Society Reviews*, 40(7), 3941-3994.

Nguyen, T.K.T. (2012). Chapter 5.3.1. Antibody-Antigen. In: *Magnetic Nanoparticles: From Fabrication to Clinical Applications*. Florida, USA: CRC Press, 138-139. ISBN 1439869332.

Nilghaz, A., Wicaksono, D.H., Gustiono, D., Majid, F.A.A., Supriyanto, E. and Kadir, M.R.A. (2012). Flexible microfluidic cloth-based analytical devices using a low-cost wax patterning technique. *Lab on a Chip*, 12(1), 209-218.

Norde, W. (1996). Driving forces for protein adsorption at solid surfaces. *Macromolecular Symposia,* 103, 5-18.

Nosonovsky, M. and Bhushan, B. (2007). Hierarchical roughness makes superhydrophobic states stable. *Microelectronic engineering*, 84(3), 382-386.

Orelma, H., Filpponen, I., Johansson, L.-S., Laine, J. and Rojas, O.J. (2011). Modification of cellulose films by adsorption of CMC and chitosan for controlled attachment of biomolecules. *Biomacromolecules,* 12(12), 4311–4318.

Orelma, H., Filpponen, I., Johnsson, L.-S., Österberg, M., Rojas, O.J. and Laine, J. (2012a). Surface functionalized nanofibrillar cellulose (NFC) film as a platform for immunoassays and diagnostics. *Biointerphases,* 7(1), 1–12.

Orelma, H., Johansson, L.-S., Filpponen, I., Rojas, O.J. and Laine, J. (2012b). Generic method for attaching biomolecules via avidin-biotin complexes immobilized on films of regenerated and nanofibrillar cellulose. *Biomacromolecules*, 13(9), 2802–2810.

Ostuni, E., Chapman, R.G., Liang, M.N., Meluleni, G., Pier, G., Ingber, D.E. and Whitesides, G.M. (2001). Self-assembled monolayers that resist the adsorption of proteins and the adhesion of bacterial and mammalian cells. *Langmuir*, 17(20), 6336-6343.

O'sullivan, M.J., Bridges, J. W. and Marks, V. (1979). Enzyme immunoassay: a review. *Annals of clinical biochemistry*, 16(1-6), 221-239.

Parolo, C. and Merkoçi, A. (2013). Paper-based nanobiosensors for diagnostics. *Chemical Society Reviews*, 42(2), 450-457.

Pelton, R. (2009). Bioactive paper provides a low-cost platform for diagnostics. *Trends in Analytical Chemistry*, 28(8), 925-942.

Peresin, M.S., Vartiainen, J., Kunnari, V., Kaljunen, T., Tammelin, T. and Qvintus, P. (2012), Large-scale nanofibrillated cellulose film: an overview on its production, properties, and potential applications. In: *Book of abstracts international conference of pulping, papermaking and biotechnology*.

Pesonen-Leinonen, E., Kuisma, R., Redsven, I., Sjöberg, A. and Hautala, M. (2006). Can contact angle measurements be used to predict soiling and cleaning of plastic flooring materials. *Contact angle, wettability and adhesion*, 4, 203-214.

Petersen, S., Gattermayer, M. and Biesalski, M. (2010). Hold on at the right spot: bioactive surfaces for the design of live-cell micropatterns. In: *Bioactive Surfaces*. Berlin, Germany: Springer Berlin Heidelberg, 35-78.

Prime, K.L. and Whitesides, G.M. (1991). Self-assembled organic monolayers: model systems for studying adsorption of proteins at surfaces. *Science*, 252, 1164-1167.

Protopopova, A.D., Barinov, N.A., Zavyalova, E.G., Kopylov, A.M., Sergienko, V.I. and Klinov, D.V. (2015). Visualization of fibrinogen αC regions and their arrangement during fibrin network formation by high-resolution AFM. *Journal of Thrombosis and Haemostasis*, 13(4), 570-579.

Putnam, F.W., Liu, Y.S. and Low, T.L. (1979). Primary structure of a human IgA1 immunoglobulin. IV. Streptococcal IgA1 protease, digestion, Fab and Fc fragments, and the complete amino acid sequence of the alpha 1 heavy chain. *Journal of Biological Chemistry*, 254(8), 2865-2874.

Qvintus, P., Tammelin, T., Hippi, U. and Salminen, A. (2013). Method for the preparation of NFC films on supports. Patent WO 2013/060934A2.

Rabe, M., Verdes, D. and Seeger, S. (2011). Understanding protein adsorption phenomena at solid surfaces. *Advances in colloid and interface science*, 162(1-2), 87-106.

Roero, C. (2006). Contact-angle measurements of sessile drops deformed by a DC electric field. *Contact Angle, Wettability and Adhesion*, 4, 165-176.

Ross, P.D. and Subramanian, S. (1981). Thermodynamics of protein association reactions: forces contributing to stability. *Biochemistry*, 20(11), 3096-3102.

Rusmini, F., Zhong, Z. and Feijen, J. (2007). Protein immobilization strategies for protein biochips. *Biomacromolecules*, 8(6), 1775-1789.

Schasfoort, R.B.M. (2017). *Handbook of surface plasmon resonance*. 2nd edition, London, UK: Royal Society of Chemistry, 524. ISBN 1788011392.

Salas, C., Nypelö, T., Rodriguez-Abreu, C., Carrillo, C. and Rojas, O.J. (2014). Nanocellulose properties and applications in colloids and interfaces. *Current Opinion in Colloid & Interface Science*, 19(5), 383-396.

Sauerbrey, G., (1959). Verwendung von Schwingquarzen zur Wägung dünner Schichten und zur Mikrowägung. *Zeitschrift für physik*, 155(2), 206-222.

Schultz, J.S. and Taylor, R.F. 1996. Chapter 1 Introduction to chemical and biological sensors, In: *Handbook of Chemical and Biological Sensors*. IOP Publishing Ltd., 1-10. ISBN 0-7503-0323-9.

Shetty, N. (2005). Chapter 4. Antigens and Immunogenicity. In: *Immunology: Introductory Textbook.* 2nd edition, New Delhi, India: New Age International Publishers, 22.

Shors, T. (2011). Chapter 5. Laboratory Diagnosis of Viral Diseases and Working with Viruses in the Research Laboratory. In: *Understanding Viruses,* 2nd edition. Massachusetts, USA: Jones & Bartlett Publishers, 103–104. ISBN 978-0-7637-8553-6.

Sigal, G.B., Mrksich, M. and Whitesides, G.M. (1998). Effect of surface wettability on the adsorption of proteins and detergents. *Journal of the American Chemical Society*, 120(14), 3464-3473.

Stokes, D. (2008). Chapter 2 Principles of SEM, In: *Principles and Practice of Variable Pressure/Environmental Scanning Electron Microscopy (VP-ESEM)*. West Sussex, UK: John Wiley & Sons Ltd., 17-60. ISBN 0470758740.

Tammelin, T. and Vartiainen, J. (2014), Chapter 13: Nanocellulose Films and Barriers. In: *Handbook of Green Materials Volume 3*. London, UK: World Scientific Publishing Company, 213-229.

Van Der Merwe, P.A. (2001). Surface plasmon resonance. *Protein-ligand interactions: hydrodynamics and calorimetry*, 1, 137-170.

Vikholm-Lundin, I. (2005). Immunosensing based on site-directed immobilization of antibody fragments and polymers that reduce nonspecific binding. *Langmuir*, 21(14), 6473-6477.

Vuoriluoto, M., Orelma, H., Johansson, L.-S., Zhu, B., Poutanen, M., Walther, A., Laine, J. and Rojas, O.J. (2015). Effect of Molecular Architecture of PDMAEMA–POEGMA Random and Block Copolymers on Their Adsorption on Regenerated and Anionic Nanocelluloses and Evidence of Interfacial Water Expulsion. *The Journal of Physical Chemistry B*, 119(49), 15275-15286.

Vuoriluoto, M., Orelma, H., Zhu, B., Johansson, L.-S. and Rojas, O.J. (2016). Control of protein affinity of bioactive nanocellulose and passivation using engineered block and random copolymers. *ACS applied materials & interfaces*, 8(8), 5668-5678.

Vuoriluoto, M., Orelma, H., Lundahl, M., Borghei, M. and Rojas, O.J., (2017). Filaments with Affinity Binding and Wet Strength Can Be Achieved by Spinning Bifunctional Cellulose Nanofibrils. *Biomacromolecules*, 18(6), 1803-1813.

Vuoriluoto, M. (2017). Engineering Nanocellulose Biointerfaces Toward Bioactivity and Strength. Doctoral dissertation, Aalto University, School of Chemical Engineering, Department of Bioproducts and Biosystems, Espoo. ISBN 978-952-60-7592-1 (pdf).

Wenzel, R.N., 1936. Resistance of solid surfaces to wetting by water. *Industrial & Engineering Chemistry*, 28(8), 988-994.

Wertz, J.-L., Mercier, J.P. and Bédué, O. (2010). Chapter 3.3. Morphological Structure. In: *Cellulose Science and Technology*. Lausanne, Switzerland: EPFL Press, 350. ISBN 143980799X.

Wilson, C.J., Clegg, R.E., Leavesley, D.I. and Pearcy, M.J. (2005). Mediation of biomaterial–cell interactions by adsorbed proteins: a review. *Tissue engineering*, 11(1-2), 1-18.

Woof, J.M. and Burton, D.R. (2004). Human antibody-fc receptor interactions illuminated by crystal structures. *Nature Reviews. Immunology,* 4(2), 89-99.

Wu, P., Castner, D.G. and Grainger, D.W. (2008). Diagnostic devices as biomaterials: a review of nucleic acid and protein microarray surface performance issues. *Journal of Biomaterials Science, Polymer Edition*, 19(6), 725-753.

Xiao, Y. and Isaacs, S.N. (2012). Enzyme-linked immunosorbent assay (ELISA) and blocking with bovine serum albumin (BSA) - not all BSAs are alike. *Journal of immunological methods*, 384(1-2), 148-151.

Yang, W., Jiao, L., Min, D., Liu, Z. and Dai, H. (2017). Effects of preparation approaches on optical properties of self-assembled cellulose nanopapers. *RSC Advances*, 7(17), 10463-10468.

Yuan, Y. and Lee, T.R. (2013). Chapter 1. Contact angle and wetting properties. In: *Surface science techniques*. Berlin, Germany: Springer Berlin Heidelberg, 3-34.

Appendices

APPENDIX 1

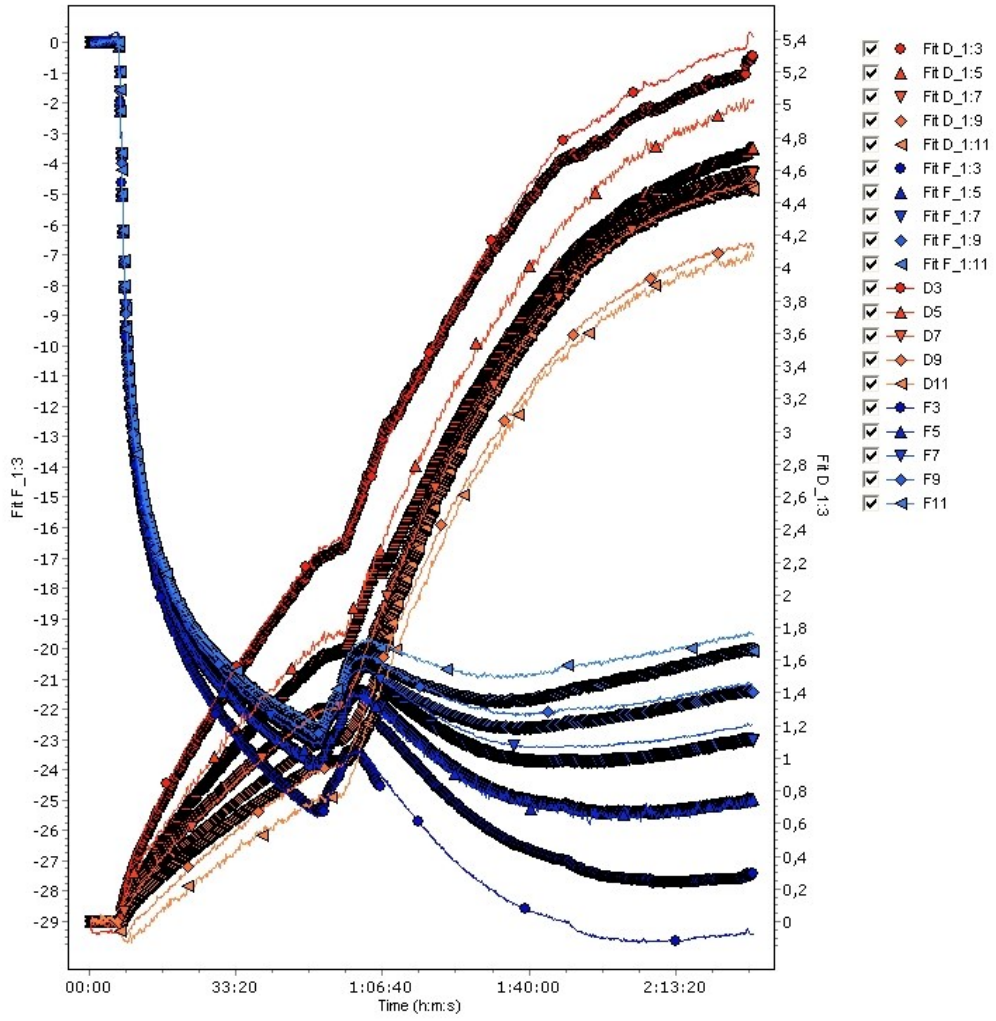

Figure S1. Fit of adsorbed hIgG layer on CNF via Voigt viscoelastic model.

APPENDIX 2

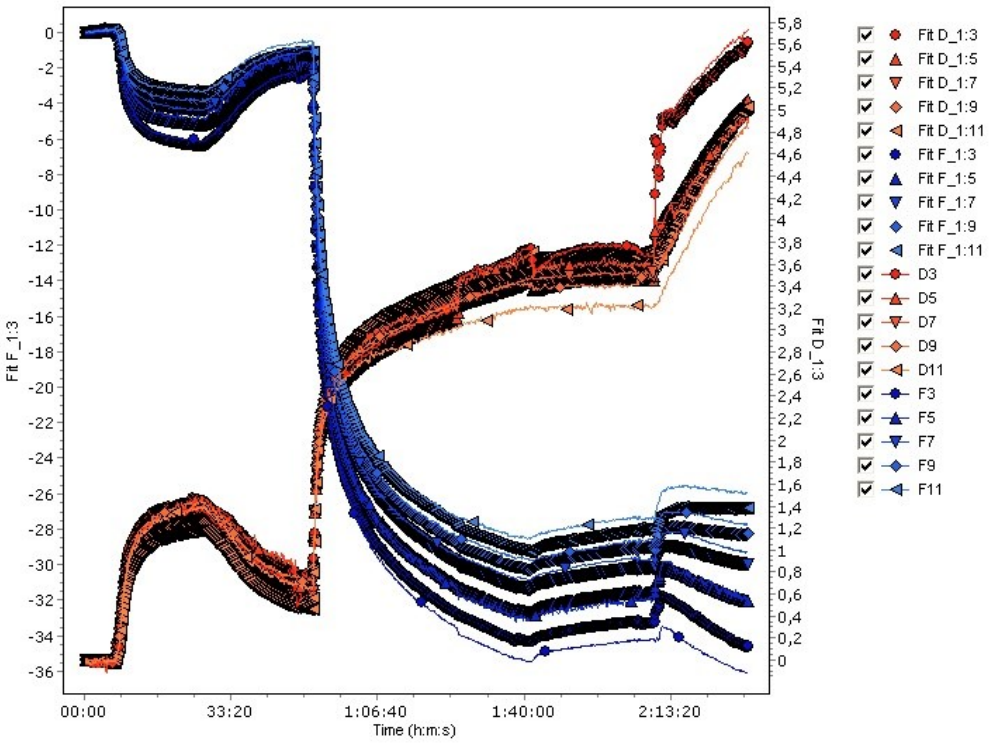

Figure S2. Fit of adsorbed fibrinogen+hIgG layer on CNF via Voigt viscoelastic model.

APPENDIX 3

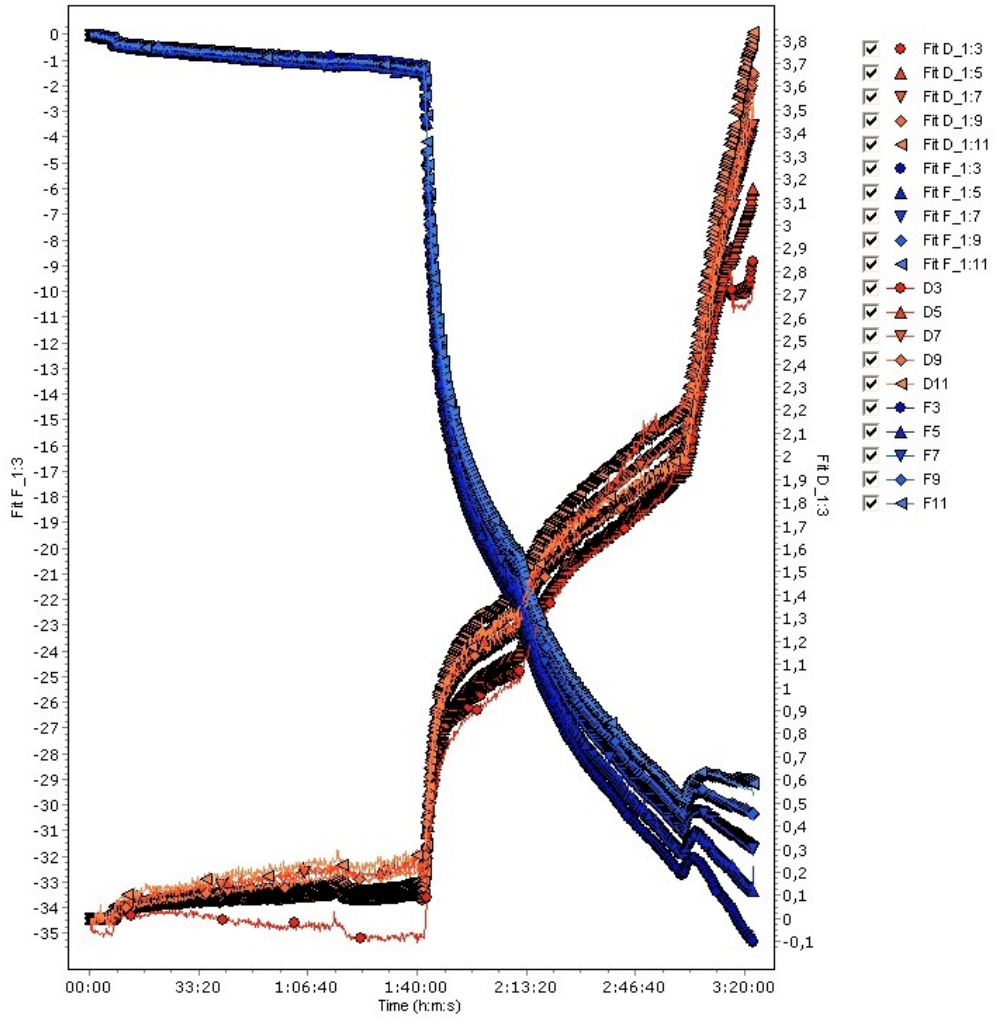

Figure S3. Fit of adsorbed BSA+hIgG layer on CNF via Voigt viscoelastic model.

APPENDIX 4

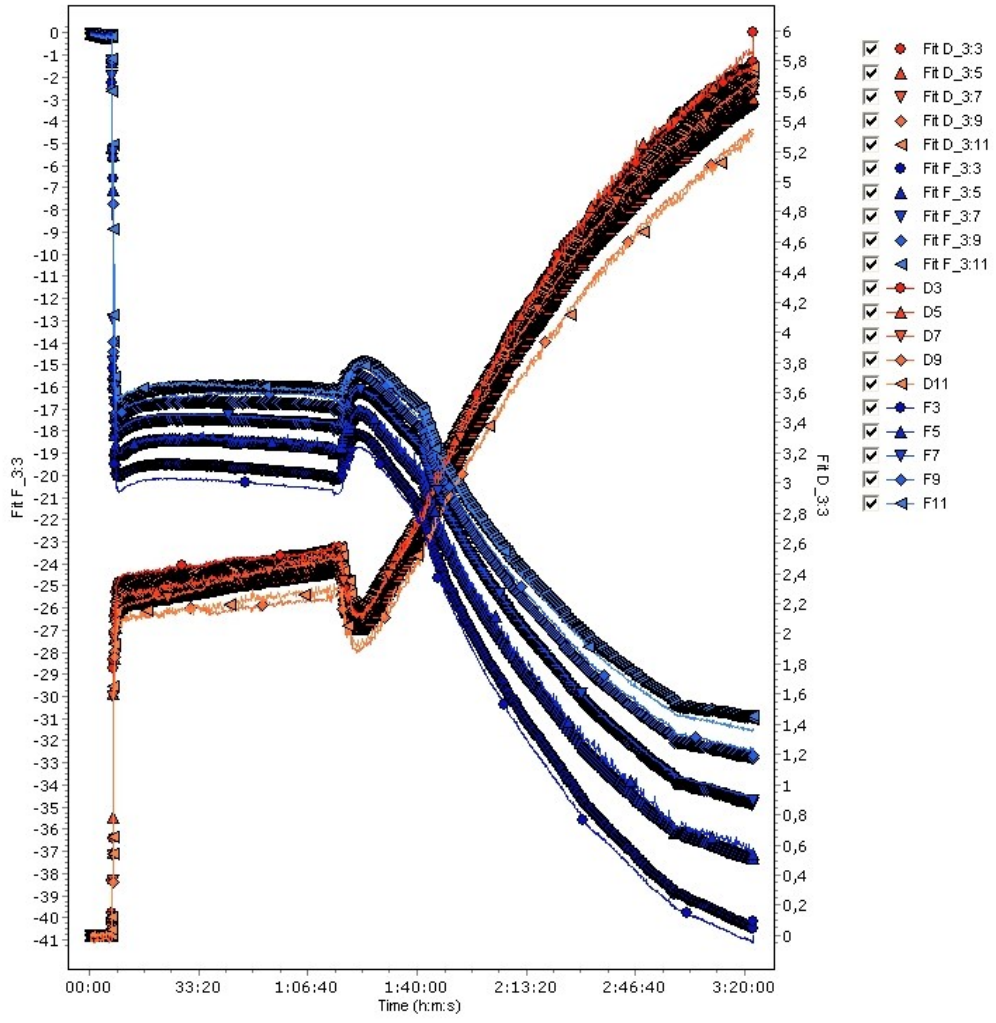

Figure S4. Fit of adsorbed D33-EGMA-137+hIgG layer on CNF via Voigt viscoelastic model.

APPENDIX 5

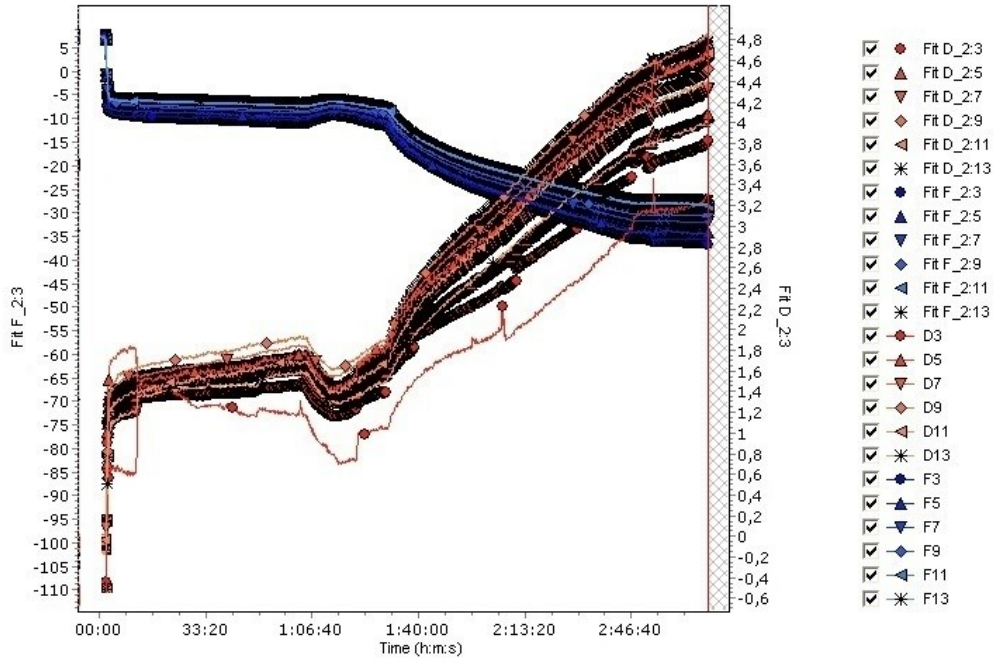

Figure S5. Fit of adsorbed D58-EGMA-118+hIgG layer on CNF via Voigt viscoelastic model.

APPENDIX 6

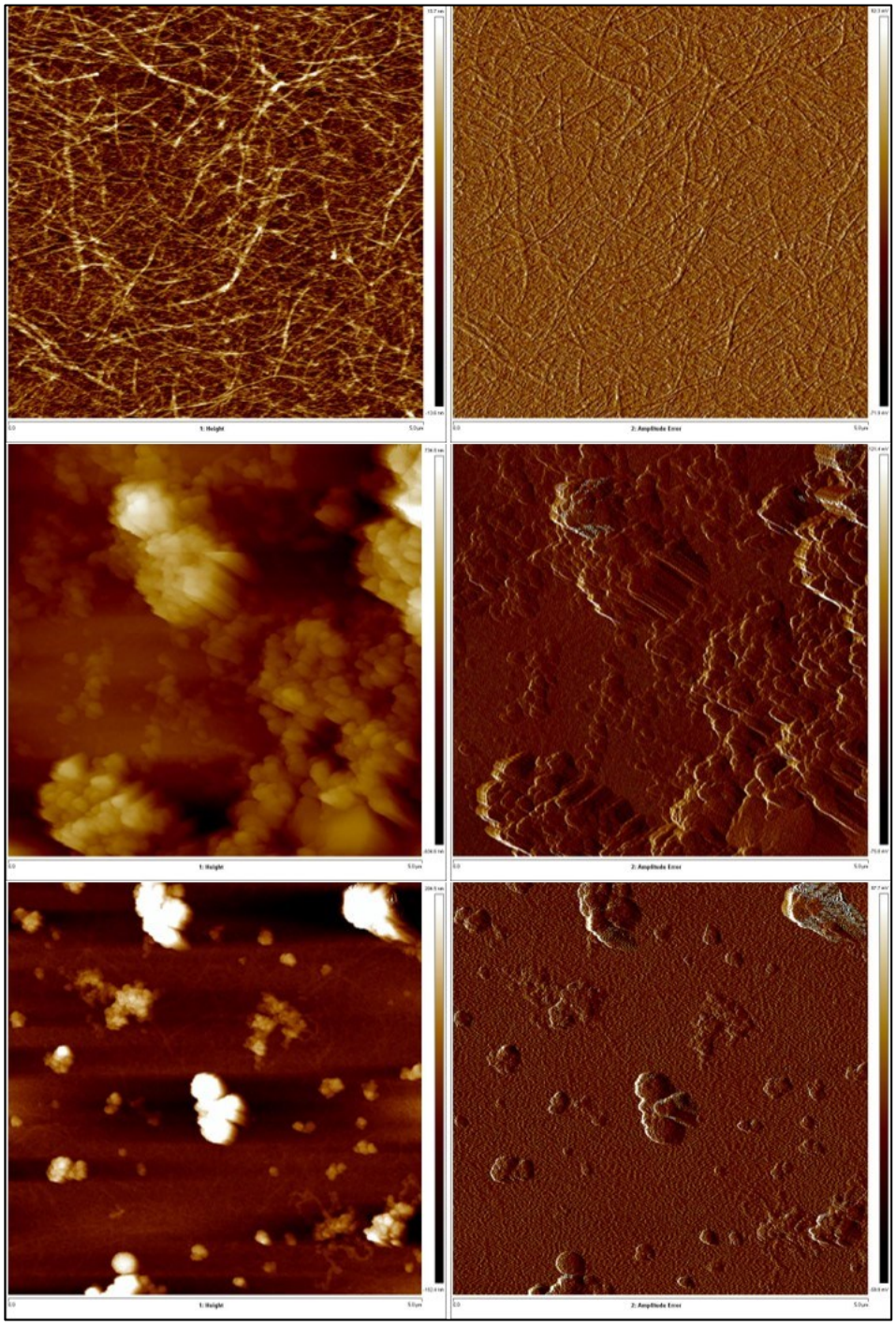

Figure S6. AFM height and amplitude error images of unmodified CNF (top), cysteamine hydrochloride modified CNF (middle) and 2-mercaptoethanol modified CNF (bottom).